

DIRECT ANALYSIS OF ENDOGENOUS AND EXOGENOUS COMPOUNDS IN
WHOLE-ANIMAL TISSUE SECTIONS BY IMAGING MALDI MASS
SPECTROMETRY

By

Sheerin Khatib-Shahidi

Dissertation

Submitted to the Faculty of the
Graduate School of Vanderbilt University

in partial fulfillment of the requirements

for the degree of

DOCTOR OF PHILOSOPHY

in

Chemistry

December, 2007

Nashville, Tennessee

Approved:

Professor Richard Caprioli

Professor Dennis Hallahan

Professor Michael Stone

Professor David Wright

Copyright© 2007 by Sheerin Khatib-Shahidi
All Rights Reserved

This work is dedicated to my father and mother, Mo and Sima Khatib-Shahidi.
Your love, strength, and encouragement have inspired me to always reach for
the stars. Thank you.

ACKNOWLEDGEMENTS

Never did I imagine the tremendous dedication and perseverance that would be required to earn a Ph.D. I am truly grateful to all who have provided me with limitless support and encouragement along my path towards achieving this goal. It would be prudent of me to specifically acknowledge the many people without whom this work would not have been possible.

First and foremost, I must thank my advisor, Richard Caprioli, for giving me the opportunity to learn and grow as an independent scientist. I appreciate all of the guidance and infinite wisdom you have provided me. I will always carry this advice with me to manage life both in and away from the laboratory. To each of my committee members, Dennis Hallahan, Larry Marnett, Michael Stone, and David Wright, thank you for all your guidance and invaluable input to help progress this project to its successful completion.

I must also acknowledge the many people I have had the pleasure of working with throughout my studies at Vanderbilt University. Thank you to the all the current and former members of the Mass Spectrometry Research Center, as colleagues and friends, you have been an amazing (and amusing!) group of people. I will always cherish the wonderful times we've shared. I would also like to thank the many collaborators here at Vanderbilt University, including the Institute for Imaging Sciences and the Department of Radiation Oncology, as well as, collaborators at Eli Lilly and Co, Jennifer Herman, Enaksha Wickremsinhe, and Todd Gillespie. I am deeply indebted to you for the many opportunities

provided to me to participate and contribute to the advancement of our scientific disciplines. I have learned a great deal from you and our candid discussions have provided me with insightful perspectives that I will always treasure. Of course, this work would not have been possible without the financial support provided by the NIH (NIH/NIGMS GM58008), Department of Defense (W81XWH-05-1-0179), and Eli Lilly and Co. (VUMC 31425). I would also like to acknowledge support from the NCI Biochemical and Chemical Training for Cancer Research Grant (CA09582).

No one knows the importance of what this accomplishment means to me more than my close friends and family. I appreciate all of your love and encouragement throughout these many years of graduate school. Thank you to the Oppenheimer family for welcoming me into your home. I feel truly blessed to have met such a warm, generous, and loving family. I am proud to regard you as my home away from home. Thank you to my best-friend, Tatum Pritchard. Despite the distance and my infrequent communication, you have been a patient, kind, and loyal friend. To my parents, Mo and Sima, you have taught me more than I could ever give you credit for here. You both have shown me by example what a good, honest, and caring person should be and, for this, I will always be appreciative. Thank you to my sister, Shari, for all of your love and support.

Finally, I must thank my best-friend and husband-to-be, Joey Latham. I met you here at Vanderbilt University four years ago and, now I can't imagine my future without you. You are the most sensitive, caring, and intelligent person I know; truly an inspiration to me. Thank you for the immeasurable love, support,

and encouragement you have given me throughout our years at Vanderbilt. I genuinely couldn't have done this without you. I love you!

TABLE OF CONTENTS

	Page
DEDICATION	iii
ACKNOWLEDGEMENTS.....	iv
LIST OF TABLES	x
LIST OF FIGURES	xi
LIST OF ABBREVIATIONS	xiv
Chapter	
I. BACKGROUND AND OBJECTIVES	1
Recent Advances in Drug Discovery and Development	1
Drug Discovery and Development Process.....	2
Technological Trends in Pharma.....	4
Mass Spectrometry in Pharmaceutical Analyses	5
Matrix-Assisted Laser Desorption/Ionization Mass Spectrometry.....	6
MALDI	7
Imaging MALDI	9
Instrumentation for MALDI Mass Spectrometry	12
Advantages of MALDI Tandem Mass Spectrometry	15
Direct Tissue Analysis using MALDI MS/MS.....	17
Current Methodologies for Drug Distribution Studies.....	19
Nuclear Imaging	20
Whole-Body Autoradiography	23
Summary and Research Objectives	25
II. PROTOCOL DEVELOPMENT FOR WHOLE-ANIMAL DIRECT TISSUE ANALYSIS	28
Tissue Preparation Protocols	28
Animal Dosing and Sacrifice	28
Carcass Embedding.....	32
Tissue Sectioning and Mounting	37
Matrix Deposition.....	42
General Considerations	42

	Matrix/Solvent Selection.....	42
	Matrix Application.....	44
	Whole-Body Drug Analysis by MALDI MS/MS	48
	General Considerations	59
	Instrument Parameter Optimization.....	51
	Data Processing.....	51
	Whole-Body Image Reconstruction.....	55
	Summary and Conclusions.....	59
	Materials and Methods	59
III.	PREDICTING MATRIX CONDITIONS FOR THE ANALYSIS OF EXOGENOUS COMPOUNDS IN TISSUE BY MALDI MS/MS	62
	Introduction.....	62
	Results	63
	Discussion	77
	Materials and Methods	79
	Materials	79
	Tissue Preparation.....	80
	Model Assay Preparation	81
	MALDI MS/MS Analysis	82
	Data Processing.....	82
IV.	DRUG AND METABOLITE IMAGING IN WHOLE ANIMAL SAGITTAL TISSUE SECTIONS USING MALDI MS/MS.....	83
	Introduction.....	83
	Results	85
	Whole-Rat Olanzapine and Metabolite Imaging	85
	Olanzapine Quantitation by HPLC-MS/MS	95
	Discussion	95
	Materials and Methods	99
	Materials	99
	Tissue Preparation.....	100
	MALDI MS/MS Imaging.....	101
	Data Processing.....	101
	Drug Quantitation	102
V.	IMAGING MALDI MASS SPECTROMETRY FOR THE DISCOVERY OF MOLECULAR FEATURES INDICATIVE OF EARLY DRUG EFFICACY	104
	Introduction.....	104

Results	107
Experimental Design	107
LDI MS Imaging of Lithium Distribution in Mouse Brain	110
MALDI MS Imaging of Proteome in Mouse Brain	113
Discussion	121
Materials and Methods	126
Materials	126
Tissue Preparation	126
LDI and MALDI MS Imaging	127
Data Processing	128
Statistical Analysis	128
 VI. CONCLUSIONS AND PERSPECTIVES.....	 130
Endogenous and Exogenous Compound Analysis in Whole-Animal Tissues by Imaging MALDI Mass Spectrometry	 130
Research Perspectives.....	132
Future Research Directions	134
Conclusions.....	142
 REFERENCES	 144

LIST OF TABLES

	Page
1. Common radionuclides used for positron emission tomography.....	22
2. List of matrices and solvents.....	65
3. List of compounds based on drug class.....	70
4. Comparison of average signal intensity for drug detected by dosed tissue model assay	76
5. List of tissue abbreviations.....	90
6. Bulk quantitation results of OLZ from tissue extracts.....	96
7. Comparison of OLZ tissue ratios from MALDI MS/MS imaging signals to HPLC-MS/MS quantitation.....	96
8. Results of the pairwise comparisons for the statistically significant features.....	118
9. List of 30 statistically significant features indicative of lithium efficacy ...	119
10. Results of the pairwise comparisons for determining the contribution of lithium or radiation	122
11. Comparison of voxels with high 3D MALDI-MS ion signal and corresponding MR data.....	141

LIST OF FIGURES

	Page
1. Schematic diagram of the steps taken to successfully introduce a pharmaceutical compound to market.....	3
2. Structures of the common matrices used in MALDI MS analyses	8
3. Cartoon depiction of the MALDI ionization process	10
4. Cartoon representation of the imaging MALDI MS experiment.....	11
5. Schematic representation of the MALDI-QqTOF mass spectrometer.....	18
6. Example of whole-body autoradiography of coronal rat section bearing Hras5 tumor xenografts	24
7. Images of metal frame used to maintain proper carcass form during freezing process	33
8. Diagram of three slicing orientations.....	35
9. Use of carboxymethylcellulose embedding media suppresses MALDI MS ion signal from tissue	36
10. Rice paper transfer of whole-body tissue sections at various thicknesses	39
11. Total ion current images of rat head section analyzed by MALDI-TOF MS	41
12. Comparison of protein spectra acquired from whole-mouse head sections using two different matrix application techniques.....	47
13. Internal standard normalizes MALDI MS/MS ion image.....	53
14. Histogram of tissue specific ion suppression effects of 2 pmol compound on tissue	54
15. Extraction efficiencies of drug compounds through brain, liver, and kidney tissues	56
16. Custom software developed for reconstruction of a whole-body MALDI MS/MS ion image	58

17.	Reconstructed whole-body ion image	60
18.	Analytical workflow for the dosed tissue model assay	64
19.	Comparison of the model assay response to dosed brain	66
20.	Comparison of the model assay response to dosed liver.....	67
21.	Comparison of the model assay response to dosed kidney.....	68
22.	Overall comparison of matrix/solvent trends across three drug classes and three tissue types.....	71
23.	Comparison of matrix/solvent preferences for the dosed brain model assay	72
24.	Comparison of matrix/solvent preferences for the dosed liver model assay	73
25.	Comparison of matrix/solvent preferences for the dosed kidney model assay	74
26.	Comparison of extraction efficiencies of OLZ and SPN	75
27.	Fragmentation spectra for OLZ, metabolites, and internal standard	86
28.	Example spectra from control liver tissue contain no interfering endogenous or matrix signals	87
29.	Comparison of WBA and MALDI MS/MS detection of olanzapine at 2 h post-dose in a whole-rat sagittal tissue section.....	88
30.	Comparison of WBA and MALDI MS/MS detection of olanzapine at 6h post-dose in a whole-rat sagittal tissue section.....	91
31.	Comparison of WBA and MALDI MS/MS detection of olanzapine at 24 h post-dose in a whole-rat sagittal tissue section.....	93
32.	Plot of average OLZ MALDI MS/MS signal from skeletal muscle across four sample plates	94
33.	Schematic representation of the experimental design	108
34.	Optical images displaying the high-density array of SA matrix droplets	109

35.	Schematic representation of analytical workflow	111
36.	Evaluation of spectral variability in the cortex region of mouse brain	112
37.	Lithium distribution as detected by imaging LDI-MS	114
38.	Temporal lithium dose response in proteome of hippocampus region detected by imaging MALDI MS	115
39.	Overlay of average spectra from each treatment group.....	116
40.	Protein signal plots of the average signal intensity of two features indicative of lithium efficacy	120
41.	Co-registered blockface and quantitative MR images obtained on a 7T magnet.....	137
42.	Reconstructed blockface volume of glioma mouse head	138
43.	Co-registered blockface volume, 3D MALDI MS, and ADC MR data.....	140

LIST OF ABBREVIATIONS

ADME	absorption, distribution, metabolism, and elimination
CHCA	α -cyano-4-hydroxycinnamic acid
CID	collision induced dissociation
CMC	carboxymethylcellulose
CNS	central nervous system
Da	Dalton
DHB	2,5-dihydroxybenzoic acid
FDA	Food and Drug Administration
HPLC	high-performance liquid chromatography
IMS	imaging mass spectrometry
IS	internal standard
LC	liquid chromatography
Li-/IR+	radiation only
Li+/IR-	lithium only
Li+/IR+	lithium plus radiation
m/z	mass-to-charge
MALDI	matrix-assisted laser desorption/ionization
MRI	magnetic resonance imaging
MS	mass spectrometry
MS/MS	tandem mass spectrometry
OLZ	Olanzapine

PD	pharmacodynamic
PET	positron emission tomography
PK	pharmacokinetic
QIT	quadrupole ion trap
QqTOF	quadrupole time-of-flight
RF	radio frequency
SA	sinapinic acid
SLD	soft laser desorption
TOF	Time-of-Flight
WBA	whole-body autoradiography

CHAPTER 1

BACKGROUND AND OBJECTIVES

Recent Advances in Drug Discovery and Development

Diseases and infections are diagnosed every year and the demand for reliable and effective therapies is ever-growing. Originally, drugs were discovered by identifying the active ingredient in traditional remedies, or by fortuitous discovery of an efficacious compound.^[1] Today, a more rigorous approach is taken to identify and understand key molecular components (i.e. therapeutic targets) of disease and infection. In recent years, genomic and proteomic studies have identified a large number of disease markers, providing a myriad of potential therapeutic targets.^[2-6] These new targets have spurred the pharmaceutical industry to produce many more potential drug compounds in the hopes of improving and extending lives. Despite advances in understanding biological systems, drug discovery and development is still a lengthy process with a low rate of novel therapeutic discovery.^[7-9] Much of this bottle-neck comes from the analytical evaluation of potential compounds.^[9, 10] New technologies are needed to minimize the attrition rate of lead compounds, especially in the areas of early drug disposition screening and evaluation.

Drug Discovery and Development Process

In the pharmaceutical industry, drug discovery and development is the process by which drugs are discovered and designed for treating, curing, or preventing disease in human beings or animals. In general, many steps are taken for the successful introduction of a drug to market (Figure 1).^[9] Simply, the process can be divided into two phases: 1) drug discovery and 2) drug development. The discovery phase (1) involves the identification of drug candidates, typically by high-throughput screening assays of small molecule libraries against a target to identify compounds with strong binding affinities. The compounds that achieve the acceptable criteria for a lead compound are then further optimized with the synthesis of many new structural analogs. These analogs are also assayed to determine binding affinities to the target. The best compounds are then examined under a wider set of parameters such as metabolic stability, bioavailability, safety, and efficacy. The compounds that successfully exhibit the best profile will be promoted to the development phase (2).

In the development phase, steps are taken to evaluate the pharmacokinetic (PK) and pharmacodynamic (PD) effects of the lead compound. This can include collecting data on the therapeutic or toxicological response in a small animal model, as well as, preparing the compound for clinical trials through formulation, purity, and stability studies. Once the lead compound fulfills all the necessary requirements, it enters into the clinical trials. Several reviews are available that give greater detail of a compound's path to market.^[9, 11-13]

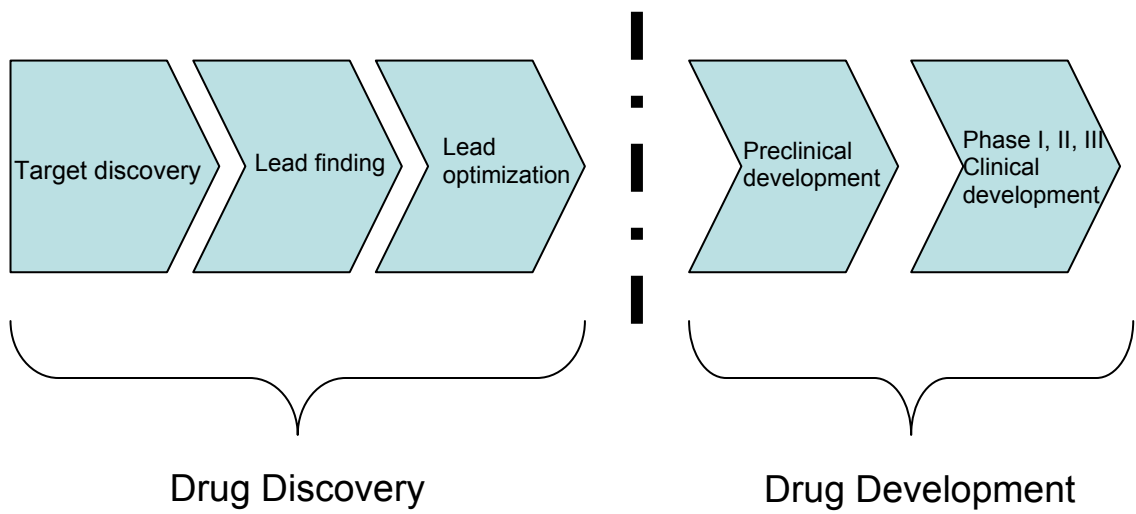


Figure 1. Schematic diagram of the steps taken to successfully introduce a pharmaceutical compound to market. Adapted from Honing *et al.*^[14]

Technological Trends in Pharma

The introduction of a new drug to market takes on average eight years or more and costs approximately \$500 million to develop.^[8] A bulk of the time and money is spent on following lead compounds that all too often prove to be unsuccessful in clinical trials. Rapidly identifying and validating potential drug therapies has become a major driving force in the pharmaceutical industry and has led to new technological developments that can facilitate the rapid screening of promising lead compounds earlier in the drug discovery and development process. This strategy has created a technological paradigm of “more, faster, and cheaper.” For example, small-molecule libraries have increased the number of novel compounds that can be synthesized (e.g. “more”).^[15, 16] As a result, analytical techniques that can quickly screen for optimal lead compounds were developed such as multiplexed *in vitro* binding or enzymatic assays (e.g. “faster”).^[17] Of even greater value were the technologies that were capable of making such evaluations by consuming less sample while at the same time providing increased sensitivity, such as micro-total analysis systems (e.g. “cheaper”).^[18]

Despite these advancements, there is still plenty of room to grow. Particularly, in the area of drug disposition where the cost and man-hours required to synthesize a radiolabeled drug compound significantly hinder throughput. For this reason, imaging studies in small animal models are reserved for the more promising lead compounds in the much later development stage. However, only 5-10% of the compounds that go into the development

stage actually ever make it to market.^[7, 11] The main reason that compounds fail is due to unacceptable ADME properties which are determined by the imaging studies. Being able to see where a drug candidate is distributed in a whole-animal helps to better assess the potential value of that compound. To that end, better imaging technologies are needed that can provide “more, faster, cheaper” analyses early in the discovery phase, before the compound moves into the more costly drug development phase.

Mass Spectrometry in Pharmaceutical Analyses

Many scientific disciplines are involved in the discovery and development of new drugs, from medicinal chemistry, toxicology, pharmacology, and analytical chemistry. These disciplines must work cooperatively to unravel the complex processes involved in disease and therapeutic intervention. In the case of analytical technologies, mass spectrometry (MS) has been widely used in many aspects of pharmaceutical research and development, from structural characterization of new chemical entities, metabolite identification, and pharmacokinetic studies.^[14, 19] This widespread use of mass spectrometry can be owed to its high sensitivity, molecular specificity, and rapid analysis times. Most of mass spectrometric analyses rely on separation techniques such as capillary electrophoresis, gas chromatography, and especially liquid chromatography (LC). With the advent of electrospray ionization, LC separations gained popularity due to the robust interface with the mass analyzer, providing a relatively straightforward means of drug analysis. Although valuable

information can be gained using LC-MS techniques, the spatial context of both the drug and metabolite compounds within the tissue is lost in these studies.

Matrix-Assisted Laser Desorption/Ionization Mass Spectrometry

The ionization technique known today as matrix-assisted laser desorption/ionization (MALDI) was introduced by Karas and Hillenkamp in 1985.^[20] This initial paper described the influence of laser wavelength on the desorption of various organic molecules. The authors noticed the increasing ion yields of non-absorbing amino acids and dipeptides in the presence of ultraviolet (UV) energy absorbing amino acids at much lower irradiance thresholds. The wavelength absorbing amino acids were hypothesized to serve as a low irradiance energy absorbing matrix that allowed for the ionization of intact non-absorbing species. The authors realized the value of this observation and postulated the future application of the wavelength absorbing matrix molecules for the analysis of small organic molecules by laser desorption mass spectrometry and hence the term MALDI was coined.^[21]

The breakthrough for large molecule analysis by laser desorption ionization arrived in 1988 with the work of Tanaka and colleagues and was awarded the 2002 Nobel Prize in Chemistry.^[22] Tanaka found that by using a mixture of ultra fine metal powder (e.g. cobalt) in glycerol as a matrix, a large protein or polymer could be ionized without fragmentation. This ionization technique became known as “soft laser desorption” (SLD). While MALDI was developed prior to SLD, it was not used to ionize proteins until after Tanaka's

work. Karas and Hillenkamp were able to ionize albumin (67 kDa protein) using nicotinic acid as a MALDI matrix.^[23] Further experiments identified derivatives of cinnamic acid to be relatively inexpensive, yet effective MALDI matrices.^[24] Today, many researchers rely on the soft nature of MALDI MS for the molecular analysis of many endogenous and exogenous analytes from biological samples.

MALDI

In MALDI MS analyses, the use of a low molecular weight organic compound that absorbs the laser energy, known as a matrix compound, is necessary to assist in the desorption and ionization process of non-volatile analytes. Prior to analysis, the matrix compound is allowed to co-crystallize with analytes in a given sample, at a typical matrix to analyte ratio of 5000:1. The most commonly used matrix compounds include 3,5-dimethoxy-4-hydroxycinnamic acid (sinapinic acid, SA), α -cyano-4-hydroxycinnamic acid (CHCA), and 2,5-dihydroxybenzoic acid (DHB) (Figure 2). The selection of a matrix compound can depend on the chemical properties of the analyte, sample conditions, and the wavelength of the laser. Most commercially available instruments are equipped with the relatively inexpensive nitrogen laser (337 nm) or the more expensive solid-state Nd:YAG laser (355 nm). While most instruments employ UV lasers, infrared (IR) lasers have been successfully used in MALDI MS applications.^[25-27] Absorption of the UV radiation from a laser pulse by the crystals subsequently causes matrix and analyte molecules to desorb from the sample surface. Gas-phase ionization occurs in the desorbed MALDI plume

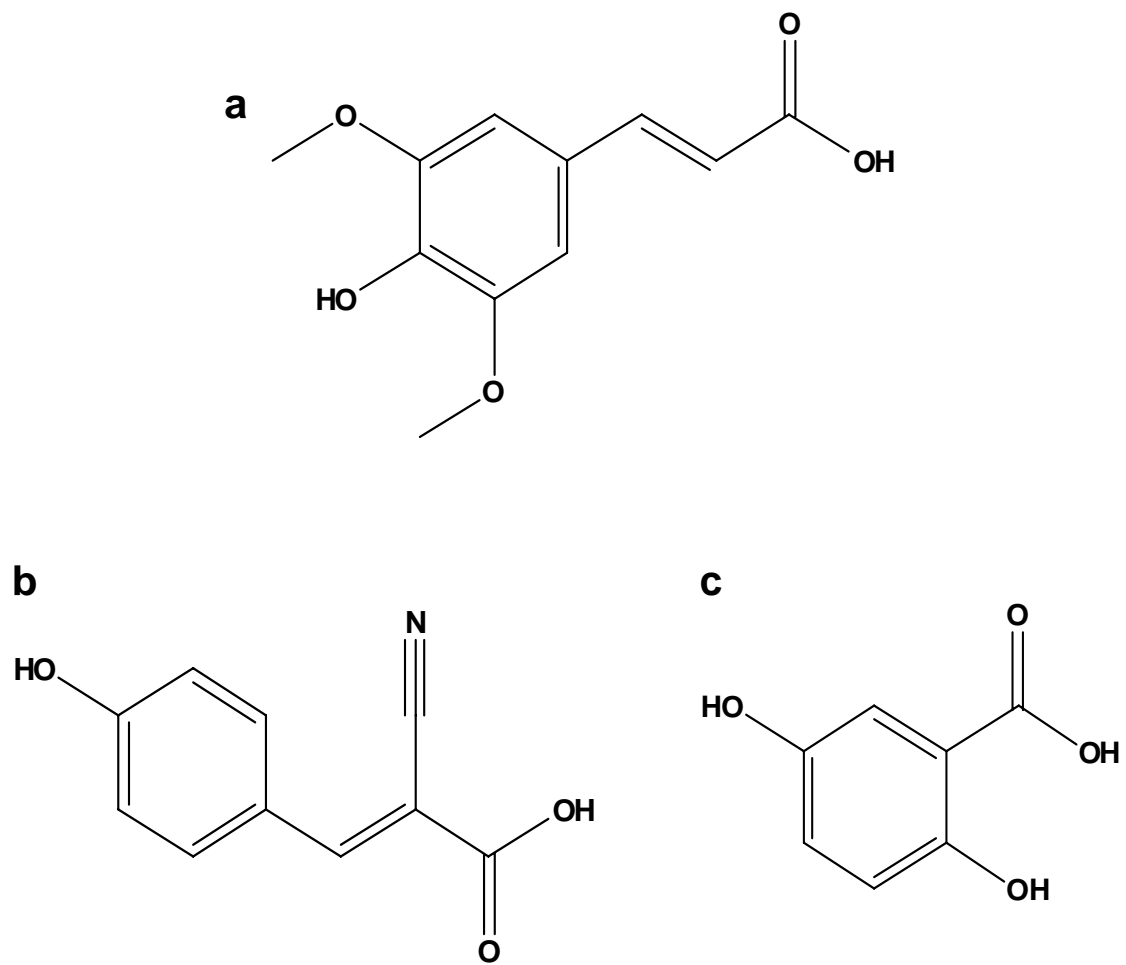


Figure 2. Structures of the common matrices used in MALDI MS analyses. a) 3,5-dimethoxy-4-hydroxycinnamic acid (sinapinic acid, SA), b) α -cyano-4-hydroxycinnamic acid (CHCA), and c) 2,5-dihydroxybenzoic acid (DHB).

to generate ions, predominantly singly protonated intact molecular ions $[M+H]^+$ (Figure 3).

Imaging MALDI

Extending the MALDI MS technology to map the location of analytes from an original sample is known as Imaging MALDI MS. The procedure uses MALDI MS to systematically raster over a sample to produce ions at known x,y locations for downstream analysis. Each mass spectrum at a specific coordinate becomes a pixel in a two-dimensional molecular map of the sample, with each pixel containing the analyte signals and associated relative abundances. A molecular ion image of the sample is produced when an m/z value is selected and its intensity at specific locations is displayed (Figure 4).

The concept of using mass spectrometry to investigate the spatial arrangements of analytes dates back several decades and is termed imaging mass spectrometry (IMS). Much of the early work in IMS was performed by secondary ion mass spectrometry (SIMS). Early imaging SIMS experiments were performed to study the elemental compositions of inorganic metals and molecular distributions within samples.^[28, 29] Current applications of SIMS technology has been limited to low mass analytes (<1000 Da) due to low ion yields and damage to the analyte during the ionization process.^[31]

With the introduction of MALDI in the mid- to late-1980s, a soft-ionization technique was established for the analysis of labile analytes. The first imaging MALDI MS experiments were reported in 1997 by the Caprioli laboratory. In this

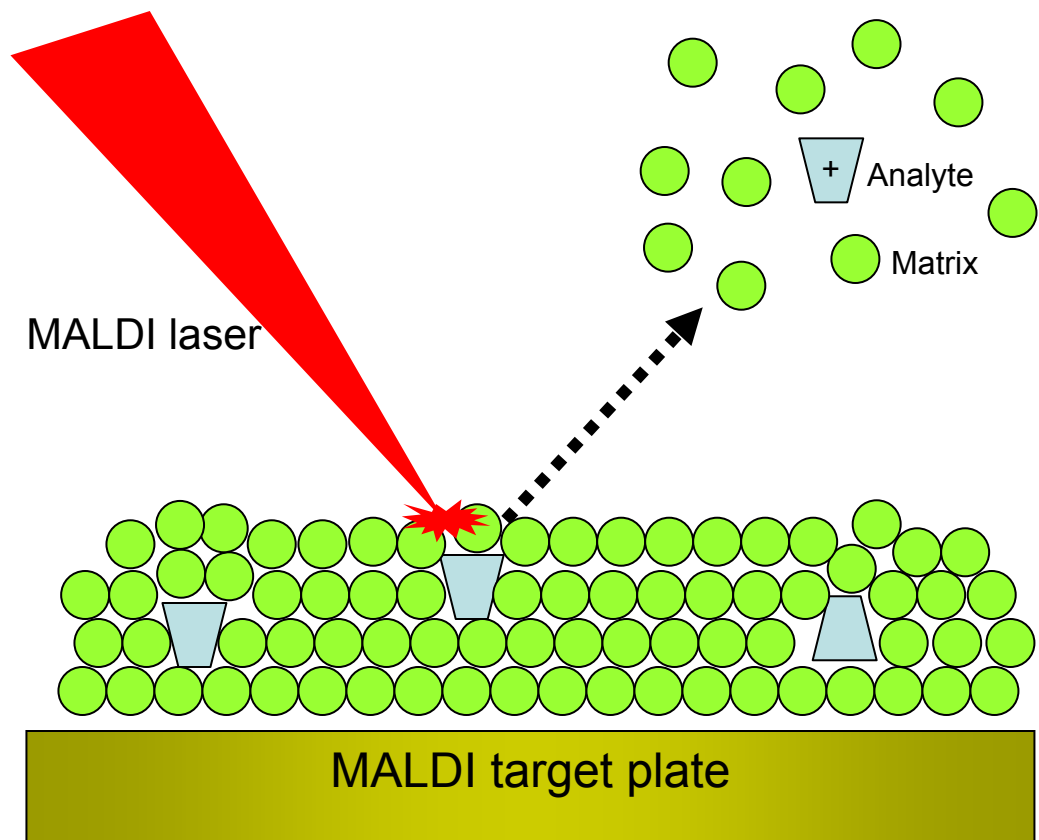


Figure 3. Cartoon depiction of the MALDI ionization process. Matrix and analyte molecules are allowed to co-crystallize on the target plate. A laser pulse causes both molecules to desorb from the sample surface and subsequent protonation of the analyte by the matrix occurs in the gas-phase.

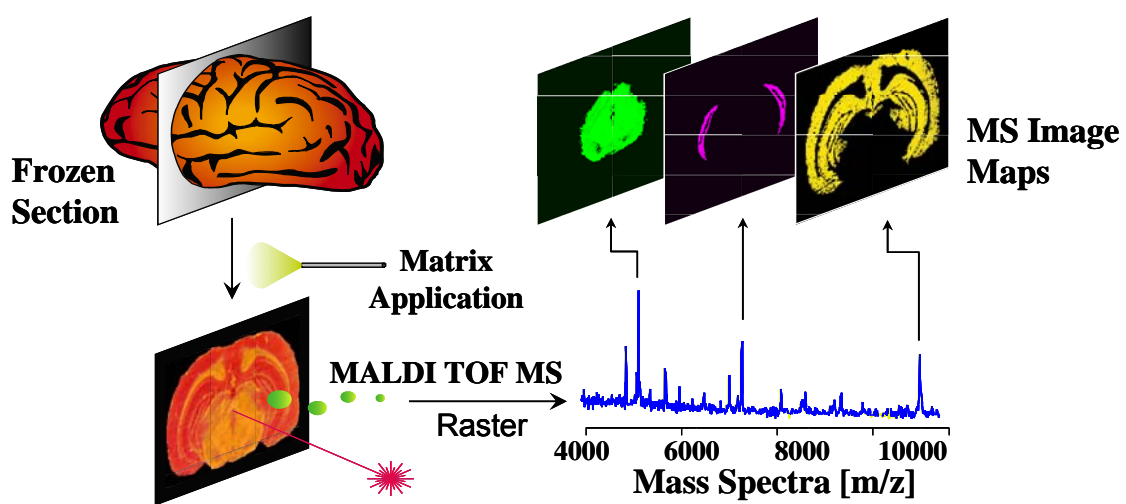


Figure 4. Cartoon representation of the imaging MALDI MS experiment. Adapted from Stoeckli *et al.*^[30]

first report, imaging experiments were successfully demonstrated by the desorption of endogenous peptide and protein compounds directly from tissue sections, as well as, from tissue blots prepared on C-18 coated membranes.^[32] Since then, imaging MALDI MS experiments have been successfully employed to desorb and detect drugs, lipids, peptides, and proteins directly from tissue samples.^[25, 33-43]

Imaging MALDI MS experiments can be performed with minimal preparative steps, with the most notable step being matrix application. The area to be ablated must be uniformly covered in matrix, whether by a continuous coating or a droplet array, to produce high-quality and reproducible images. Practical aspects of tissue sample preparation, as well as, instrument parameters for an Imaging MALDI MS experiment are described in more detail in Chapter II or can be referenced elsewhere.^[39, 44, 45]

Instrumentation for MALDI Mass Spectrometry

Owing to the soft ionization of intact analyte species by MALDI, the ionization technique gained popularity for the analysis of a broad mass range of molecular ions. The capability of the MALDI process to desorb and ionize versatile analyte species requires an equally accommodating mass analyzer. Therefore, MALDI is commonly coupled to time-of-flight (TOF) mass analyzers. TOF mass analyzers are relatively simple and are capable of analyzing ions ranging from a few Dalton (Da) to greater than 200 kDa.

A MALDI-TOF mass spectrometer is composed of two regions: 1) an ion source where ions are produced and accelerated, and 2) a field-free drift tube terminates at the ion detector. The two regions are maintained under vacuum, with pressures in the range of 10^{-7} to 10^{-8} Torr. Following a laser pulse, all desorbed ions are accelerated into the mass analyzer by a homogeneous electric field of known strength, generally ± 20 kV. From basic principles, it is understood that the potential energy of a charged particle in an electric field is related to its charge and to the strength of the electric field:

$$E_p = q \cdot U \quad (1)$$

where E_p is the potential energy, q is the charge of the particle, and U is the electric potential or voltage.

The acceleration caused by U results in ions of the same charge to have equivalent kinetic energies (E_k):

$$E_p = E_k \quad (2)$$

The kinetic energy of a given mass is defined as:

$$E_k = \frac{1}{2} \cdot m \cdot v^2 \quad (3)$$

where m is the mass and v is the velocity.

Based on equation (2), equations (1) and (3) can be combined:

$$q \cdot U = \frac{1}{2} \cdot m \cdot v^2 \quad (4)$$

The velocity of an ion can be determined by measuring the flight time of an ion (t_{TOF}) down a flight tube of known length (d):

$$v = \frac{d}{t_{TOF}} \quad (5)$$

Equation (5) can now be substituted into equation (4):

$$q \cdot U = \frac{m}{2} \cdot \left(\frac{d}{t_{TOF}} \right)^2 \quad (6)$$

and rearranged to solve for time of flight (t_{TOF}):

$$t_{TOF} = d \cdot \sqrt{\frac{m}{2 \cdot q \cdot U}} \quad (7)$$

Delayed extraction is the term used to describe the time-lag that occurs after the laser pulse, but before the accelerating potential is applied. Since mass resolution and accuracy is dependent on the spatial homogeneity and energy distribution of the ions as they are accelerated into the TOF, delayed extraction is used to correct for initial energy differences and spatial heterogeneity that occurs in an expanding MALDI plume. Once the accelerating voltage is applied, the ions furthest from the voltage source will be accelerated more and the ions closest to the voltage source will be accelerated less. When the delay time is properly adjusted, the ions will be spatially focused at the detector. Given that the ion spends some time in the source of fixed length (d_0) under delayed extraction conditions, this time period (t_s) must also be considered for the total flight time, since the time-of-flight measurement is triggered by the laser pulse:

$$t_s = 2 \cdot d_0 \cdot \sqrt{\frac{m}{2 \cdot q \cdot U}} \quad (8)$$

Therefore, the total time-of-flight (T) can be expressed as:

$$T = t_{TOF} + t_s = (d + 2d_0) \cdot \sqrt{\frac{m}{2 \cdot q \cdot U}} \quad (9)$$

Since instrument dimensions and operating potentials are known, these variables can be replaced with a constant, k , in the equation:

$$T = k \cdot \sqrt{\frac{m}{q}} \quad (10)$$

Consequently, equation (10) describes the flight time of an ion to be inversely proportional to its m/z (where the q has been replaced by a z). As a result, lower molecular weight ions will reach the detector in a shorter time than larger molecular weight ions. More detailed descriptions of the MALDI-TOF instrumentation and delayed extraction conditions can be found in several reviews.^[46-48]

Advantages of MALDI Tandem Mass Spectrometry

MALDI-TOF instrumentation has gained popularity for the analysis of complex biological samples for the detection of carbohydrates, lipids, peptides, proteins, and polynucleotides.^[49-51] The broad range of application can be owed to the high sensitivity, “limitless” mass range, and simplicity of spectral interpretation for the MALDI-TOF technique. Typically, complex mixtures of analytes as low as a few femtomoles can be routinely detected and since the MALDI process produces predominately singly charged ions, the peaks can be interpreted without the need for deconvolution. Despite these clear advantages, in the case of small molecule detection, MALDI-TOF MS analyses prove to be

disadvantageous due to the chemical noise from excess matrix molecules. The matrix molecules (see Figure 2) can complicate the low mass region of interest, masking the presence of an analyte by ion suppression effects or isobaric peaks. For this reason, tandem mass spectrometry is often employed for small molecule analyses.

Tandem mass spectrometry, or MS/MS analysis, requires an additional mass analyzer in the instrument design. Mainstream MALDI MS/MS instruments include quadrupole ion traps (QIT), TOF-TOF, and quadrupole-TOF (QqTOF) analyzer configurations. The advantage of a tandem mass spectrometer can be two-fold, selectivity (ultimately providing increased sensitivity) and structural identification. The advantage of selectivity occurs in the first mass analyzer region, where customarily, a narrow mass window of ions centered on an analyte ion of interest is allowed to persist while ions falling outside that mass window are rejected. The ions that remain in the mass spectrometer (i.e. precursor ions) are then subjected to fragmentation by collision induced fragmentation (CID) with neutral gas molecules. The fragment ions (i.e. product ions) are then detected and can be used to relate back to the structure of the precursor ion. Therefore, the product ion pattern affords an added level of confidence by providing structural confirmation of the precursor ion. Consequently, tandem mass spectrometry can resolve a matrix ion that is isobaric to the precursor ion, provided the matrix ion does not share an identical peak in the product spectra.

Currently, the standard instrument for small molecule analysis by MALDI MS/MS is the QqTOF configuration.^[52] Briefly, the QqTOF is similar to a triple

quadrupole with the last quadrupole replaced by a TOF analyzer (described in previous section). A detailed review of triple quadrupoles can be referenced for more information.^[53] A schematic representation of a MALDI-QqTOF instrument can be seen in Figure 5. In the case of the QqTOF mass spectrometer, an additional radio frequency (RF) only quadrupole (Q0) is added to provide collisional cooling and focusing of the ions from the MALDI source. Minimal extraction voltages (± 10 V) are needed to accelerate the ions from the MALDI source into Q0. During an MS/MS analysis, the second quadrupole (Q1) acts as a mass filter allowing ions within mass windows of ± 0.1 -2.5 Da to continue on into the mass spectrometer. The ions are then accelerated (20-200 eV) into the collision cell (Q2), where they undergo CID. After leaving Q2, the product ions are reaccelerated in the orthogonal direction by a pulsed electric field (kHz) into the TOF analyzer for detection. Ultimately, the advantage of a QqTOF over other MALDI MS/MS instruments is the high mass resolution (10,000) and very high mass accuracy (a few ppm).

Direct Tissue Analysis using MALDI MS/MS

MALDI-TOF MS has proven to be a valuable discovery tool for the identification of disease biomarkers from biological samples, including the analysis of proteins directly from tissue sections.^[36, 37, 54-57] The success of direct tissue analysis by MALDI-TOF MS can be attributed to the minimal sample pretreatment steps and the technique's high tolerance for tissue impurities (e.g. salts).^[39]

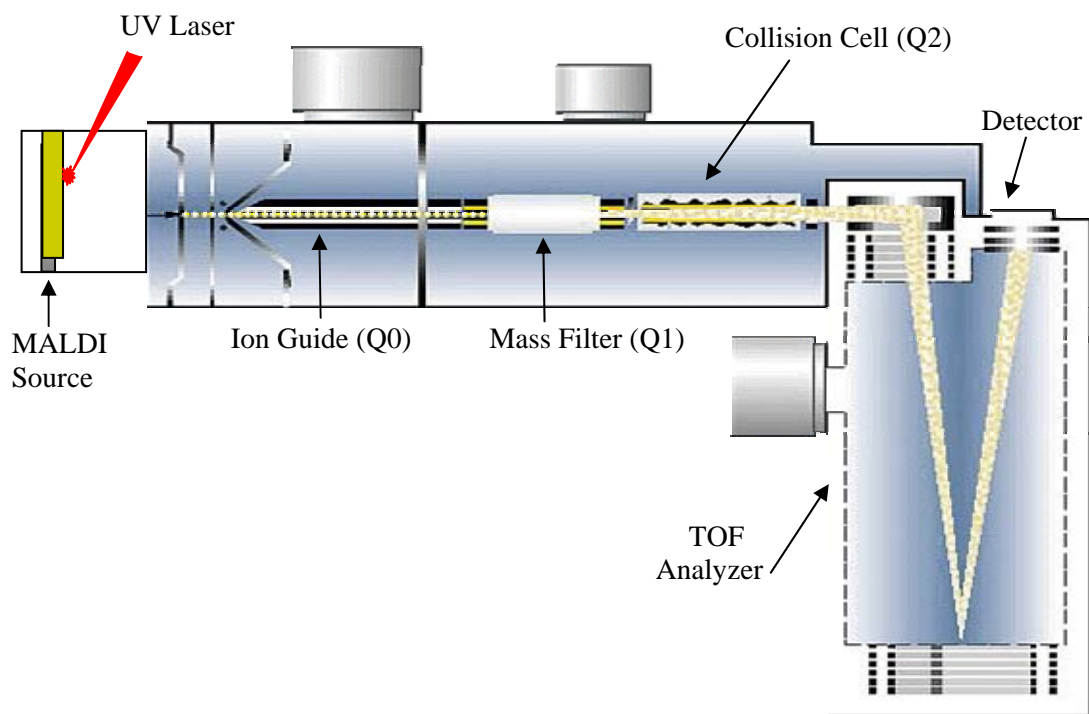


Figure 5. Schematic representation of the MALDI-QqTOF mass spectrometer. Adapted from www.appliedbiosystems.com/Qstar

The analysis of tissues by MALDI-TOF MS was further extended to preserve the spatial location from which spectra are acquired, and is termed imaging MALDI MS.^[30, 32, 58] Published results using imaging MALDI-MS/MS for the analysis of pharmaceutical compounds in tissue are limited. One of the first reports was published by Troendle et al. using a MALDI-QIT-MS to detect the drug paclitaxel in a human ovarian tumor sample.^[40] More recently, drug imaging of dosed tissue sections was reported by Reyzer et al. using a MALDI-QqTOF MS.^[38] The authors initial studies with a MALDI-TOF MS revealed matrix interference (m/z 695.2, $[3SA+Na]^+$) with the protonated SCH 226 374 drug signal (m/z 695.4) and the peaks could not be differentiated. Therefore, the authors employed the MALDI-QqTOF MS in order to overcome some of the limitations from the MALDI-TOF analysis. The imaging tandem mass spectrometry experiment was able to show the unambiguous localization of the major CID fragment from SCH 226 374 across a dosed tumor section. This study shows the value and potential of MALDI MS/MS for detecting drug and metabolite distributions directly from whole-animal sections, thus providing a label-free, molecularly specific imaging technology.

Current Methodologies for Drug Distribution Studies

Within the last quarter-century, important imaging technologies have been innovated for use in the medical field to help make individual patient diagnoses and guide therapeutic decisions.^[59] In the past decade, a broader interest has been seen in recognizing the value of these technologies for use beyond medical

diagnoses. With better animal models of disease, the ability to image an administered drug can help validate potential drug targets, as well as, aid in assessing therapeutic efficacy.^[60] For drug distribution studies in whole-animals, two approaches can be taken: 1) *in vivo* imaging or 2) *ex vivo* imaging. Both approaches require a labeled drug which can be time consuming and costly to synthesize. In addition, the chemical tag may alter the pharmacological properties of the compound, which could affect the bioavailability and localization of the labeled pharmaceutical within an animal. The disadvantage of current drug imaging technologies is that only the label is monitored, preventing the differentiation of a drug from a metabolite that has retained the label. On the other hand, these imaging technologies have the ability to interrogate anatomical, molecular, or physiological parameters of an animal model, but again, give little information as to the molecular identity of many biological end-products that result from administration of a drug compound. Early determinations of tissue distributions and PK/PD profiles of a novel therapeutic compound play a major role in the drug discovery and development process and more sophisticated technologies are needed to overcome the apparent limitations of the currently available imaging modalities.

Nuclear Imaging

In vivo imaging, which includes magnetic resonance imaging (MRI), computed tomography (CT), positron emission tomography (PET), and single photon emission computed tomography (SPECT), is currently being used by

many researchers to facilitate the drug discovery and development process.^[60-62] The noninvasive nature of these nuclear imaging modalities allows for repetitive or continuous measurements of the physiological or pharmacological response to be performed. Recently, these imaging technologies have been used to measure the early PK profile of a variety of new pharmaceutical compounds in small animal models, with the most common techniques being SPECT and PET imaging.^[60, 63, 64] PK studies by these *in vivo* techniques require a radiolabel to be incorporated into the drug structure. The selection of a radiolabel is based on the imaging modality employed.

For example, a gamma- (i.e. SPECT) or positron-emitting (i.e. PET) radiolabel must provide enough radiation to escape the animal, while at the same time, the energy must not be so high that it cannot be collimated or detected efficiently.^[63] A frequently incorporated radiolabel in SPECT imaging of pharmaceuticals is ^{99m}Tc which decays to its normal ground state with a half-life of 6.03 h by emitting an easily detectable gamma ray at 140.5 keV.^[63] Similarly, a PET radiolabel, ¹⁸F, can be used as an efficient label for fluorinated drugs with a half-life of 110 min, emitting two 511 keV photons in opposite directions.^[64] A list of common radiolabels used in PET imaging can be seen in Table 1. PET imaging has the potential to provide quantitative information similar to that of *ex vivo* techniques (see following section) in a variety of tissues at a spatial resolution of 1-6 mm, while SPECT imaging has a lower spatial resolution of 7-18 mm and is less applicable for quantitation.^[64] Overall, these techniques can provide valuable, noninvasive measurements of the three-dimensional (3D)

Table 1. Common radionuclides used for positron emission tomography (PET).
Adapted from Fischman *et al.*^[64]

Radiolabel	Half-life (min)
¹⁵ O	2.0
¹³ N	10.0
¹¹ C	20.4
¹⁸ F	110
⁷⁶ Br	972
¹²⁴ I	6048

distribution of a radiolabeled pharmaceutical *in vivo*.

Whole-body Autoradiography

The *ex vivo* imaging technique, known as whole-body autoradiography (WBA), has become a valuable tool for tissue distribution studies and is a mandatory procedure for drug approval by the Food and Drug Administration (FDA).^[65] Classically, a lead compound is radiolabeled and administered to an animal model, a technique that was first introduced by Ullberg in 1954.^[66] The selection of a radiolabel can depend on the timescale of the study, chemical structure, and known metabolic pathways of the compound. Typically, radiolabels used for drug administration in animals include ^{14}C and ^3H . After administration of the radiolabeled compound, the animal is sacrificed on a time-scale equivalent to the compound's known pharmacokinetics, which is often obtained by high-performance liquid chromatography tandem mass spectrometry (HPLC MS/MS).^[67] Whole-body tissue sections are collected at a thickness of 20-40 μm and WBA images are collected at a spatial resolution of $<50 \mu\text{m}$.^[68] In the case of PK distribution studies, 8-10 week old male rats are commonly used for WBA, where sections are collected in the coronal or sagittal orientation to maximize the visualization of multiple organs of interest.^[69] Much information about the absorption, distribution, and route of clearance of the radiolabeled pharmaceutical can be acquired by WBA with an average turnover time of 5 days (Figure 6). However, the detected signal does not distinguish between the

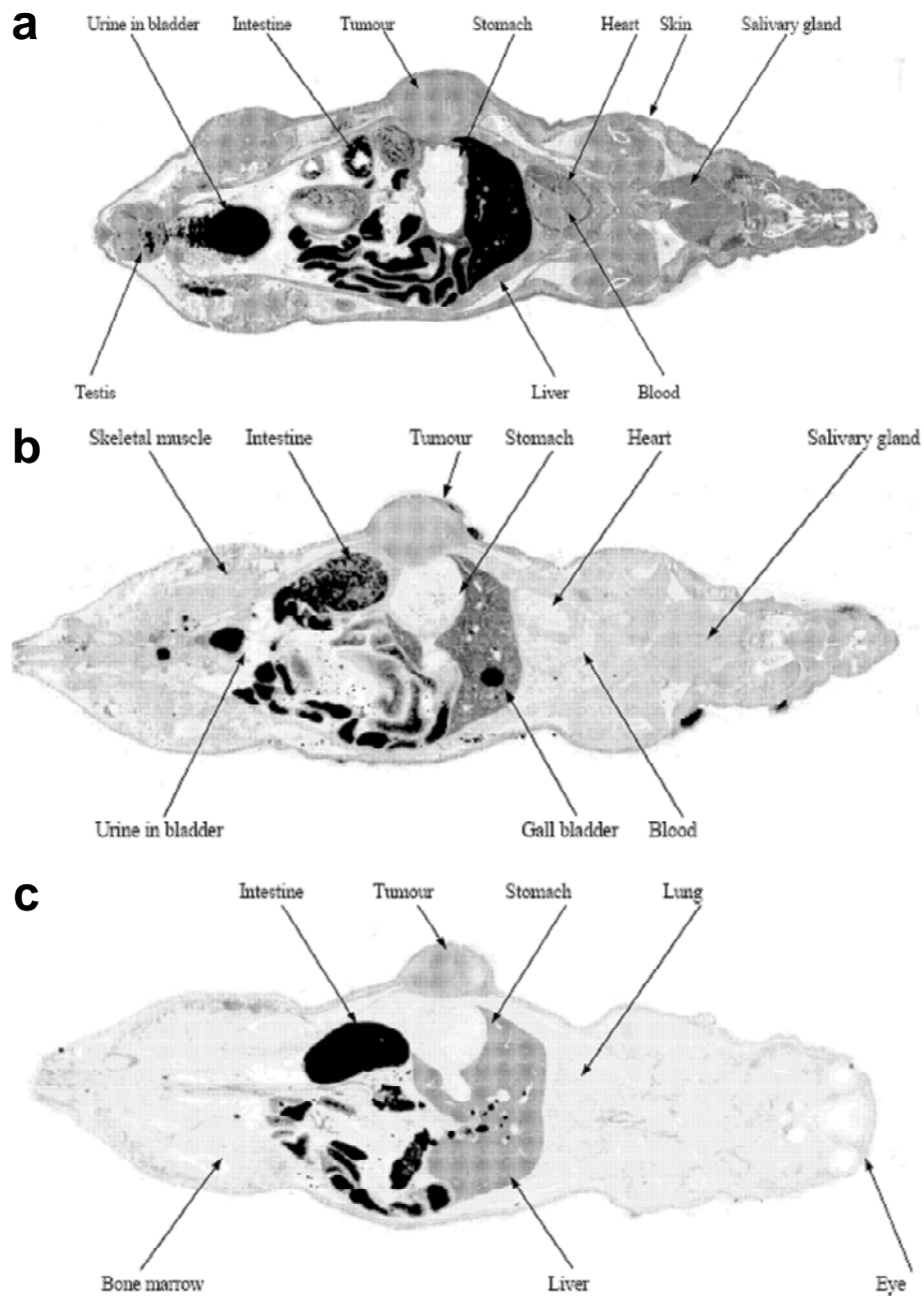


Figure 6. Example of whole-body autoradiography of coronal rat section bearing Hras5 tumor xenografts. a) 0.25 h, b) 1 h, and c) 2 h following administration of a single intravenous dose of ^{14}C -ZD6126. ^[70]

original radio-labeled compounds from metabolites that have retained the radiolabel and represents a significant limitation of WBA.

Summary and Research Objectives

Improvements in the preclinical steps of drug discovery and development are needed to better identify potentially successful drug candidates, while at the same time eliminating inferior drug compounds early in the process. A key component of this process is the ability to gain knowledge about the distribution and delivery of a novel therapeutic compound to a target organ or tissue, since tissue distributions play an essential role in the PK behavior of a drug. Of even greater interest would be the development of a detection system that allows for the correlation between drug tissue distribution and pharmacological or toxicological effects.

This research focuses on the development and application of a new methodology for the analysis of exogenous (drug) and endogenous (protein) compounds in whole-organ and whole-body animal tissue sections by imaging MALDI mass spectrometry (IMS). Data obtained by this novel methodology shall demonstrate the capacity to detect and determine the relative concentrations of drug in tissues and more importantly, at the same time, the distribution of various metabolites. Such information about the individual contributions of a drug and its metabolites is not easily obtainable by currently available imaging techniques such as autoradiography. In addition, detecting protein changes with both spatial and molecular specificity will allow for the correlation of drug tissue distribution

and therapeutic response within the same sample. Identifying specific protein patterns that relate to drug efficacy or toxicity would lead to important PD assessments of novel therapeutic compounds early in the drug discovery and development process.

This work was focused on the following research objectives:

Objective 1: Develop a reliable, reproducible method for the direct tissue analysis of endogenous and exogenous compounds from whole-animal tissue sections by imaging MALDI MS.

Objective 2: Employ the methods developed in Objective 1 to image the individual distributions of exogenous drug and subsequent metabolites in whole-rat sagittal tissue sections. From these images, determine the relative concentrations of the exogenous compound across multiple organs.

Objective 3: Employ methods developed in Objective 1 to evaluate the pharmacodynamic effects of drug administration. Identify early protein markers of drug efficacy.

Development of an MS imaging methodology capable of characterizing individual drug and metabolite distributions, as well as protein changes as a result of drug administration, in whole animal tissues will advance the ever-

growing need for rapid evaluations of PK and PD parameters of lead compounds.
Application of this novel methodology will save the pharmaceutical companies
valuable time and money.

CHAPTER II

PROTOCOL DEVELOPMENT FOR WHOLE-ANIMAL DIRECT TISSUE ANALYSIS

Tissue Preparation Protocols

The direct analysis of pharmaceuticals from dosed tissue sections by imaging MALDI MS/MS has great potential, as was described in Chapter I. Extending the application to whole-animal tissues will provide a label-free, molecularly specific approach to detect the individual distributions of an administered drug and its subsequent metabolites, all of which can be determined from a single imaging experiment. Development of this technology will have an enormous impact on the pharmaceutical workflow by providing early PK/PD assessments of novel therapeutic candidates in small animal models.

This chapter outlines the sample preparation, analysis, and image processing protocols that were developed throughout the context of this research, including practical aspects of animal dosing and sacrifice, tissue sectioning and mounting, matrix application, and general strategies for direct analysis of endogenous and exogenous compounds from whole-animal tissue sections by imaging MALDI MS and MS/MS.

Animal Dosing and Sacrifice

When designing an MALDI MS/MS imaging experiment to determine the disposition of an administered pharmaceutical compound, it is important to select

the proper small animal model. In the early phases of drug discovery and development, therapeutic candidates cannot be administered to humans, and therefore, predictions about the PK/PD properties have to be made from an *in vivo* animal model. The two most common species include rats and mice, which have different metabolic rates and pathways; hence providing vastly different metabolite and distribution information. In general, rats are used for PK/PD studies due to their similarity to human pathways for the adsorption, distribution, metabolism, and elimination (ADME) of an administered pharmaceutical.^[71] In other cases, mice may be preferred, since many more models of disease are available in mice rather than rats. In addition, the imaging MALDI MS/MS analysis may require more time for the larger rat than a mouse, depending on the experimental parameters and should also be considered (to be discussed in ensuing sections). For these reasons, proper thought must be given to the choice of a small animal model.

Once an animal model has been chosen, the amount of drug to administer must be determined. Generally, there are two levels of dosing, 1) physiological or 2) pharmacological. Their differences are subtle, but have important implications for the success of a MALDI MS/MS imaging experiment. Physiological dosing (1) refers to the minimal dose required to elicit a physical change in the animal that returns a process to normal functioning. For example, this can be a hormone replacement therapy that requires very low doses of hormone equivalent to endogenous levels. Pharmacological dosing (2) refers to the amount of drug needed to educe a change in function, typically at a level

where therapeutic or toxicological effects can be monitored (i.e. over-dosing), including the ADME properties of a therapeutic candidate. On the whole, physiological doses are much lower in amount than pharmacological doses and may accumulate in tissues at much lower concentrations. The lower concentration of drug throughout the organs in a whole-body tissue section may be difficult to detect by MALDI MS/MS and should be tested on an individual compound basis. Therefore, it is recommended that for drug distribution studies, pharmacologically relevant doses should be administered to determine PK and ADME profiles (MALDI MS/MS), while physiologically relevant doses should be used to determine the appropriate PD profile of a drug through proteomic analysis (MALDI MS).

The route of drug administration also plays a key role in the detected PK/PD profile studies by IMS. There are many ways to administer a drug and they can be divided into three main categories: 1) topical, 2) enteral, and 3) parenteral. The most common routes of administration for drug distribution studies include the enteral and parenteral routes. The enteral route (2) includes oral dosing by pills or liquid (i.e. per orum or p.o.) where the desired effect is systemic (non-local). For small animals, this often requires forced administration via an oral gavage, which is an apparatus, much like a feeding tube, that is guided down the throat of an animal to deliver a precise liquid dose of drug directly into the stomach. The parenteral route (3) includes intravenous (i.v.) or subcutaneous injections where the desired effect is also systemic, but instead, the drug is administered by routes other than the digestive tract. Depending on

the route of administration, the same drug can produce different results. For example, some drugs are not significantly absorbed into the bloodstream from the gastrointestinal tract and their ADME properties will vary greatly after an enteral administration rather than a parenteral administration. Enteral routes are generally the most preferred for the treatment of chronic disease in humans, because of the ease of administration. However, some drugs can not be used enterally because their absorption in the digestive tract is low or unpredictable, so parenteral administration is generally used to increase the bioavailability of the drug. Since small animal studies are used to predict a human response, the route of drug administration should be carefully chosen to match the ultimate route of administration to be used in humans.

After successful administration of the pharmaceutical compound, the animal must be sacrificed for analysis by IMS. The time from which an animal was dosed to when it is sacrificed will depend on the parameters of the experiment. Generally, the time-points for sacrifice are based on pharmacokinetic parameters of the drug determined from earlier *in vitro* studies. In any case, the animal must be properly exsanguinated to avoid ion suppression effects in the MALDI ionization process^[39], as well as, to avoid artificially increased detection of drug in highly vascularized tissues and organs. In the case of whole-body tissue sections, cardiac puncture is the preferred method of exsanguination, since the integrity of the animal carcass will be preserved. Cardiac puncture is performed by anesthetizing the animal, usually with isoflurane, and puncturing the heart with a heparin needle and drawing the blood

into the syringe, all while the heart is still beating. The gauge of the needle is usually between 18 to 24, and no longer than one inch. Successful exsanguination will result in approximately 1 cc of blood for mice and 3 cc for rats. The removal of all the blood from the animal is what ultimately causes death.

Immediately after the animal has been sacrificed, the carcass must be frozen to minimize any delocalization or enzymatic degradation of the analytes.^[39] Care must be taken during the freezing process, to maintain a symmetrical form of the carcass. This can be accomplished by the use of a u-shaped metal frame that runs the length of the carcass but is slightly narrower than the width of the carcass. The carcass is placed on its back in the metal frame so the spine is straight and its paws pointed upward (Figure 7). The metal frame is then placed in a mixture of hexane and dry ice (-60 °C) to produce a rapid freeze, but not too harsh where “shock” such as cracking of the tissue can occur, as is often seen with the flash freezing of tissues in liquid nitrogen. The metal frame holding the carcass is submerged for approximately 5 min for mice and 10 min for rats. The frozen carcass is then rinsed with cold distilled water to remove excess hexane, patted dry with paper towels, and stored at -80 °C until the embedding step.

Carcass Embedding

The orientation of the carcass during the embedding step is an important consideration. Depending on the parameters of the experiment, the carcass can be positioned on the metal sample stage to collect coronal (back to stomach), axial (nose to tail), or sagittal (left flank to right flank) whole-body sections (Figure

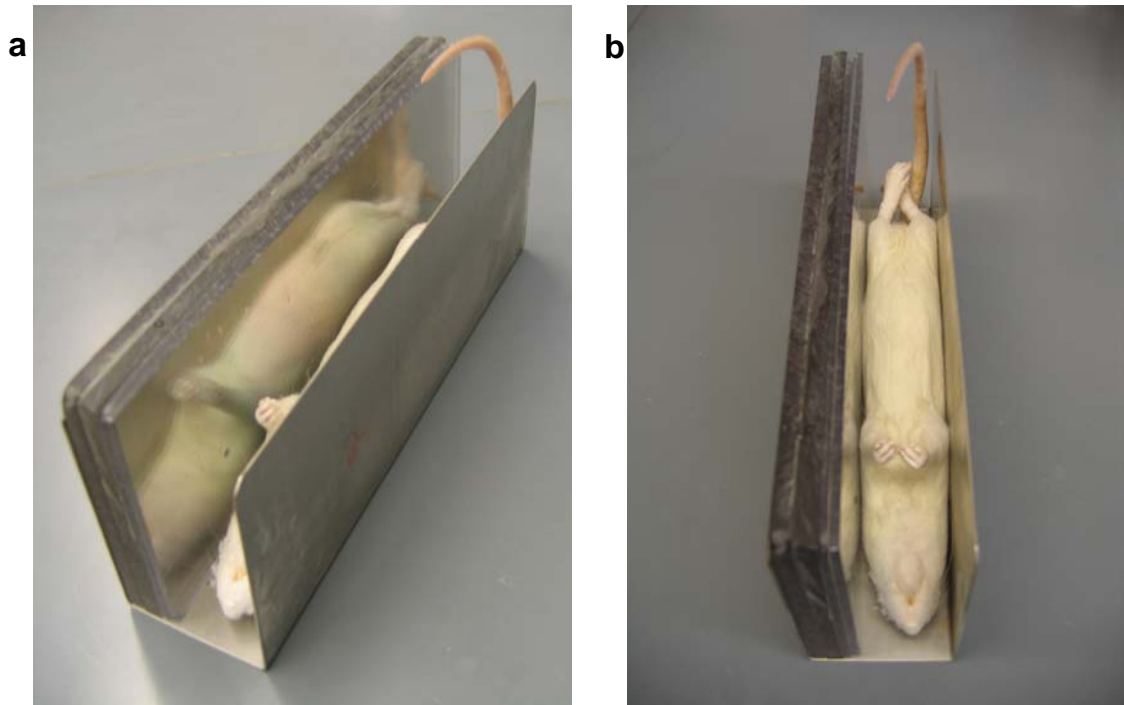


Figure 7. Images of metal frame used to maintain proper carcass form during freezing process in hexane and dry ice. a) u-shaped metal frame, b) bird's eye view of animal position.

8). For drug distribution studies, the animal is usually positioned for sagittal sections, since this orientation maximizes the number of organs represented in a single whole-body slice.

When the orientation of the carcass has been decided, it must be set in embedding media to preserve the integrity of the tissue during the cutting process. In WBA studies, it is customary to embed the carcass in carboxymethylcellulose or CMC; however, for MALDI MS/MS studies, CMC is not practical since it can smear across the tissue during the sectioning process and cause significant suppression of the analyte signal (Figure 9). It was determined that the carcass could be embedded in distilled water and still provide the necessary support during the sectioning process.

For appropriate embedding, a metal sample stage is fitted with a frame to help form the sample block (i.e. embedded carcass). The two pieces are placed in a -80 °C freezer for 30 min. While still in the freezer, a wax platform is placed on the sample stage to elevate the carcass in order to provide a margin from the metal stage for the blade of the cryomacrocut. Next, the carcass is positioned in the proper orientation on the wax. A small amount of distilled water is added to quickly freeze the wax platform and carcass in place (approximately 5 min). After an adequate anchor has been achieved, the frame is filled with distilled water until the carcass is completely covered. To create a frozen sample block, the whole assembly is allowed to freeze at -80 °C for a minimum of 4 hours.

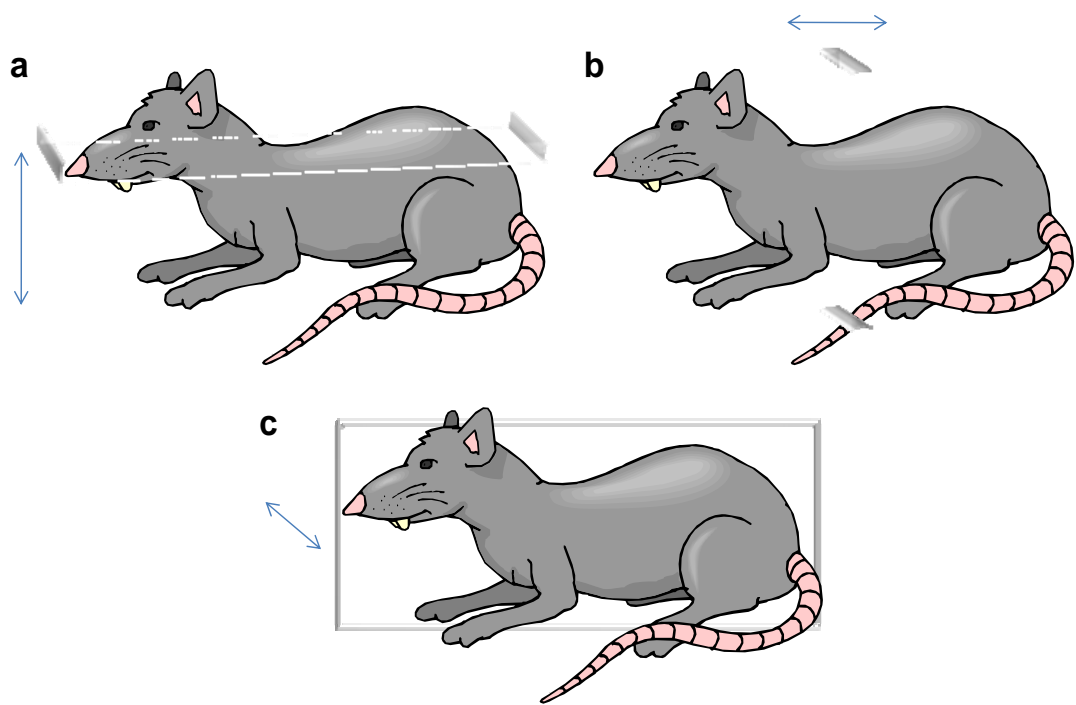


Figure 8. Diagram of three slicing orientations a) coronal, b) axial, and c) sagittal. Arrows indicate z direction of sectioning.

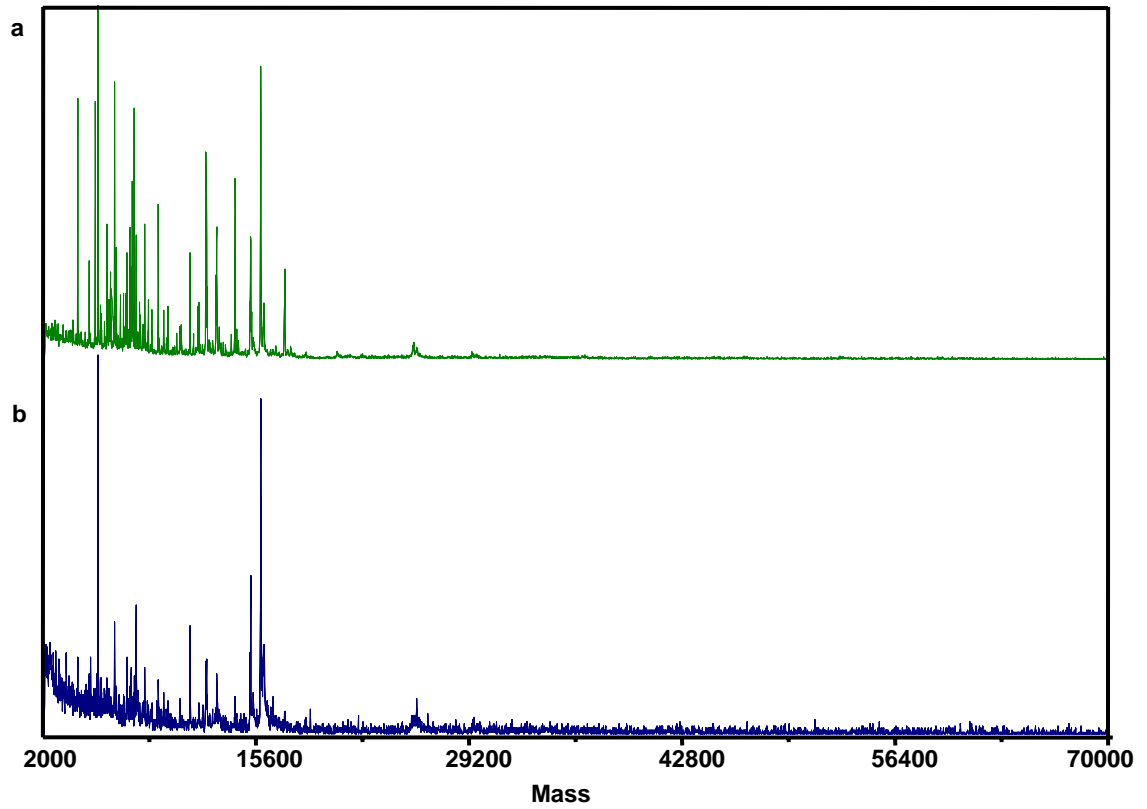


Figure 9. Use of carboxymethylcellulose (CMC) embedding media suppresses MALDI MS ion signal from tissue. a) protein spectra from control tissue and b) protein spectra from CMC embedded tissue

Tissue Sectioning and Mounting

Sectioning takes place at -20 °C in a whole-body cryostat, known as a cryomacrocut. However, before whole-body tissue sectioning can be performed, the frame must be removed and the sample block must be equilibrated at -20 °C for 1 h to avoid cracking of the ice. Once equilibrated, the sample block is secured onto a translational sledge that moves the sample block underneath a stainless-steel blade, cutting from left to right. The blade assembly is motorized and precisely advances the blade into sample block at a designated thickness.

The process of collecting a whole-body tissue section can be tedious, as there are many variables to consider. At a desired level in the carcass, a piece of acetate film tape is placed onto the sample blockface and any air-pockets smoothed out. The tape acts as a support to maintain a flat tissue section, otherwise the tissue would curl as it came off the blade. An acrylic block is used by the right hand to gently apply pressure onto the sample block just before it passes under the blade, in order to ensure the tissue adheres to the tape. As the tissue comes off the blade, the left hand guides the tape at ~45° angle away from the blade to prevent the tape from getting caught and torn. Outside the cryomacrocut, the movement and speed of the sledge is controlled by the amount of pressure applied to a lever that is driven by the operator's leg. Altogether, these elements must be performed simultaneously to properly obtain a whole-body tissue section.

The sectioning process and tissue thickness depends on the analysis to be performed. For drug distribution imaging by MALDI MS/MS, whole-body tissue

sections are collected directly onto acetate film tape at 20 μm thickness. The tissue sections are allowed to freeze dry overnight inside the cryomacrocut chamber prior to analysis. For proteomic analysis by MALDI-TOF MS, whole-body sections cannot be collected directly onto the acetate film tape. Tissue sections that are collected and analyzed directly on acetate film tape are not electrically conductive, and therefore accumulate charge on the tape surface during the acceleration of the ions into the TOF analyzer, as described in Chapter I. In general, the charging effect produces poor quality spectra and, when the build up of charge is large, analyte signal is lost completely. To compensate for the charging effect, the sectioning process is modified to include a piece of rice paper between the sample blockface and acetate film tape. Collecting the tissue onto the non-sticky rice paper provides a medium from which the tissue can be transferred onto a conductive substrate and, until then, the sections are stored at $-20\text{ }^{\circ}\text{C}$. The sectioning thickness of the tissue is now dependent on the adequate tissue transfer off the rice paper and onto the MALDI target plate, as well as, the production of high-quality spectra. The optimal thickness was determined to be 20-30 μm (Figure 10).

The whole-body tissue sections must be prepared in a manner that accommodates the sample introduction system of the MALDI mass spectrometer. This process is different for the exogenous small molecule analysis than the endogenous proteomic analysis; however, both require the use of MALDI target plates. Each MALDI target plate measures 4 x 4 cm and, accordingly, a sagittal mouse section typically requires two plates, while a sagittal rat section requires

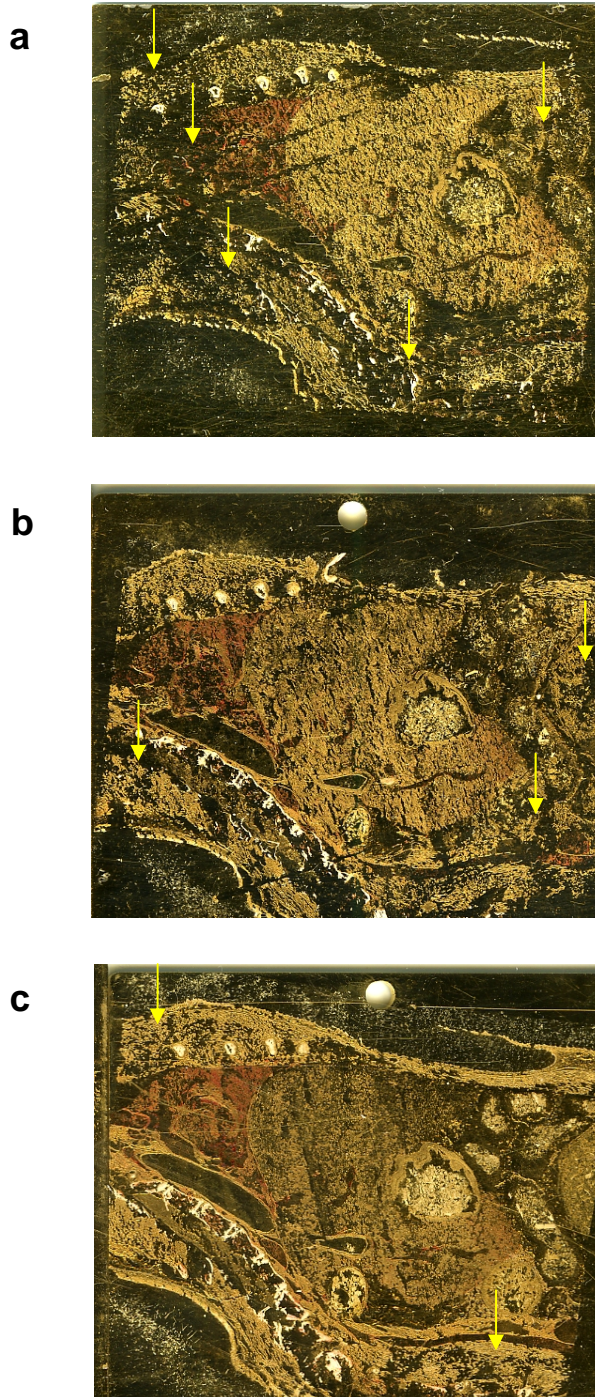
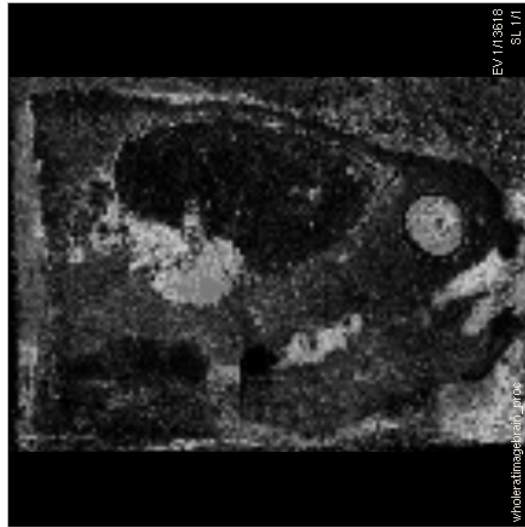


Figure 10. Rice paper transfer of whole-body tissue sections at various thicknesses. a) 10 μm , b) 20 μm , and c) 30 μm . Arrows indicate areas of poor tissue transfer onto MALDI target plate.

four. For small molecule analysis on the MALDI-QqTOF-MS, the tissue mounting procedure is relatively simple and straightforward. The freeze-dried tape section is mounted (tissue side up) directly onto consecutive plates using double-sided conductive tape and the excess acetate film tape is trimmed. The rice paper sections are transferred via thaw-mounting and require the tissue to make contact with a pre-chilled plate. The tissue is pulled off the rice paper and onto the plate by placing a warm hand on the opposite side of the plate. This can be performed for a single sagittal section simultaneously on multiple plates. After approximately 10 s of warming, the rice paper is pulled away from the plate, leaving the tissue behind.

By and large, the rice paper transfer technique has its limitations of poor tissue transfer and inadequate reproducibility and should only be performed when absolutely necessary, such as for proteomic analyses on a MALDI-TOF-MS due to charging effects when tissue is left on tape (Figure 11). Prior to matrix deposition, four fiducials are drawn on each plate (discussed in image reconstruction section) and a digital scan is acquired at 1200 dpi. The plates are then separated using a razor blade along the seams between each plate, since only one plate can be introduced into the mass spectrometer at a time.

a



b

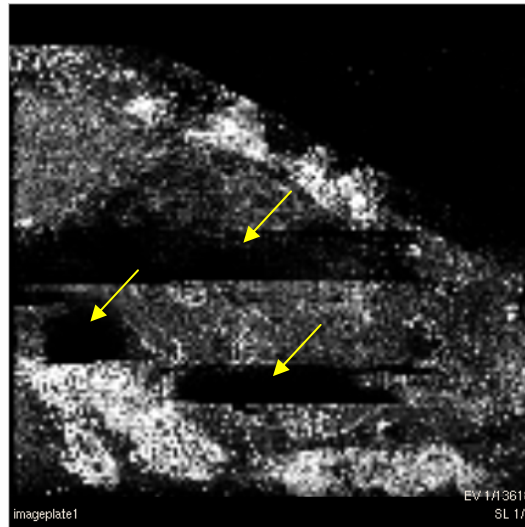


Figure 11. Total ion current images of rat head section analyzed by MALDI-TOF MS. a) rice paper transfer and b) tissue on tape. Arrows indicate areas of charging (i.e. loss of ion signal).

Matrix Deposition

General Considerations

Once the tissue preparation protocols are complete, the next step towards analysis by IMS requires matrix solution to be deposited onto the tissue surface. For the analysis of whole-body tissue sections, the selection of matrix conditions and optimizing application parameters are extremely vital to obtaining high-quality mass spectra, since many organs with varying surface properties are present in a single sample. The selection of a matrix/solvent combination can greatly influence the effective extraction, co-crystallization, and ionization of analytes directly from a tissue section, and must be considered for each analyte species. In addition, the method of matrix application must maintain the spatial integrity of the analytes within a tissue sample at a desired image resolution, while providing homogeneous coverage so as not to negatively affect the accuracy of the MS analysis. This section provides general guidelines for the selection and application of matrix conditions for the successful analysis of endogenous and exogenous compounds directly from whole-body tissue sections by IMS.

Matrix/Solvent Selection

The choice of matrix compound plays an essential role in the MALDI ionization process. The three most commonly used matrix compounds are SA, CHCA, and DHB. Each compound has a preferred mass range for application.

For example, SA is routinely used in the analysis of proteins and high-molecular weight analytes, while CHCA is more commonly used for the analysis of peptides and low molecular weight species. The choice of matrix concentration can also affect the eventual crystal coverage and quality of the mass spectra acquired directly from a tissue section. It is known that higher matrix concentrations result in higher quality mass spectra by providing increased ion yields and signal resolution.^[39] And, lastly, the choice of a solvent can influence the effective extraction of the analyte out of the tissue, as well as, proper crystal formation. Thus, appropriate solvent conditions may vary depending on the chemical properties of the analyte, as well as, the chemical properties of the tissue from which the analyte will be analyzed.

In the case of endogenous protein analysis directly from tissue, SA matrix at 25 mg/mL in 50:50 acetonitrile:0.2% trifluoroacetic acid (TFA) in water yields the best combination of crystal coverage and signal quality for most tissue types tested.^[39] Be as it may, in the case of whole-body tissue sections, many tissues with varying surface properties are present and the matrix must simultaneously crystallize over all areas of the sample in a homogeneous manner to obtain high-quality, reproducible spectra. SA matrix alone does not adequately achieve this effective coverage from a single application event, since pockets of uncoated or amorphous crystal layers can be observed on various tissues across the whole-body section. Therefore, matrix selection was optimized by testing a variety of matrix combinations to effectively yield the necessary homogeneous crystal coverage on all tissue types. It was determined that a homogenous crystal layer

could be achieved using a combination of SA (20 mg/mL) and DHB (5 mg/mL) in 50:50 acetonitrile: 0.2% TFA in water while still providing high quality protein mass spectra.

In the case of exogenous small molecule analysis, the selection of a matrix/solvent combination is of even greater importance, since ionization yields are more dramatically affected.^[72] This is due to the chemical formula and the structure of a drug compound, which are the two important factors that determine its chemical properties. At this time, a universal matrix/solvent combination is not available, and therefore combinations should be tested and selected for sufficient co-crystallization of the analyte of interest, effective desorption/ionization in the MALDI process, and any possible interfering isobaric matrix peaks. Streamlining the selection of a proper matrix/solvent combination for the analysis of pharmaceutical compounds directly from dosed tissue will be discussed in more detail in Chapter III. As a rule for whole-body analysis, the matrix/solvent combination that is optimal for *most* tissues and organs should be selected, since many different tissue types are present in an entire animal section. Also, an internal standard that is a structural analog to the analyte compound of interest should be incorporated into the matrix/solvent combination (~2 μ M spike) for normalization reasons.

Matrix Application

When a proper matrix/solvent combination has been determined for the analysis at hand, the matrix must then be deposited onto the tissue surface.

Generally, there are two approaches for matrix application, 1) spotting or 2) spray-coating, and either approach can be performed manually or robotically. The spotting technique (1) involves the dispensing of discrete droplets of matrix onto a tissue section. For imaging studies, this is routinely performed by a piezo ink-jet or nozzle-less acoustic-wave robotic spotting system. Both robotic systems allow for the precise ejection of picoliter volume droplets of matrix at high resolutions ($\sim 150\text{-}300\ \mu\text{m}$). This process requires several iterations of droplet ejection (7-15 passes), which can be very time consuming and, as a result, usually reserved for small tissue samples. For the global analysis of an analyte species, such as the proteome, spotted tissue samples generally produce highly-reproducible, signal-rich mass spectra.

The spray-coating technique (2) involves covering the entire sample with a homogeneous layer of matrix crystals. This can be achieved by manually (glass reagent nebulizer) or robotically (piezo spray-head) by nebulizing a solution of matrix to create a mist of droplets that land on the tissue surface and dry independently. Again, several iterations of spray passes (~ 30) are required to adequately produce an even crystal layer, with a 1-2 min ambient drying time between each pass. Crystal coverage is evaluated by visual inspection using a microscope. The goal of a spray-coating approach is to maximize analyte extraction from the tissue, while minimizing analyte delocalization. Therefore, care must be taken to sufficiently wet the tissue with matrix solution, but not to saturate the tissue to cause the movement of analytes across the tissue surface. Highly reproducible spray-coated spectra can be acquired in global analyses, but

by comparison to spotted spectra, are generally of lower-quality since fewer peaks are observed in the mass spectra (Figure 12).

An additional factor to consider, when deciding on a matrix application approach, is the spatial resolution of the imaging MALDI MS analysis. The resolution of a spotted tissue will be limited by the matrix spot itself. Depending on the tissue properties, solvent conditions, and the number of ejection passes, automatic spots can be reproducibly produced as small as 140 μm in diameter. The resolution of a spray-coated tissue is limited by the laser diameter of the MALDI source. Most commercial MALDI MS systems have lasers that can be reliably focused down to a 50 μm diameter, before any significant analyte sensitivity is lost.

Also, the average crystal size produced by spray-coating can vary based on the matrix/solvent conditions, but are generally around 20-35 μm in size. Consequently, the spray-coating approach allows for images to be acquired at a much higher spatial resolution than would be possible by spotting. A recent publication was reported where the laser diameter limitation was by-passed using a technique known as “over-sampling.”^[73] This technique steps the laser at dimensions smaller than the diameter of the beam, but requires that the matrix at each pixel be completely ablated, since the laser ablation areas are overlapped. In this approach, the image resolution is no longer limited by the laser, but by the crystal size instead.

In the case of whole-body tissue sections, the spray-coating approach is preferred since a larger sample area can be adequately coated with matrix in

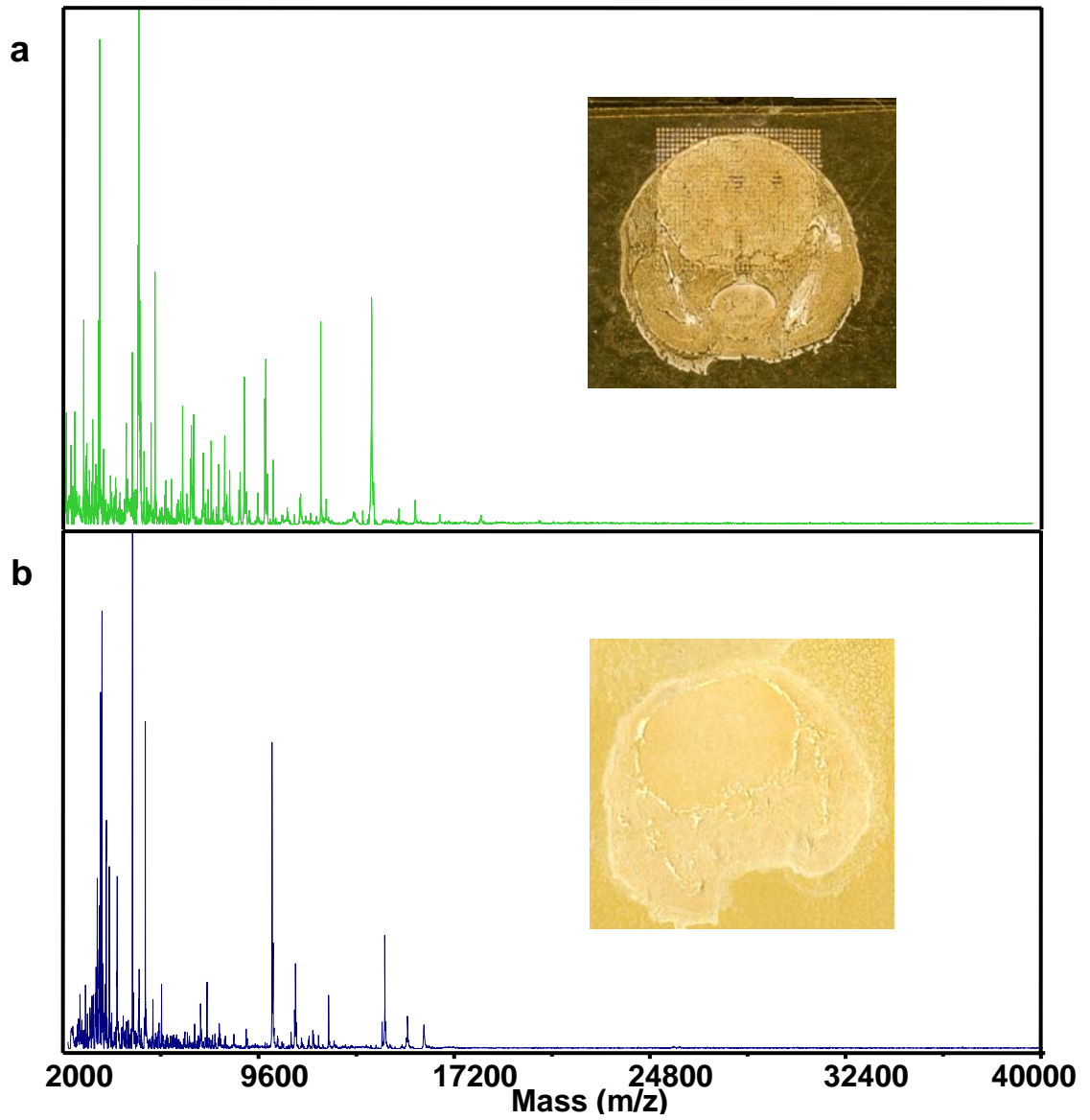


Figure 12. Comparison of protein spectra acquired from whole-mouse head sections using two different matrix application techniques. a) robotically-spotted brain and b) spray-coated brain.

much less time (~1 h/plate) than it would take to robotically spot the sample (> 8 h/plate). Time is an important consideration for whole-body tissue analysis, since one sagittal section can span multiple plates, all of which need to be analyzed in a timely manner to maximize reproducibility. In addition, the spray-coating approach can produce high-quality spectra for the analysis of exogenous small molecule analytes (i.e. pharmaceutical compound) since the matrix/solvent selection and application are specifically optimized for that analyte alone.

Whole-body Drug Analysis by MALDI MS/MS

This research is focused on developing a reliable method to image endogenous and exogenous compounds in whole-animal tissue section by MALDI MS. Previous work has shown that imaging MALDI MS is a sensitive sampling technique that can detect over 500 individual protein signals from a single tissue section, and that these signals collectively represent a snapshot of the proteome.^[32, 34] Comparing the protein signal patterns between large sets of samples can help identify key proteins directly or indirectly involved in disease progression, prognosis, and drug efficacy or toxicity.^[36, 37, 55-57, 74, 75] It has also been shown that MALDI MS/MS can be used to monitor the spatial localization of drug within a dosed tissue section.^[33, 38] A major advantage of drug imaging by MALDI MS/MS is molecular specificity. In other words, MALDI MS/MS is capable of differentiating an intact drug from metabolites that differ in mass. As a result, imaging whole-body tissue sections by MALDI MS/MS can be useful for the label-free visualization of drug and metabolite distribution. This technology will

allow for earlier analysis of therapeutic candidates in the drug discovery process since no additional synthesis of a chemically or radio-labeled drug is required.

The optimization protocols necessary for developing a whole-animal proteome analysis occur in the sample preparation and the image reconstruction stages. The image acquisition and data processing protocols have remained the same as previously established imaging MALDI MS methods, detail about which can be referenced elsewhere.^[34, 76] Therefore, this section will focus on the optimization of acquisition parameters necessary for the analysis of exogenous compounds from whole-body tissue sections by MALDI MS/MS.

General Considerations

The analysis of small molecules by MALDI-TOF MS/MS has limitations, most notably spectral noise from the matrix, matrix clusters, and fragment ions that occur in the same molecular weight range of most drug compounds (< 1000 Da).^[77] Moreover, the matrix is present in excess (5000:1) over the analyte of interest, overwhelming the low mass region of the spectrum. The problem becomes even more complex when directly analyzing tissue because there is a relatively high concentration of salt (Na^+ and K^+) on the tissue surface. The salt acts as an anchor around which multiple matrix molecules can cluster. For protein analysis, the tissue can be washed with ethanol rinses to remove excess salts; however, this is not recommended for exogenous small molecule analysis, since the drug can leach out of the tissue and into the wash solution. Another interference can be contributed by endogenous small molecule species that can

be co-crystallized and desorbed along with the analyte of interest. Therefore, it is important when optimizing the MALDI MS/MS instrument parameters that these interferences be considered, especially when selecting a window for mass filtering of the precursor ion. It is also recommended that appropriate controls are performed to ensure interfering signals do not share an isobaric signal that could be misinterpreted as drug signal.

It is imperative to take into account the time needed for the analysis of multiple plates from a single whole-body tissue section. The image resolution, signal accumulation time, and the number of signal transitions monitored all contribute to the total analysis time, and then must be multiplied by the number of plates in queue for analysis. For example, two transitions at 4 s accumulation time each that are monitored across a whole-rat sagittal section (4 plates) at 400 x 400 μm resolution will take a total of 96 h or 4 days to acquire. Therefore, experimental time constraints should be considered when optimizing the instrument parameters. Lastly, it is vital to maintain the instrument at an equal performance level for all plate analyses. The monitoring of an internal standard transition is recommended for each plate analysis. This will allow for evaluation of the instrument performance and normalization of artificial spectral variations that may occur during the analysis. Collectively, all of these considerations will minimize the plate-to-plate variations that can occur during a whole-animal imaging experiment.

Instrument Parameter Optimization

Optimizing the spectrum quality of a dosed tissue requires tuning the instrument settings to maximize the drug signal that can be detected. Ideally, the instrument parameters should be optimized for each analyte (drug and metabolites) of interest in order to achieve the best signal sensitivity. The key parameters include the mass filter window, collision energy, CID pressure, and TOF mass range. The MS/MS parameters are generally optimized using drug and metabolite standards. To maximize sensitivity, wide mass windows centered on the analyte of interest are allowed to pass into the collision chamber (± 2.5 Da). Typical collision energies are between 25 to 40 eV with a CID pressure of 0.03-0.04 mTorr. Argon or air can be used as the CID gas. A small mass range (~100 Da window) centered on the major CID fragment peak is selected in order to maximize the pulsing rate of the orthogonal TOF. In addition, the number of seconds accumulated per transition is optimized for sensitivity and total analysis time. Signal accumulation time is generally 4 s/transition.

Data Processing

Two major factors are taken into account when processing data from a whole-body analysis: 1) ionization efficiency, and 2) extraction efficiency of the analytes. Ionization efficiency (1) includes considerations for the specific ionization yield of an analyte in the MALDI process. For example, tissue specific ion suppression can occur, as well as, disparity in the amounts or properties of matrix crystals across different tissues can produce artificial variations in the

detectable analyte signal. To correct for these erroneous analyte signals, an internal standard (IS) is incorporated into the matrix application step. The IS is a structural analog of the drug and metabolites of interest and is added within the concentration range of analyte signals (typically 1-4 μM). Since the IS concentration should be equal across the whole-body section, the detected IS signal can be used to normalize any tissue specific ion suppression or uneven matrix coating effects that may occur in the imaging experiment (Figure 13). Signal suppression in the MALDI process is compound specific, as well as, tissue specific and should be tested for each analyte. If the drug and metabolite signals behave similarly, then a single IS can be employed. Figure 14 demonstrates the signal suppression that can occur for a drug, olanzapine (OLZ), and its metabolites, N-desmethyl- and 2-hydroxymethyl olanzapine, across brain, liver, and kidney tissues. In this case, 2 pmol of each compound standard was deposited onto the surface of the tissue using an ink-jet printer and allowed to dry. At the same coordinates, a matrix solution containing an IS spike was deposited. Analysis of the spots by MALDI MS/MS revealed signal variations for each of the compounds; however, normalizing against the IS signal corrected for the ionization yields within each tissue type. Variation in total ionization yields of compounds from different tissue types is an issue that cannot be corrected by the addition of an IS alone.

Extraction efficiency (2) considers the affinity of a compound for a tissue type, as well as, the effective extraction of that compound out of the tissue by the matrix solvent. Since many tissues are coated with matrix simultaneously, a

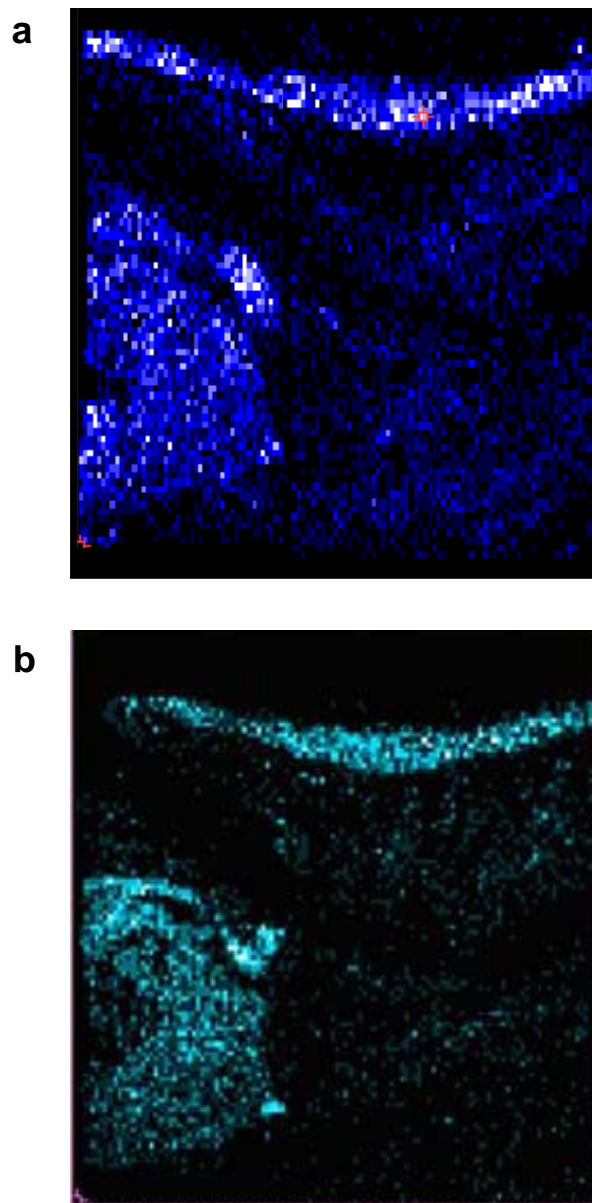


Figure 13. Internal standard normalizes MALDI MS/MS ion image. a) raw signal and b) normalized signal.

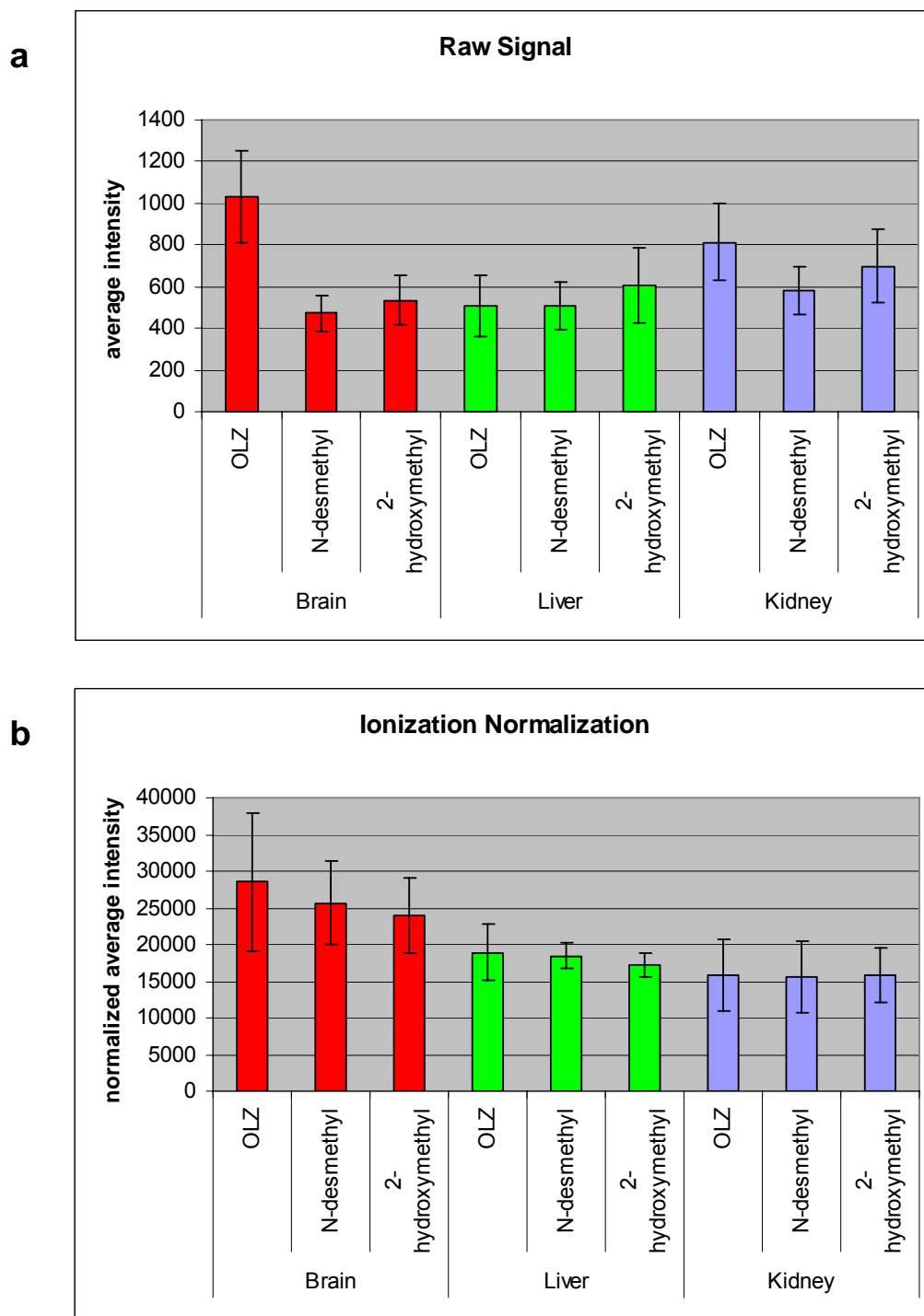


Figure 14. Histogram of tissue specific ion suppression effects of 2 pmol compound on tissue. a) raw signal and b) internal standard normalized signal.

single solvent system must be used and may not be optimal for all tissue types present in a whole-body section. For this reason, only a fraction of the analyte may be extracted out of a tissue during the matrix application step, and the subsequent image would only indicate a low level of analyte to be present in that tissue. If quantitative information is to be extracted from the MALDI MS/MS images, then signal intensity alone could misrepresent the actual concentration of drug present in the tissue and a normalization factor should be considered before interpreting the image data. For example, Figure 15 demonstrates the extraction efficiencies of OLZ and its metabolites through brain, liver, and kidney tissue sections (detailed protocol explained in Chapter III). The concentration curves show a linear response for each compound; however, their extraction efficiencies across each tissue are different, with the exception of the N-desmethyl olanzapine metabolite. This approach allowed for extraction normalization factors to be determined, which were then applied to the image signals to calculate the relative quantities of drug across a whole-body tissue section (Chapter IV). A similar approach can be taken to determine the extraction efficiencies of any pharmaceutical compound of interest and application of the extraction normalization factors will afford quantitative information to be concluded from the MALDI MS/MS imaging results.

Whole-Body Image Reconstruction

A whole-body analysis produces a very large dataset that must be managed effectively to extract any useful information. Imaging software provided

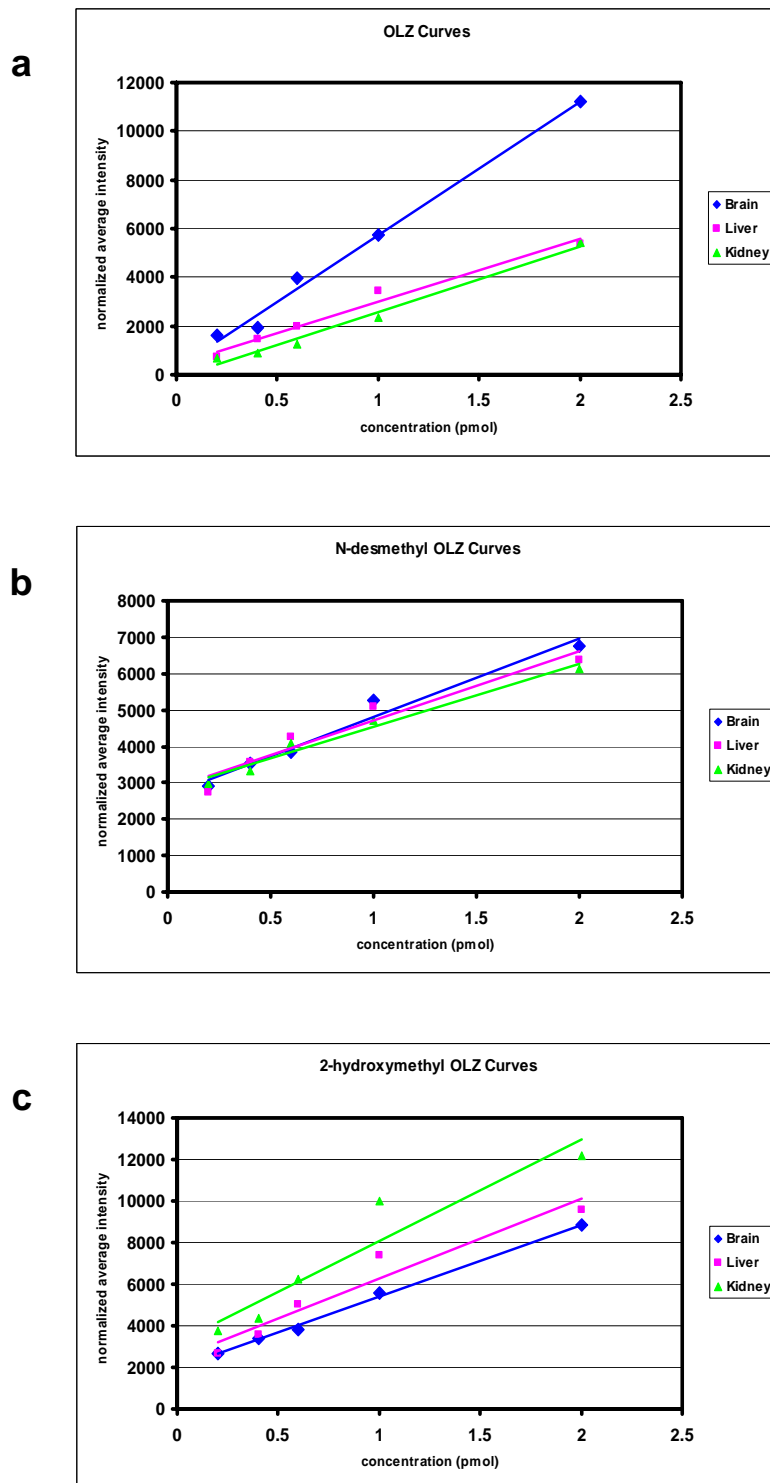


Figure 15. Extraction efficiencies of drug compounds through brain, liver, and kidney tissues. a) olanzapine standard curves, b) N-desmethyl metabolite standard curves, and c) 2-hydroxymethyl metabolite standard curves.

by the instrument manufacturer can display the imaging results adequately; however, in the case of whole-body analysis, results span multiple plates and must be combined. For this purpose, custom software was developed to assemble the individual images for reconstruction of a whole-body image (Figure 16).

During the tissue mounting step, four fiducials were placed in the corner of each MALDI plate of the sample. An optical image (1200 dpi jpeg) of the intact whole-body section was acquired and then the plates were separated for individual analysis. Before each image acquisition, the motor coordinates of the four fiducials are recorded. After data acquisition of all plates is complete, the MALDI MS/MS images are reconstructed using the manufacturer's software. In this software, the IS signal (S_{IS}) can be selected for normalization of the analyte signal (S_a):

$$S_{normalized} = \frac{S_a}{S_{IS} + 1} \cdot 100$$

Since the same concentration of IS was used for each matrix application, and the same volume of matrix was applied to each plate, the intensity threshold is set to the same value for each imaging experiment. The resulting MALDI MS/MS image is saved as a jpeg file and this process is repeated for each plate. Using the custom software, each of the MALDI MS/MS jpegs are loaded into the program along with the motor coordinates from the instrument. In addition, the jpeg pixel coordinates for each of the fiducials from the optical image of the intact whole-body section is loaded. The custom software performs a calculation to

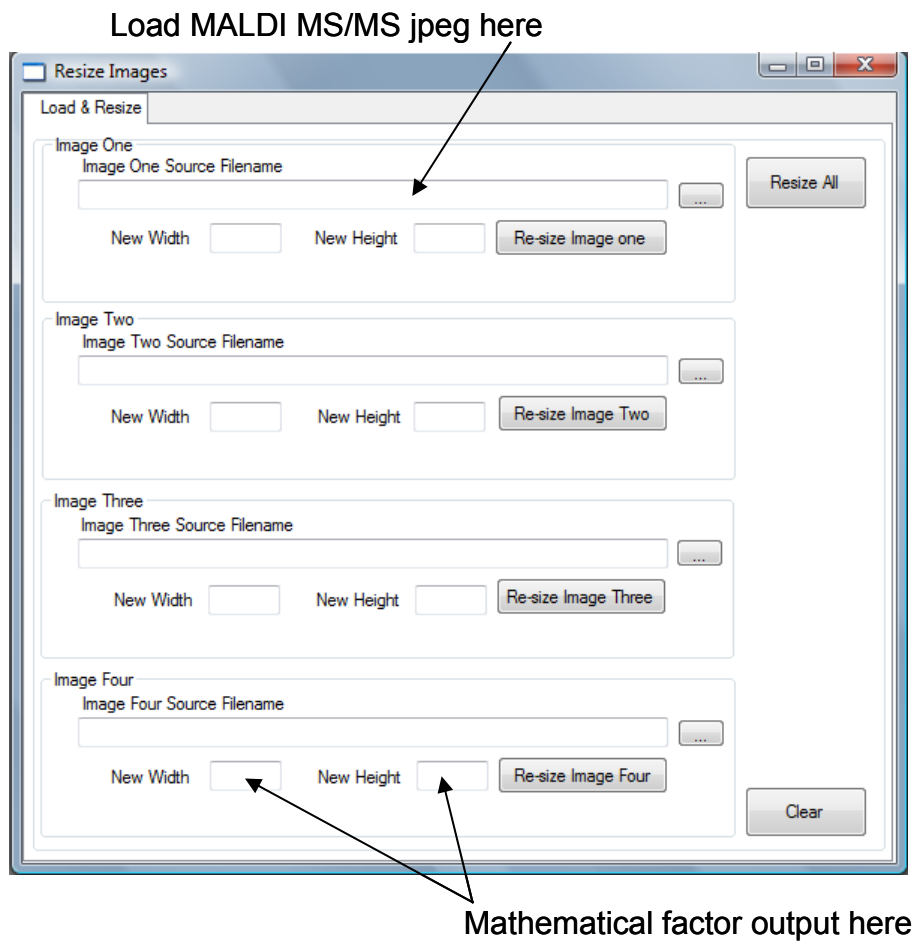


Figure 16. Custom software developed for reconstruction of a whole-body MALDI MS/MS ion image.

determine the mathematical factor necessary to match the motor coordinates to the jpeg pixel coordinates of the fiducials. The imported MALDI MS/MS jpegs are then sized accordingly and assembled to reconstruct the whole-body image (Figure 17).

Summary and Conclusions

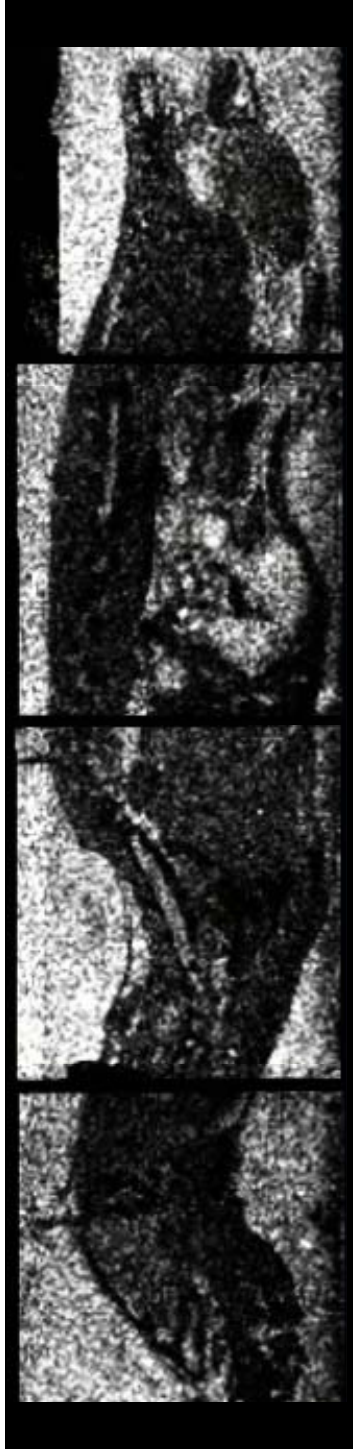
Successful application of a MALDI MS based imaging methodology for the detection of exogenous small molecules from whole-body tissue sections can provide unique information on the individual drug and metabolite distributions, as well as, endogenous protein changes as a result of drug administration. The methods discussed here were effectively applied to the analysis of drug, metabolite, and protein compounds in whole-animal tissue sections. This MALDI MS imaging methodology has great potential and the tissue preparation, matrix deposition, analysis, and data processing protocols outlined in this chapter can serve as a guide for future applications.

Materials and Methods

The MALDI matrices, sinapinic acid (SA) and 2,5-dihydroxybenzoic acid (DHB), were purchased from Sigma Chemical Co. (St. Louis, MO). HPLC grade acetonitrile, ethanol, hexane, isopropanol, and methanol were purchased from Fisher Scientific (Suwanee, GA). Trifluoroacetic acid (TFA) was purchased from Burdick and Jackson (Muskegon, MI). Acetate film tape and conductive double-sided tape were purchased from 3M Laboratories (St. Paul, MN).



a



b

Figure 17. Reconstructed whole-body ion image. a) optical image and b) reconstructed total ion current image.

Tissue sections were cut on a Leica CM3600 cryomacrocut (Leica Microsystems Inc., Germany). Endogenous protein images were acquired on either an Autoflex II MALDI-TOF-MS (Bruker Daltonics Inc., Billerica, MA) equipped with a 200 Hz Smartbeam laser or a Voyager DE STR MALDI-TOF-MS equipped with a 337 nm nitrogen laser operating at 20 Hz. Data were obtained in positive, linear mode with an accelerating voltage of 20 kV, under optimized delayed extraction conditions (200-300 ns). Imaging MALDI-MS/MS analyses were performed on QStar XL oMALDI-QqTOF-MS (Applied Biosystems Inc., Foster City, CA) equipped with a 337 nm nitrogen laser operating at 20 Hz. MS/MS data were obtained in positive mode, with a collision energy of 25 eV with an argon collision gas at a CID pressure of .04 mTorr. Unless otherwise noted, images were acquired at 600 x 400 μm lateral resolution with each pixel representing the signal sum of 4 s/transition.

CHAPTER III

PREDICTING MATRIX CONDITIONS FOR THE ANALYSIS OF EXOGENOUS COMPOUNDS IN TISSUE BY MALDI MS/MS

Introduction

It has been previously reported that sample preparation procedures are key for the reproducible detection and analysis of analytes directly from tissue sections by MALDI MS based technologies.^[39, 78] This becomes even more critical for the analysis of exogenous small molecules, such as drug compounds, by MALDI MS/MS. Evidence has been shown that average MALDI MS/MS signal intensity of small molecules is dependent upon matrix choice and tissue type.^[35, 78, 79] Currently, there are no established trends known for matrix/solvent preferences of small molecules in dosed tissue, and therefore, time consuming optimization procedures are needed before a MALDI MS/MS imaging study of dosed tissue can commence.

In this chapter, the development of a dosed tissue model assay for the high-throughput screening of potential exogenous small molecules for analysis by MALDI MS/MS and their preferences for matrix/solvent combinations will be discussed. By identifying drug class trends for matrix/solvent preferences, sample preparation of dosed tissues will have a guideline for analysis by MALDI MS/MS saving both time and resources.

Results

After many attempts of perfecting the model, a successful assay workflow was established and is comprised of five key steps: 1) image acquisition of a fiducial marked plate, 2) robotic printing of a 2 pmol drug standard array, 3) thaw-mounting of two 20 μm thick overlaid tissue sections over the drug array, 4) robotic printing of matrix/solvent combinations, and 5) analysis on the MALDI-QqTOF-MS (Figure 18). Each plate was prepared with only one drug compound and three tissue types, brain, liver, and kidney. The three most commonly used MALDI matrices, sinapinic acid (SA), α -cyano-4-hydroxycinnamic acid (CHCA), and 2,5-dihydroxybenzoic acid (DHB) were tested in this study. Each matrix was prepared in either 50% or 75% acetonitrile or methanol for a total of 12 matrix/solvent combinations (Table 2).

To validate the matrix/solvent preferences predicted by the model, a similar workflow was employed for the analysis of dosed tissue sections, except that no drug standard was spotted onto the plate prior to tissue mounting. Comparisons of the model assay results to the actual matrix/solvent preferences observed from dosed olanzapine and spiperone tissues demonstrates good correlation (Figure 19-21). MALDI MS/MS analysis of dosed brain, liver, and kidney tissue from rat revealed an overall preference for DHB as compared to SA and CHCA for detected drug signal. A similar preference for DHB from drug standards extracted through control liver sections was observed (model). Therefore, any trends observed by the dosed tissue model should predict for the actual matrix/solvent preference of a drug from dosed tissue.

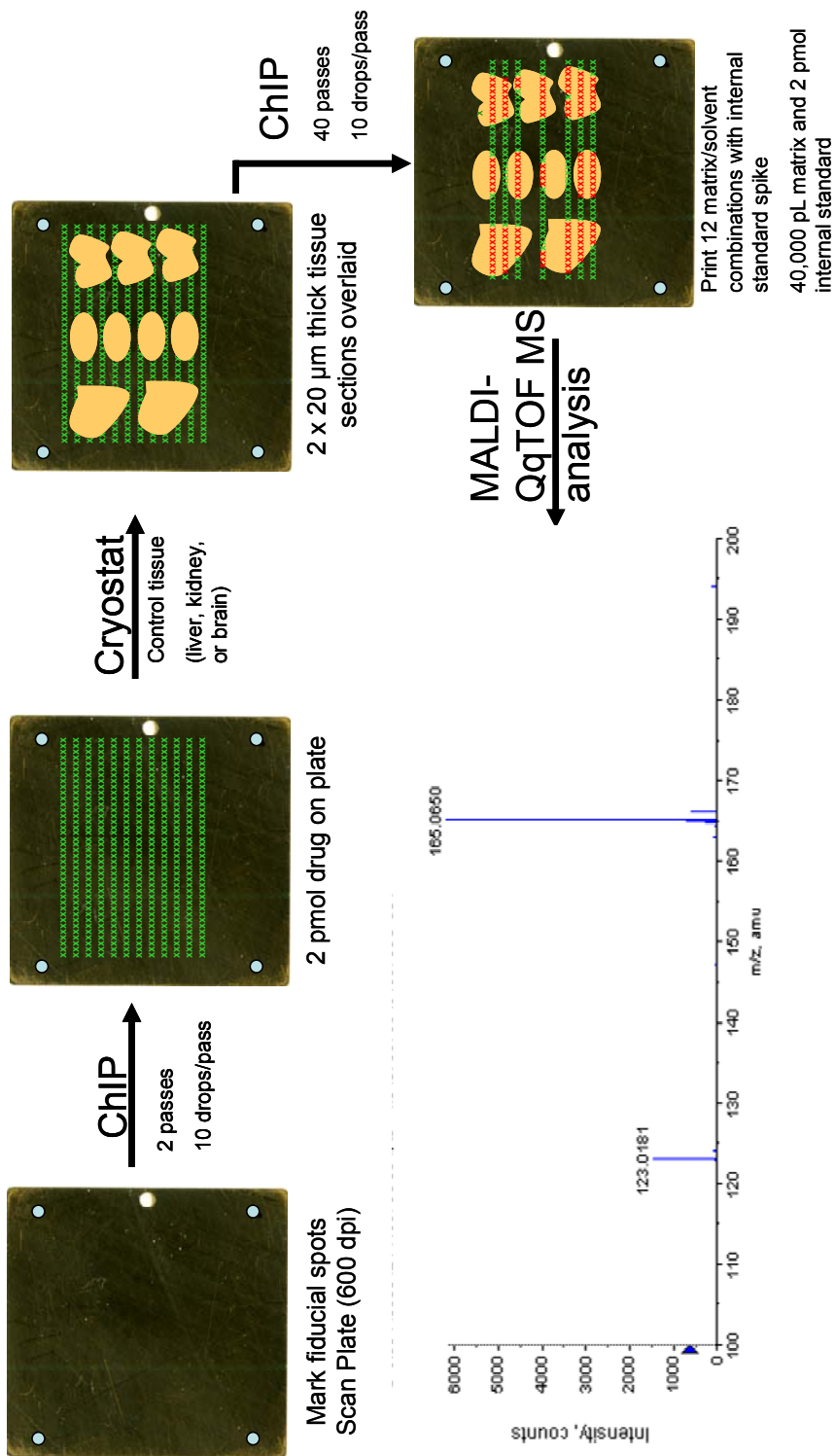


Figure 18. Analytical workflow for the dosed tissue model assay.

Table 2. List of matrices and solvents mixed to make matrix/solvent combinations.

Matrices	Solvent Compositions
sinapinic acid (SA)	50:50 acetonitrile:water (I)
α -cyano-4-hydroxycinnamic acid (CHCA)	75:25 acetonitrile:water (II)
2,5-dihydroxybenzoic acid (DHB)	50:50 methanol:water (III)
	75:25 methanol:water (IV)

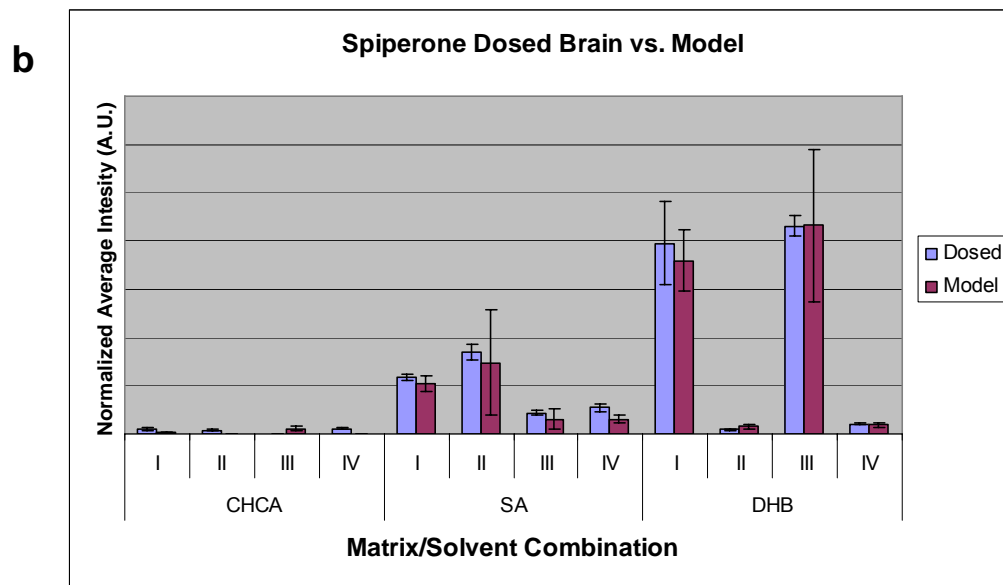
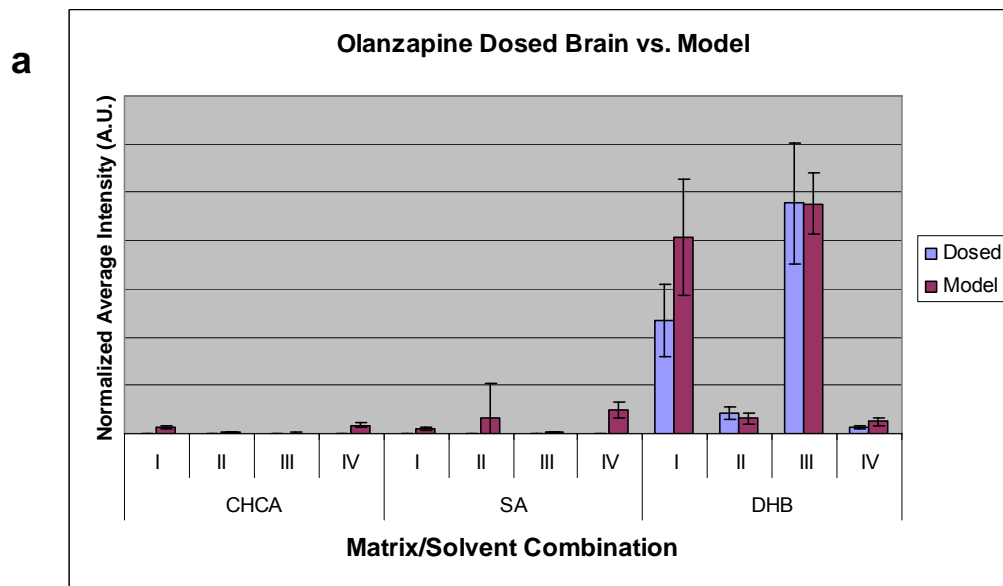


Figure 19. Comparison of the model assay response to the response from dosed brain shows good correlation.

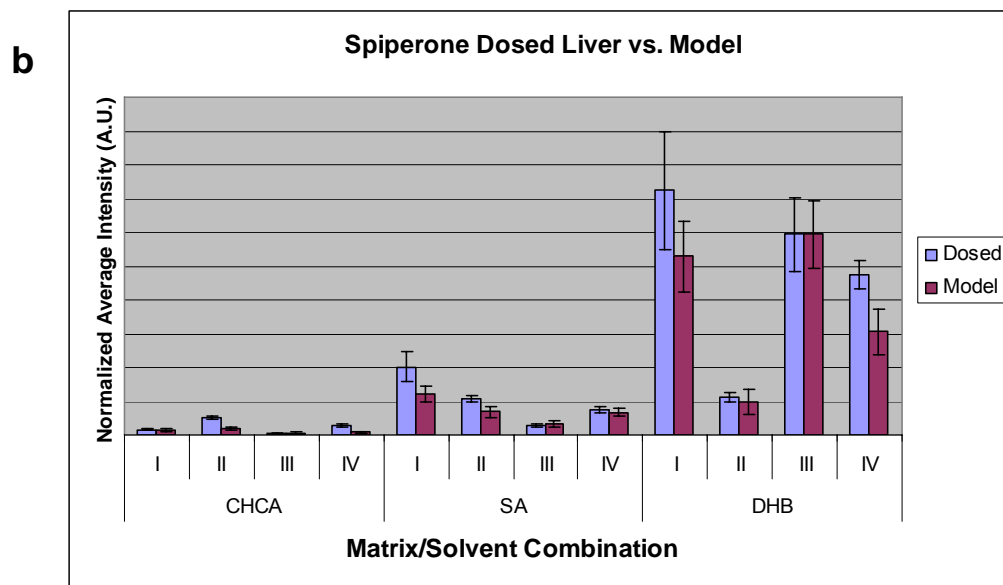
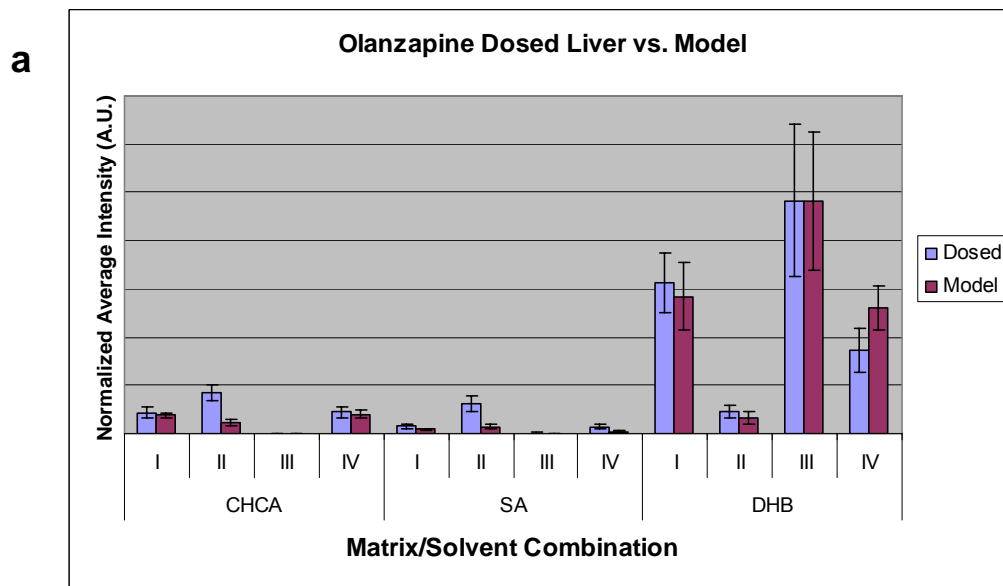


Figure 20. Comparison of the model assay response to the response from dosed liver shows good correlation.

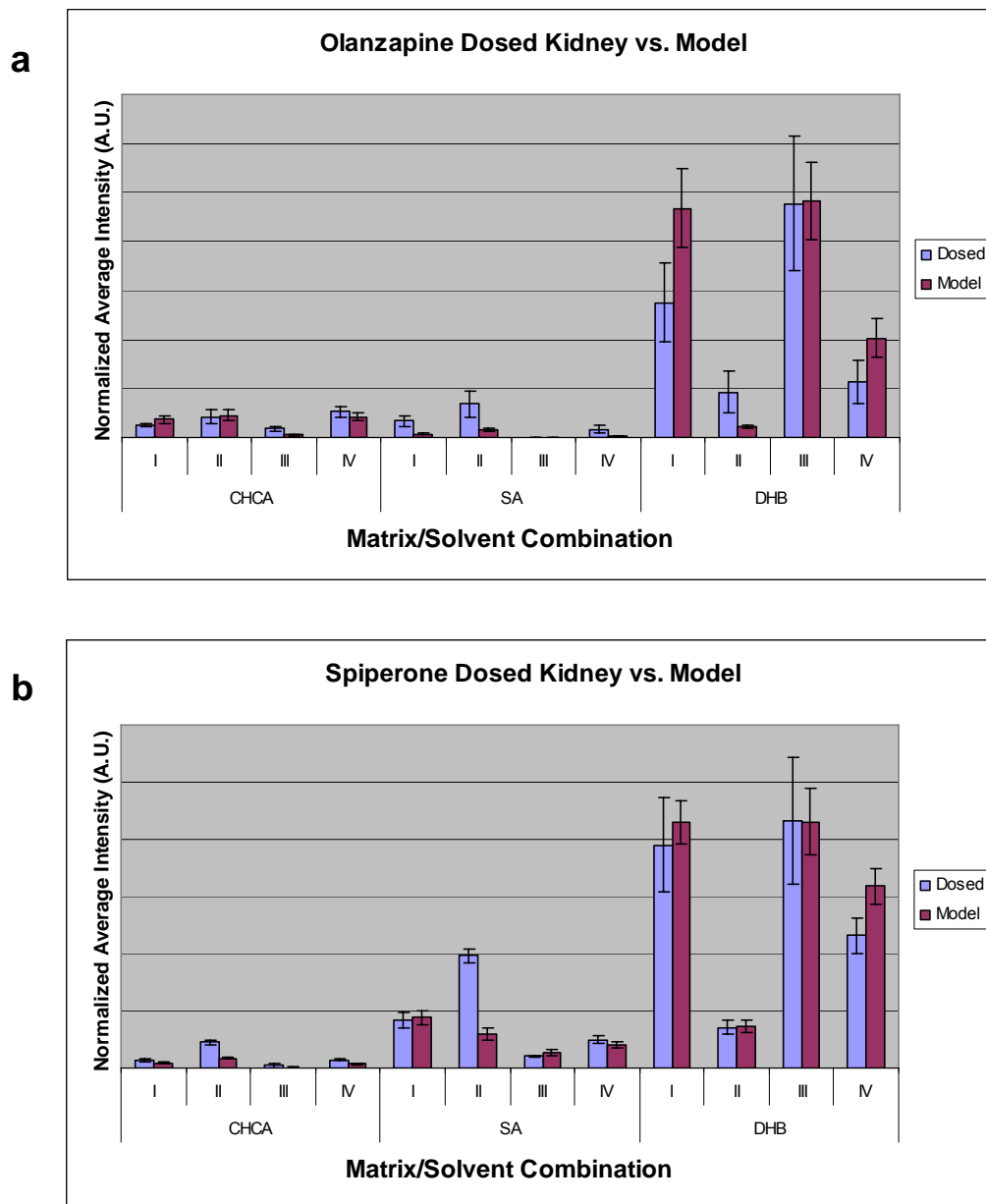
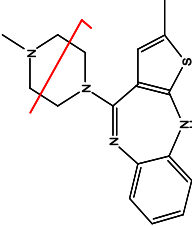
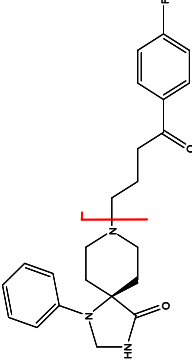
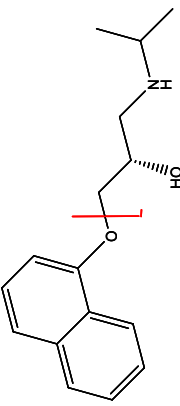
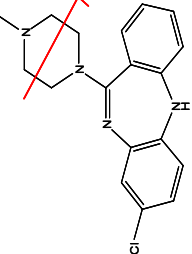
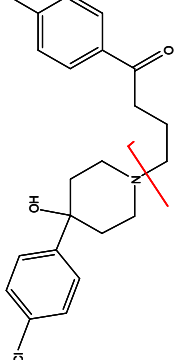
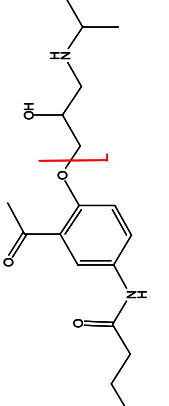
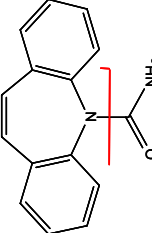
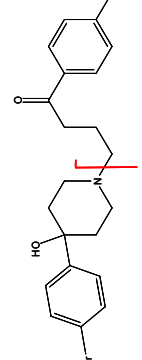
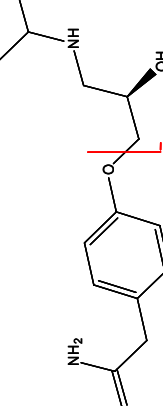


Figure 21. Comparison of the model assay response to the response from dosed kidney shows good correlation.

As a result, the model assay was then applied to three compounds within three different drug classes (Table 3). Overall, a minimum of 20 spots were analyzed per matrix/solvent combination, producing a total of ~20,000 spectra representing the matrix/solvent preferences for all 9 small molecules analyzed from the brain, liver, and kidney tissues (Figure 22). By comparing the overall response for all variables in this study, individual class trends could now be identified. For example, the benzoazepine class preferred 50% organic solvent, the butyrophenone class 50% methanol, and the isopropylamino-phenopropanol class 50% acetonitrile, all with DHB matrix. The comparison was further broken down to identify trends based on tissue type (Figures 23-25). Generally for all compounds, I preferred DHB in 50% organic solvent for brain sections, DHB in methanol for liver, and kidney data showed no strong preference for any particular matrix/solvent combination tested.

Standard curves of OLZ and SPN were also printed on the plate to compare the extraction efficiencies of the compounds through the different tissues using DHB in 50% methanol (Figure 26). Across the concentration range, OLZ had similar extraction efficiencies, while SPN exhibited more dramatic differences for each tissue type (Table 4). SPN was extracted through kidney with the highest efficiency followed by liver and brain. In addition, these curves can be used to determine extraction normalization factors needed when comparing drug signals between the different tissue types (Chapter IV).

Table 3. List of compounds based on drug class that were used in the dosed tissue model assay.

Benzoazepine Class	Butyrophenone Class	Isopropylamino-phenopropanol Class
<p>Olanzapine (OLZ) 313→256</p> 	<p>Spiperone (SPN) 396 →165</p> 	<p>Propranolol (PPL) 260 →116</p> 
<p>Clozapine (CLOZ) 327→270</p> 	<p>Haloperidol (HALO) 376 →165</p> 	<p>Acebutolol (ACE) 337 →116</p> 
<p>Carbamazepine (CARB) 237→194</p> 	<p>Bromperidol (BROM) 421 →165</p> 	<p>Atenolol (ATEN) 267 →116</p> 

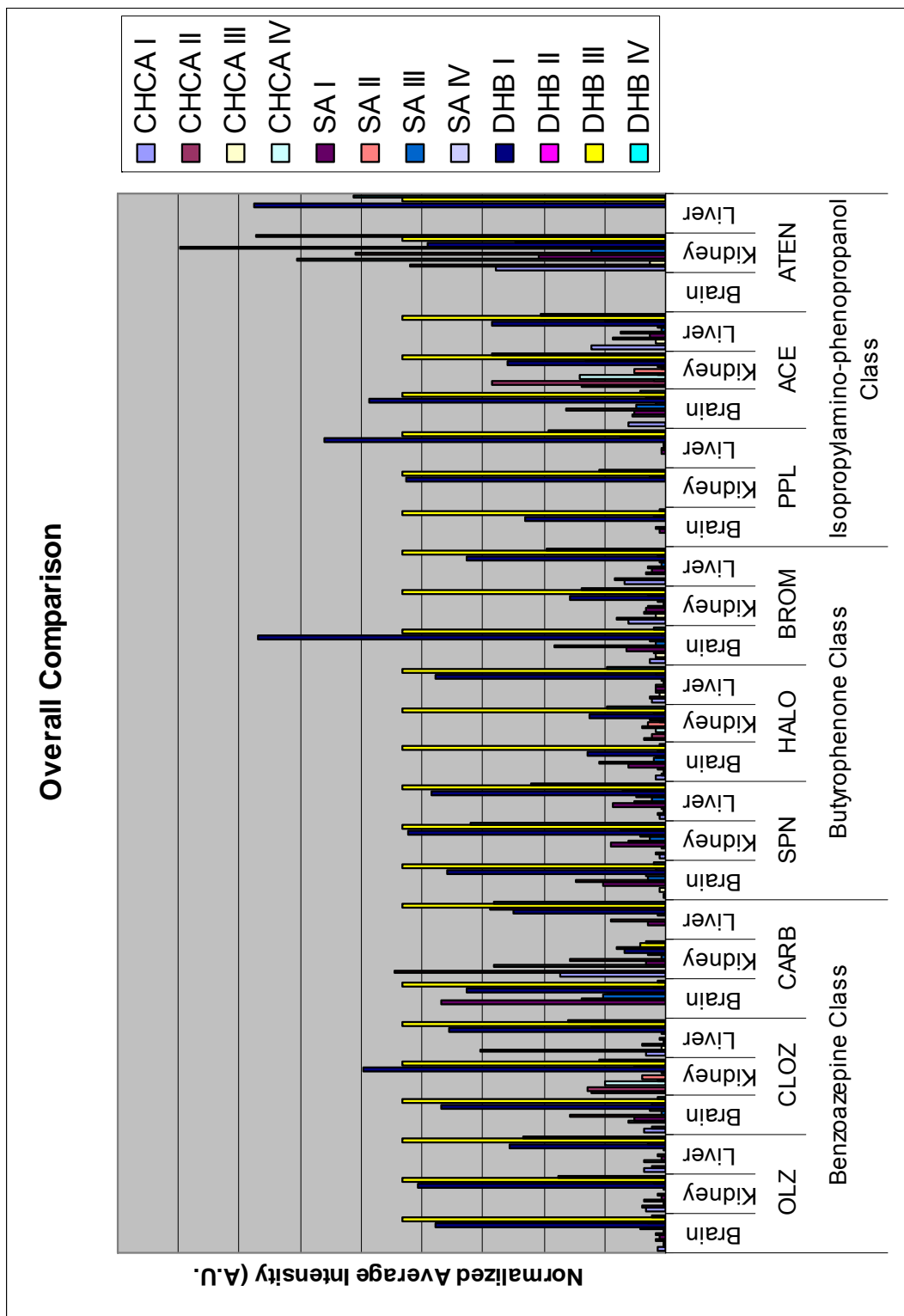


Figure 22. Overall comparison of matrix/solvent trends across three drug classes and three tissue types.

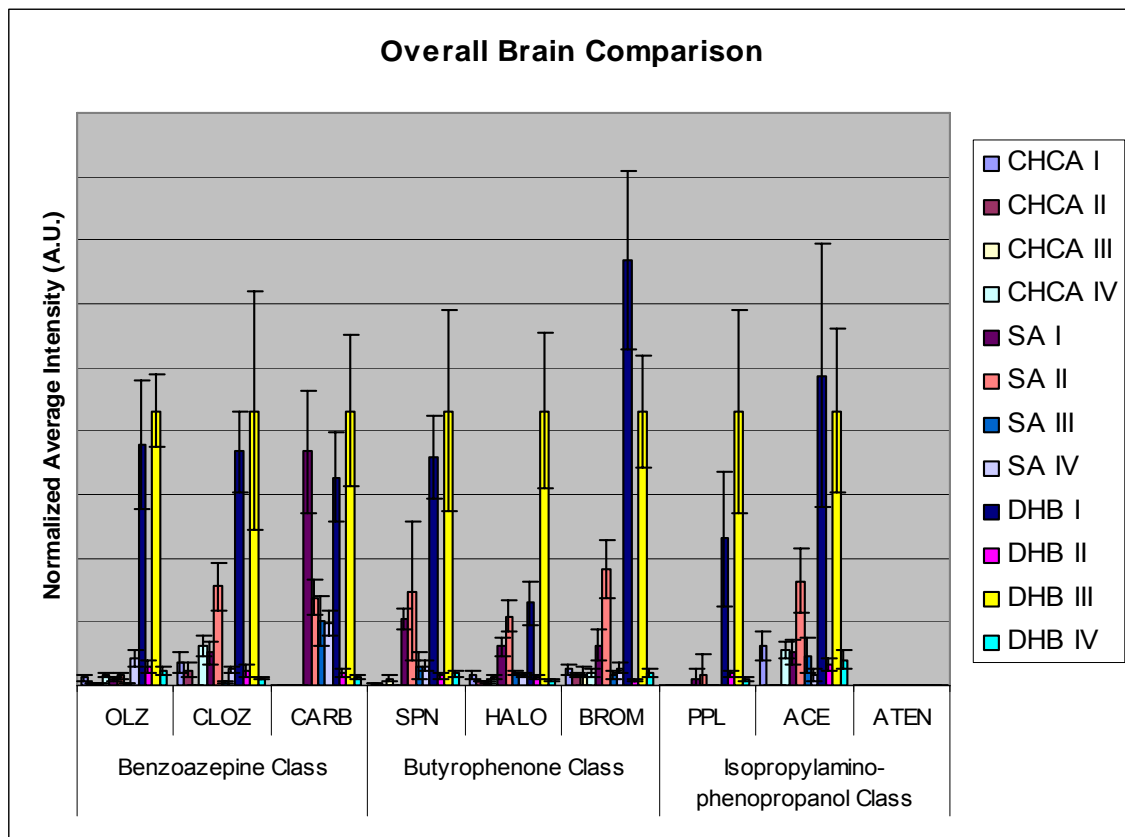


Figure 23. Comparison of the matrix/solvent preferences of three drug classes as determined by the dosed brain model assay.

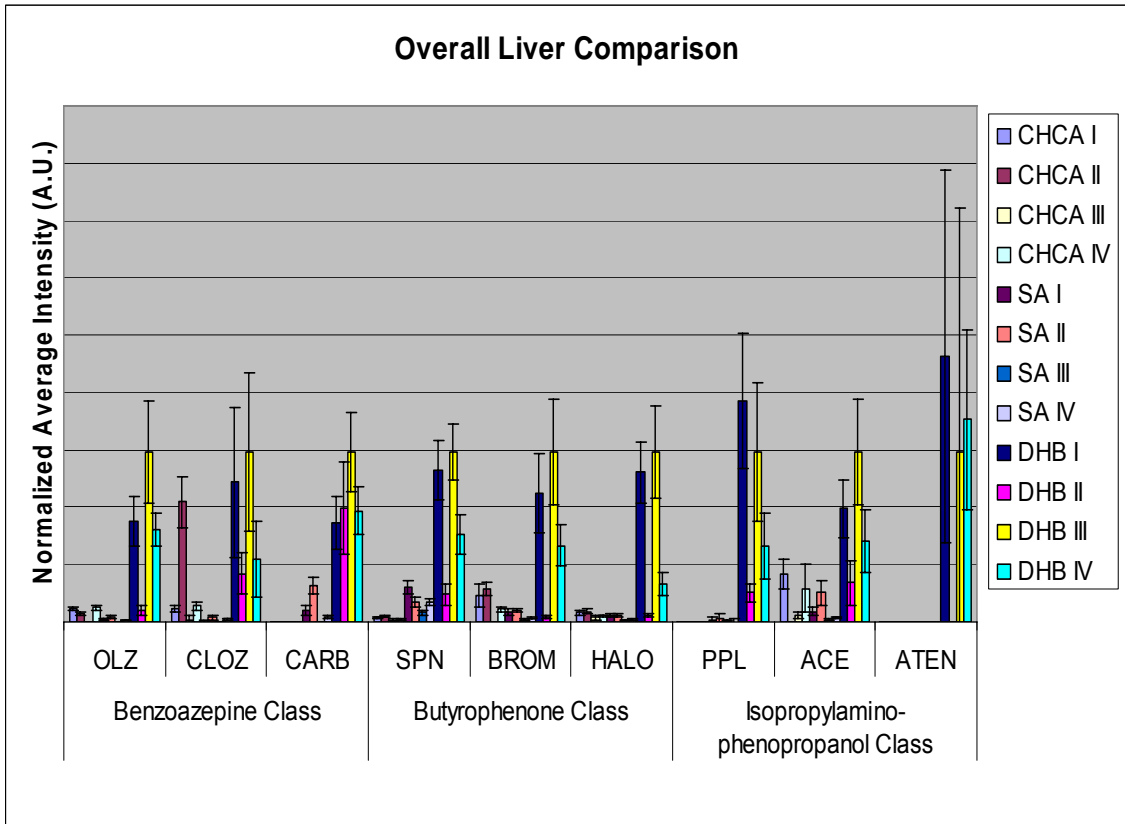


Figure 24. Comparison of the matrix/solvent preferences of three drug classes as determined by the dosed liver model assay.

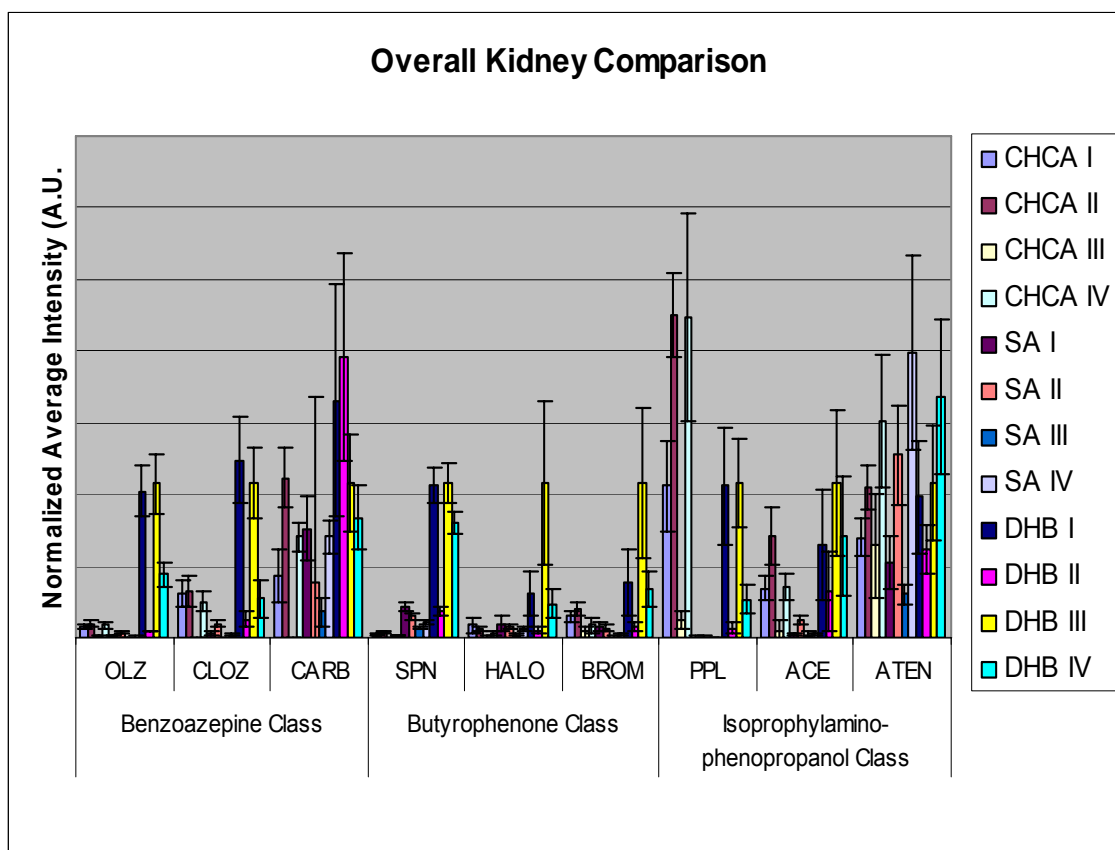


Figure 25. Comparison of the matrix/solvent preferences of three drug classes as determined by the dosed kidney model assay.

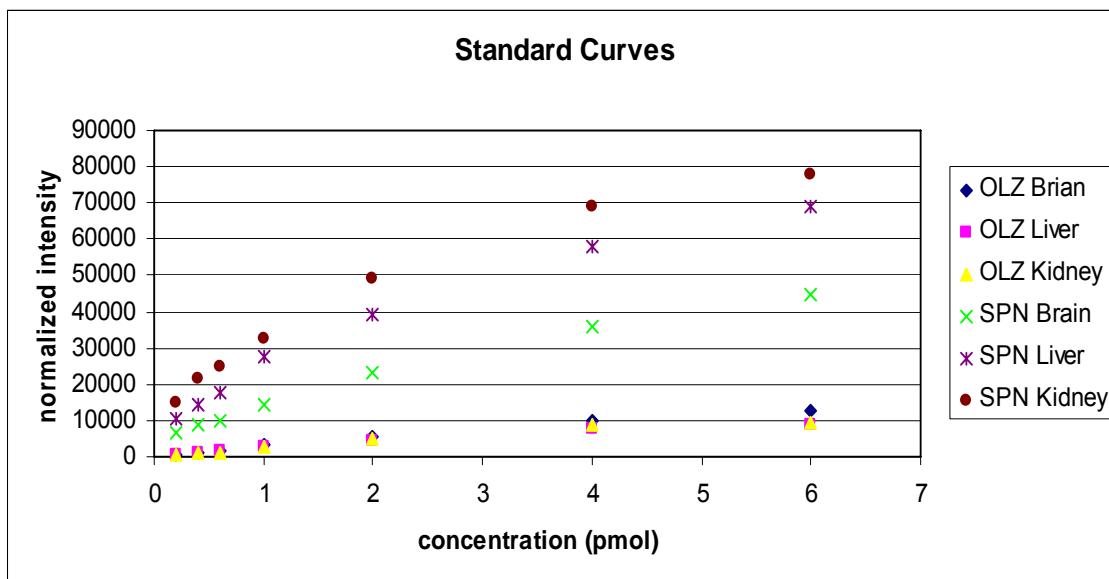


Figure 26. Comparison of the extraction efficiencies of OLZ and SPN through the different tissues using the matrix/solvent combination of DHB in 50% methanol (DHB III).

Table 4. Comparison of average signal intensity for 2 pmol of OLZ and SPN detected through brain, liver, and kidney tissue using the matrix/solvent combination of DHB in 50% methanol (DHB III).

Average Signal (2 pmol)	Brain	Liver	Kidney	Normalization Factor
OLZ	5683.3 25 %CV	4291.0 19 %CV	4855.8 39 %CV	Brain 1.0 Liver 1.3 Kidney 1.2
SPN	23192 33 %CV	39420 28 %CV	49168 23 %CV	Brain 2.1 Liver 1.2 Kidney 1.0

Discussion

It is believed that the detection of drug compounds from dosed tissue relies on solvent preferences for extraction, as well as, the incorporation of the extracted drug into the matrix crystals. It is known that several factors influence these preferences and include the molecular structure of the analyte (i.e. chemical properties) and permeability of the target tissue, for example.^[80-82] Collectively, it is reasonable to assume that the simple diffusion of a drug could vary significantly between tissues within an animal. In this study, a model was developed that mimics dosed tissue matrix/solvent preferences for drugs across three classes, the benzoazepine, butyrophenone, and isopropylamino-phenopropanol classes. Drug compounds in the benzoazepine class are sedative-hypnotic agents that are commonly used for the treatment of a variety of symptoms including seizure control, anxiety, alcohol withdrawal, and insomnia, to name a few. Butyrophenones are a class of pharmaceutical drugs used to treat various psychiatric disorders such as schizophrenia. The drug compounds representing the isopropylamino-phenopropanol class are β -adrenergic antagonists and are used for the treatment of hypertension in cardiac patients. The structures and therapeutic targets of each of these drug classes are different and it would be reasonable to expect the matrix/solvent preferences to differ across these classes.

The dosed tissue model assay was validated by selecting a compound from each class and administering a pharmacologically relevant dose to a rat. The rats were sacrificed 2 h post-dose and the brain, liver, and kidney organs

were removed. Analysis of these dosed organs identified the actual matrix/solvent preferences that should be mimicked by the model. Trends for matrix/solvent preference predicted by the dosed tissue model assay correlated very well to the dosed tissue results, indicating the model does in fact mimic dosed tissue preferences. Subsequent analysis of the 9 compounds using the dosed tissue model assay identified trends across the different drug classes and tissue types. It was determined that DHB produced the highest detected signal for most compounds analyzed and should be a good general matrix for small molecule analysis from dosed tissues. The choice of solvent was determined to be more dependent upon the tissue type chosen for the analysis than the drug structure itself. Therefore, when analyzing a whole-body tissue section containing multiple tissue types, it is important to select the solvent that is acceptable for most tissue analyzed.

To determine the extraction efficiencies of the drugs in this study, a dilution series of drug standard was automatically spotted on the MALDI plate and overlaid with tissue in the same manner as the model. A single drug was chosen to represent each class and DHB in 50% methanol was selected as the “generic” matrix/solvent combination. From the data collected the extraction efficiency of the generic matrix combination in brain, liver, and kidney was evaluated and provided a means to calculate normalization factors. The butyrophenone class demonstrated the best extraction efficiency with 71% of the drug detected by the assay, while the benzoazepine class reported an extraction efficiency of 42%. Furthermore, the standard curve was used to see if absolute

quantities of drug could be determined using the model assay. Approximately 0.1 pmol of OLZ drug was detected in the actual dosed liver tissue as determined by the extracted standard curve; however, previous HPLC-MS/MS extraction studies from liver homogenate indicate that ~0.3 pmol of drug should be present within the dosed tissue area analyzed. Therefore, DHB in 50% methanol extracted ~33% of dosed OLZ, while our model demonstrated an approximate extraction efficiency of 42% for OLZ. Thus, while the model does not precisely represent the absolute quantities from dosed tissue, it is still capable of mimicking the matrix/solvent preferences and can be used to predict optimal matrix conditions for direct tissue analysis by MALDI MS/MS without the need for expensive animal studies.

Materials and Methods

Materials

The MALDI matrices, 3,5-dimethoxy-4-hydroxycinnamic acid (sinapinic acid, SA), α -cyano-4-hydroxycinnamic acid (CHCA), and 2,5-dihydroxybenzoic acid (DHB), were purchased from Sigma Chemical Co. (St. Louis, MO). HPLC grade acetonitrile, methanol, and hexane were purchased from Fisher Scientific (Suwanee, GA). HPLC grade cyclohexane was purchased from Acros Organics (Geel, Belgium). Fischer 344 rats were purchased from Charles River Laboratory, Inc. (Wilmington, MA). Standards of clozapine (CLOZ), carbamazepine (CARB), spiperone (SPN), haloperidol (HALO), bromperidol

(BROM), propranolol (PPL), acebutolol (ACE), and atenolol (ATEN) were purchased from Sigma Chemical Co. Zyprexa tablets (OLZ) were obtained from the Vanderbilt University Hospital Pharmacy (Nashville, TN). All animal studies were approved by the Institutional Animal Care and Use Committee at Vanderbilt University.

Tissue Preparation

One drug compound from each class was administered (p.o.) at pharmacologically relevant doses to 10 week-old male Fischer 344 rats, which had fasted overnight prior to start of study. OLZ drug was administered at 8 mg/kg, SPN at 5 mg/kg, and PPL at 10 mg/kg. Animals were euthanized at 2 h post-dose by isoflurane anesthesia followed by exsanguination via decapitation. Control and dosed brain, liver, and kidney were harvested and frozen in powdered dry ice. All samples were stored at -80 °C until sectioning. Control organs were reserved for model assay (see next section). Dosed tissue sections of 20 µm thickness were collected at -20 °C using a Leica CM3050s cryomicrotome (Leica Microsystems, Inc., Germany) and thaw-mounted to gold-coated MALDI target plates. All plates were stored in a vacuum desiccator for 2 h prior to matrix deposition. Each sample was robotically spotted with 40 nL (40 passes, 10 drops/pass, 100 pL/drop) of each matrix/solvent combination (see table 2) using a piezo ejection chemical inkjet printer (ChIP, Shimadzu, Kyoto, Japan) for a total of 20 spots per combination. All matrix/solvent combinations were prepared fresh at 15 mg/mL and contained an internal standard spike of 2

pmol. All matrix spotted tissue sections were stored in a vacuum dessicator for ~12 h until MALDI MS/MS analysis.

Model Assay Preparation

At beginning of each drug analysis, a gold-coated MALDI target plate is marked with four fiducials (one in each corner of the plate) and an image is acquired on a flat-bed scanner at 600 dpi and saved as a tiff. The plate is then loaded onto the robotic spotter (ChIP, Shimadzu) and a scanned image is acquired by the instrument. The instrument acquired scan is then taught (i.e. co-registered) to the imported tiff image based on the fiducial markings. For each plate, one drug compound is printed in an array of 38 x 26 spots with 1mm spacing (988 spots total). A 1 mM solution of drug is printed in 2 passes of 10 drops/pass at 100 pL/drop resulting in 2 pmol of drug standard on plate. The plate is then removed from the spotter and allowed to dry in the dark for 15 min. Using a Leica CM3050s cryomicrotome at -20 °C, two 20 µm thick tissue sections of each control brain, liver, or kidney organ are overlaid and thaw-mounted onto gold-coated MALDI target plate covering the printed drug array. All plates were stored in a vacuum desiccator for ~2 h prior to matrix deposition. The plate was then returned to the spotter and retaught using the same fiducials (realignment error was determined to be <10 µm). At the exact same coordinates as the drug spots, 40 nL (40 passes, 10 drops/pass, 100 pL/drop) of each matrix/solvent combination is printed for a total of 20 spots per combination. Again, all matrix/solvent combinations were prepared fresh at 15 mg/mL and

contained an internal standard spike of 2 pmol. Matrix spotted tissue sections were stored in a vacuum dessicator for ~12 h until MALDI MS/MS analysis.

MALDI MS/MS Analysis

Analyses were performed on a QStar XL (MDS Sciex, Concord, Canada) equipped with an oMALDI source (20 Hz 337 nm nitrogen laser) and a hybrid QqTOF mass analyzer to obtain MS/MS data. Instrument parameters were optimized for each compound. Generally, fragmentation was achieved using a collision energy of 25-40 eV with an argon collision gas at a pressure of 0.04 mTorr. Each drug was monitored for the CID fragmentation of the parent drug into its major fragment (see Figure 21). Two transitions, analyte and internal standard, were monitored per spot with 5 s accumulation time per transition (total of 10 s/pixel). Each array was automatically acquired with intraspot rastering pattern using the oMALDI 4.0 software.

Data Processing

For the model assay and dosed tissues, the analyte signal intensity was normalized against internal standard signal intensity from each matrix/solvent spot. Within each matrix/solvent combination, normalized signals were q-tested (95% confidence level) for outliers and then averaged. Signal averages were then normalized to the DHB III signal for graphical representation (excel) of the dosed tissue model assay comparisons across all three drug classes and tissues.

CHAPTER IV

DRUG AND METABOLITE IMAGING IN WHOLE ANIMAL SAGITTAL TISSUE SECTIONS USING MALDI MS/MS

Introduction

Modern pharmaceutical research has been greatly influenced by the advent of new technologies, such as genomics, proteomics, combinatorial chemistry, and high-throughput screening, each promising to enhance the discovery of new therapeutic compounds. This has led to a large number of hypothetical targets with exponentially more potential drug candidates. It was hoped that these technologies would give rise to more “promising” lead candidates. However, the increased number of potential drug candidates and high-throughput screening assays has not yet resulted in a commensurate increase in research productivity. Of the few lead compounds that have advanced onto the development phase, even fewer (if any) can be credited to the new drug discovery paradigm.^[83] The attrition rates of these development compounds can be attributed to poor analytical pharmacokinetic (PK) assessments of the potential lead candidate in the discovery phase. Most of the discovery phase PK studies are *in vitro* assays, or computer-based *in vivo* prediction models that are necessary to evaluate the countless drug candidates produced from combinatorial libraries.^[11, 16, 17, 71] Despite their speed and throughput, these systems are poor predictors of *in vivo* PK response. Therefore, the main reason drugs fail in the development phase is unacceptable PK

parameters. The success of pharmaceutical research will now depend on new analytical technologies that can detect where a drug candidate and its metabolites are distributed in a whole-animal since tissue distribution plays an essential role in the PK behavior of a drug.

In recent years, the potential of IMS based imaging technologies has become apparent for the quick, label-free, and molecularly specific analysis of drugs directly from tissue sections.^[38, 40, 84] Development and application of IMS for the imaging of whole-animal tissue sections can help assess the potential value of a lead candidate earlier in the drug discovery process. These early PK evaluations will improve the quality of lead candidates that enter the development phase, before expensive man-hours and resources are wasted.

In the study presented here, efforts were focused on the development and application of a novel imaging MALDI MS/MS methodology that can analyze exogenous compounds directly from whole-animal tissue sections, while at the same time, providing quantitative information about the relative distribution of that compound across the various organs. Rats dosed with pharmacologically equivalent amounts of olanzapine (OLZ) were chosen since previous data using quantitative whole-body autoradiography (WBA) were available as reference^[85] for the MALDI MS/MS method development.

Results

Whole-Rat Olanzapine and Metabolite Imaging

In the case study of olanzapine and its metabolites, MALDI MS/MS analysis was performed to monitor the major fragment from the collision induced dissociation of the precursor compound (Figure 27). Standard curves of OLZ and metabolite standards were linear over a concentration range of 0.006 to 600 pg/mL with a correlation coefficient of >0.992. The lower limit of detection for OLZ and metabolite standards spiked on tissue was 1 fg.

To ensure that no interfering signal could be misinterpreted as olanzapine or metabolite signal, proper control experiments were performed using the same instrument parameters that were optimized for the imaging study. A control (non-dosed) whole-body sagittal tissue section from rat was imaged, and no interfering fragment peaks at m/z 256, 270, or 272 were detected at the transitions corresponding to drug, metabolites, or internal standard (Figure 28). In addition, the spectra indicate no matrix interference since a DHB solution was used for the analysis of the control tissues. Therefore, all detected fragment peaks represent true drug and metabolite signal.

After a single 8 mg/kg oral dose of OLZ, drug and metabolites were present in measurable amounts in almost all tissues at 2 and 6 h post-dose and fewer tissues at 24 h post-dose. At the 2 h time point, OLZ is observed to be ubiquitously distributed throughout the whole rat, with significant localization in specific organs (Figure 29). The highest OLZ signal was detected in the lung

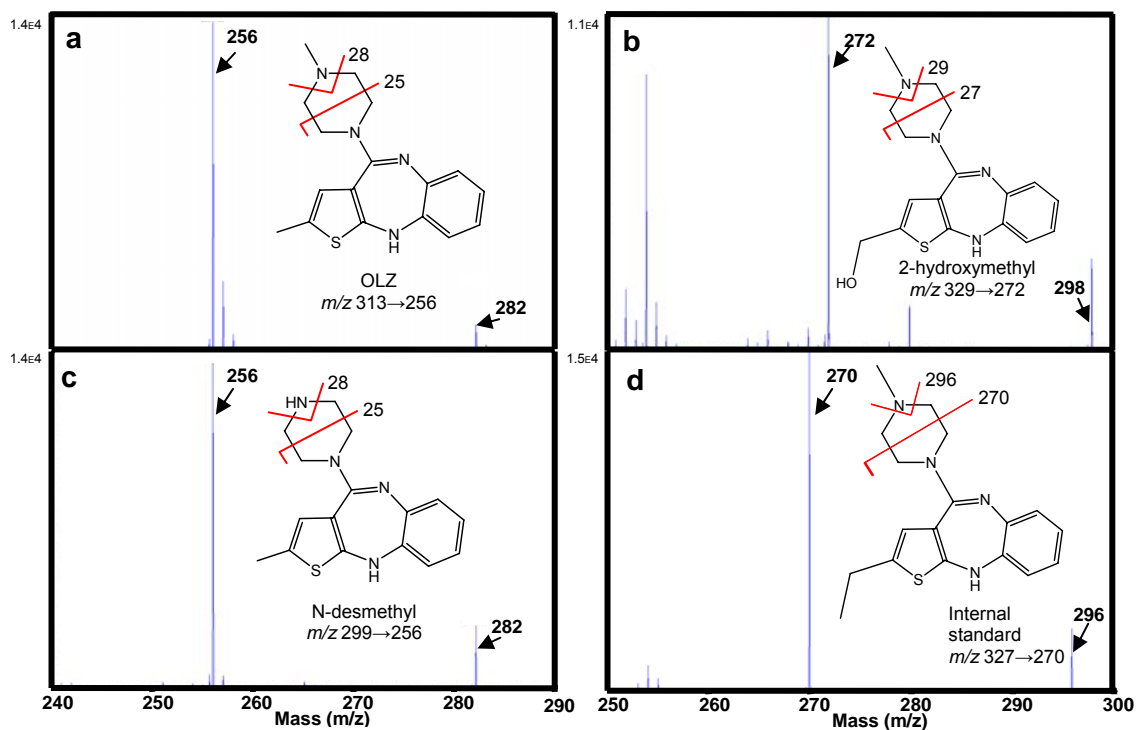


Figure 27. Fragmentation spectra for OLZ, metabolites, and internal standard. a) Olanzapine m/z 313→256, b) 2-hydroxy-methyl olanzapine metabolite m/z 329→272, c) N-desmethyl olanzapine metabolite m/z 299→256, and d) internal standard m/z 327→270.

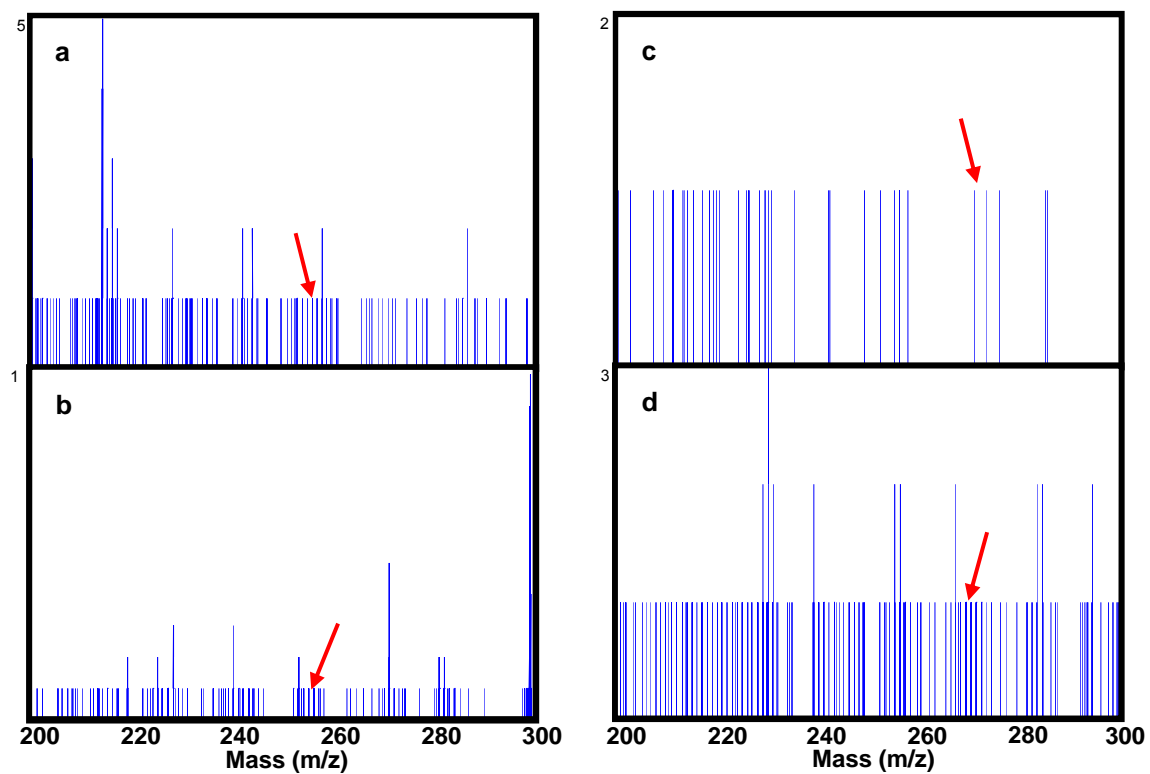


Figure 28. Example spectra from control liver tissue analysis with DHB contain no interfering endogenous or matrix signals. a) olanzapine transition m/z 313→256, b) N-desmethyl transition m/z 299→256, c) 2-hydroxymethyl transition m/z 329→272, and d) internal standard transition m/z 327→270. Arrows pointing at location of expected fragment peak.

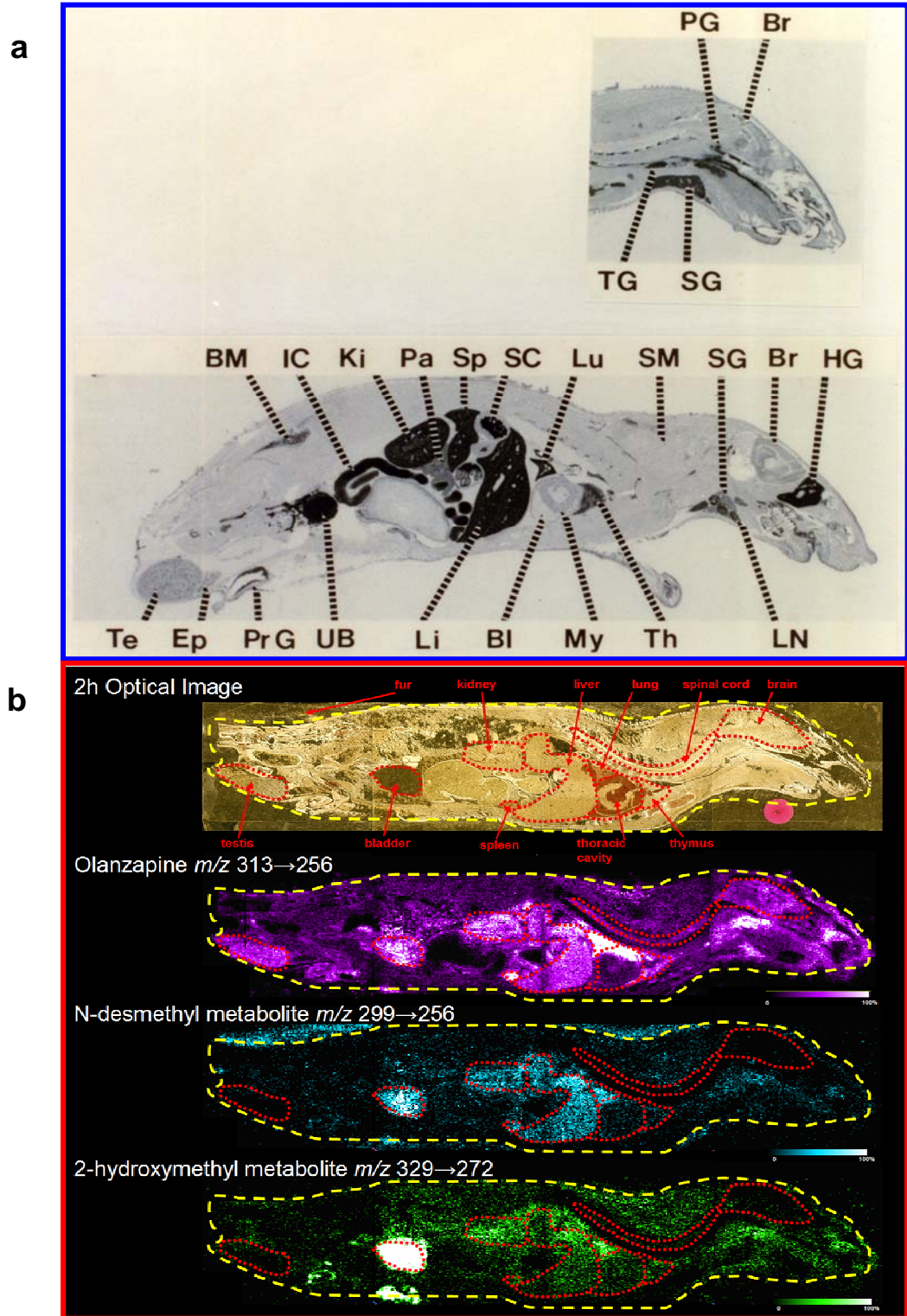


Figure 29. Comparison of WBA and MALDI MS/MS detection of olanzapine at 2 h post-dose in a whole-rat sagittal tissue section. a) whole-body autoradiography of [^{14}C] OLZ shows distribution of all labeled compounds^[85], b) MALDI MS/MS detects individual OLZ and metabolite distribution.

followed by the spleen, bladder, kidney, liver, thymus, brain and spinal cord, and testis. This observation is in full agreement with previously published OLZ WBA data.^[85] A list of abbreviations can be referenced in Table 5.

For the first time, *metabolite distribution* was detected using the whole-body MALDI MS/MS technology and revealed that the metabolites, N-desmethyl and 2-hydroxymethyl olanzapine, collectively contributed 21% of the total MS/MS signal. The N-desmethyl metabolite was detected primarily in the liver, kidney, and bladder and contributed 8% of the total MS/MS signal. The 2-hydroxymethyl metabolite was detected with the highest signal in the bladder followed by the liver and kidney. This second metabolite contributed 13% of the total MS/MS signal. It should be noted that little to none of these metabolites was detected in the brain and spinal cord. These data are consistent with previous evidence that the metabolites have no central nervous system pharmacological activity.^[86]

At 6 h following OLZ administration, static drug distribution was again detected throughout the whole-body section, with OLZ signal greatly decreased in the brain and spinal cord regions at 66% less ion signal than the 2 h time point (Figure 30). This observation correlated to previous studies that found a 78% decrease in [¹⁴C]OLZ concentration from 2 to 6 h in brain tissue.^[85] The decrease in detected OLZ signal indicated clearance of the drug from the target organ. OLZ was detected at the highest amount in lung, followed by localization in liver, bladder, testis, and thymus. Metabolite distribution remained unchanged, with localization primarily in lung, liver, and bladder. The combined metabolite signal was 28% of the total MS/MS signal, with individual contributions of 13%

Table 5. List of tissue abbreviations.

Abbreviation	Tissue
Bl	blood
BM	bone marrow
Br	brain
CC	cecum contents
Ep	epididymis
Ey	eye
Fe	feces
HG	Harderian gland
IC	intestinal contents
Ki	kidney
Li	liver
LN	lymph node
Lu	lung
My	myocardium
Pa	pancreas
PG	pituitary gland
PrG	prostate gland
SC	stomach contents
SG	salivary gland
Sk	skin
SM	smooth muscle
Sp	spleen
Te	testis
TG	thyroid gland
Th	thymus
UB	urinary bladder

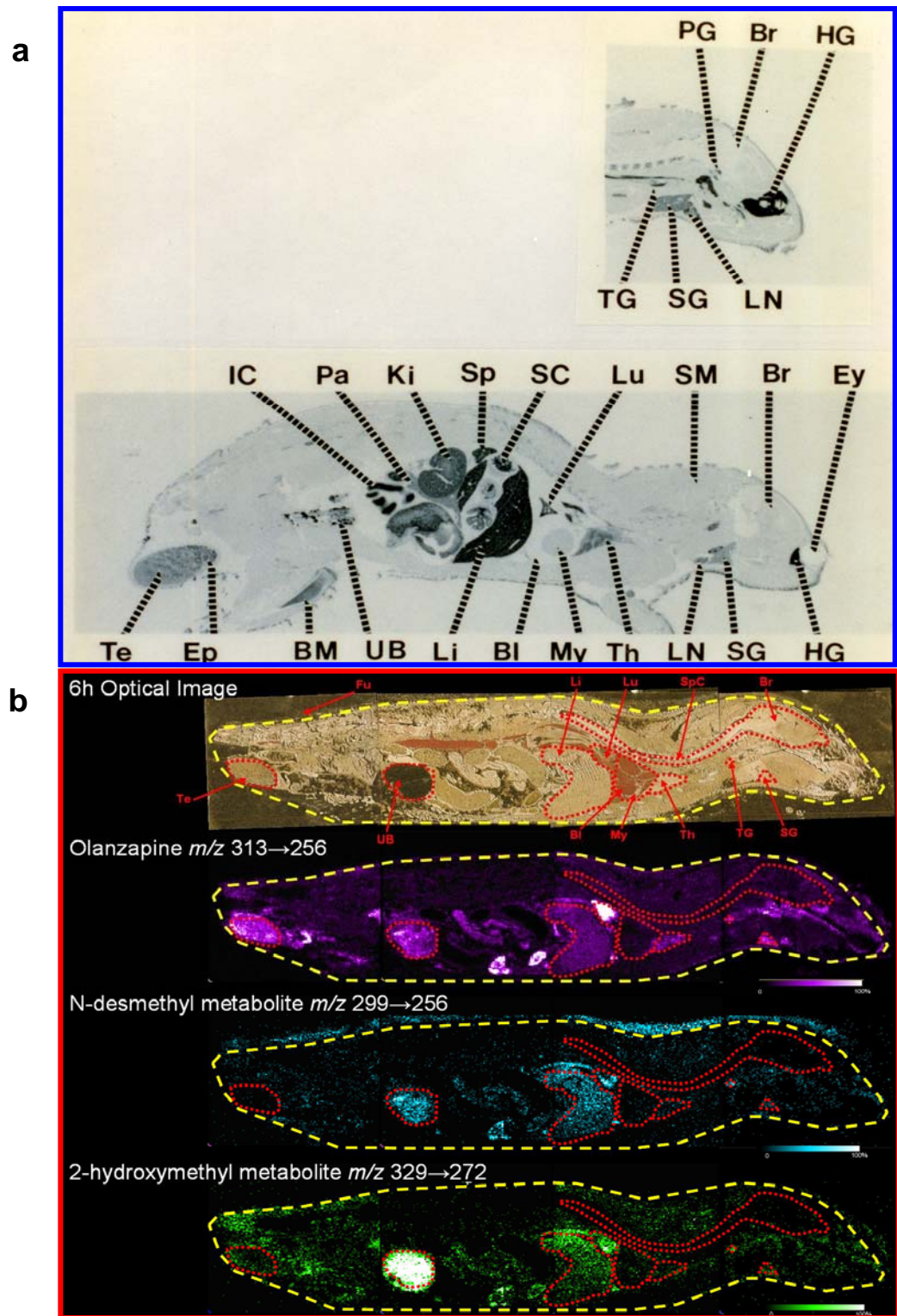


Figure 30. Comparison of WBA and MALDI MS/MS detection of olanzapine at 6 h post-dose in a whole-rat sagittal tissue section. a) whole-body autoradiography of [14 C] OLZ shows distribution of all labeled compounds^[85], b) MALDI MS/MS detects individual OLZ and metabolite distribution.

and 15% for the N- desmethyl and 2-hydroxymethyl olanzapine metabolites, respectively. Again, little to no metabolite signal was detected in the brain and spinal cord regions. Interestingly, the 2-hydroxymethyl metabolite was detected in the testis at 6 h post-dose, although it was not present in the testis at detectable levels in the 2 h post-dose section.

MALDI MS/MS images acquired at 24 h post-dose, indicate the majority of the OLZ has eliminated from the rat and is corroborated by the WBA images^[85] (Figure 31). Signals were detected at much lower levels and the image thresholds were adjusted for visualization (10x for OLZ, and 2x for the metabolites). OLZ was detected in a few organs, with the highest signal in Harderian gland, testis, and cecum. Metabolite distribution was confined primarily to the cecum and kidney. It is intriguing to note that no OLZ or metabolite signal was detected by MALDI MS/MS or WBA in the cecum at previous time points. The combined metabolite signal was 63% of the total MS/MS signal, with individual contributions of 47% and 16% for the N-desmethyl and 2-hydroxymethyl metabolites, respectively.

Reproducibility of the MALDI MS/MS image acquisition was assessed by comparing the 2 h OLZ signal detected from skeletal muscle tissue, since this tissue was represented on each of the four plates spanning a single whole-rat sagittal tissue section (Figure 32). A whole-body sagittal rat image acquired in this study contains ~27,000 pixels. A Bartlett's test for plate-to-plate signal variance, as well as, an analysis of variance (ANOVA) test were performed on sampled skeletal muscle pixels (~300) from each plate and confirmed no

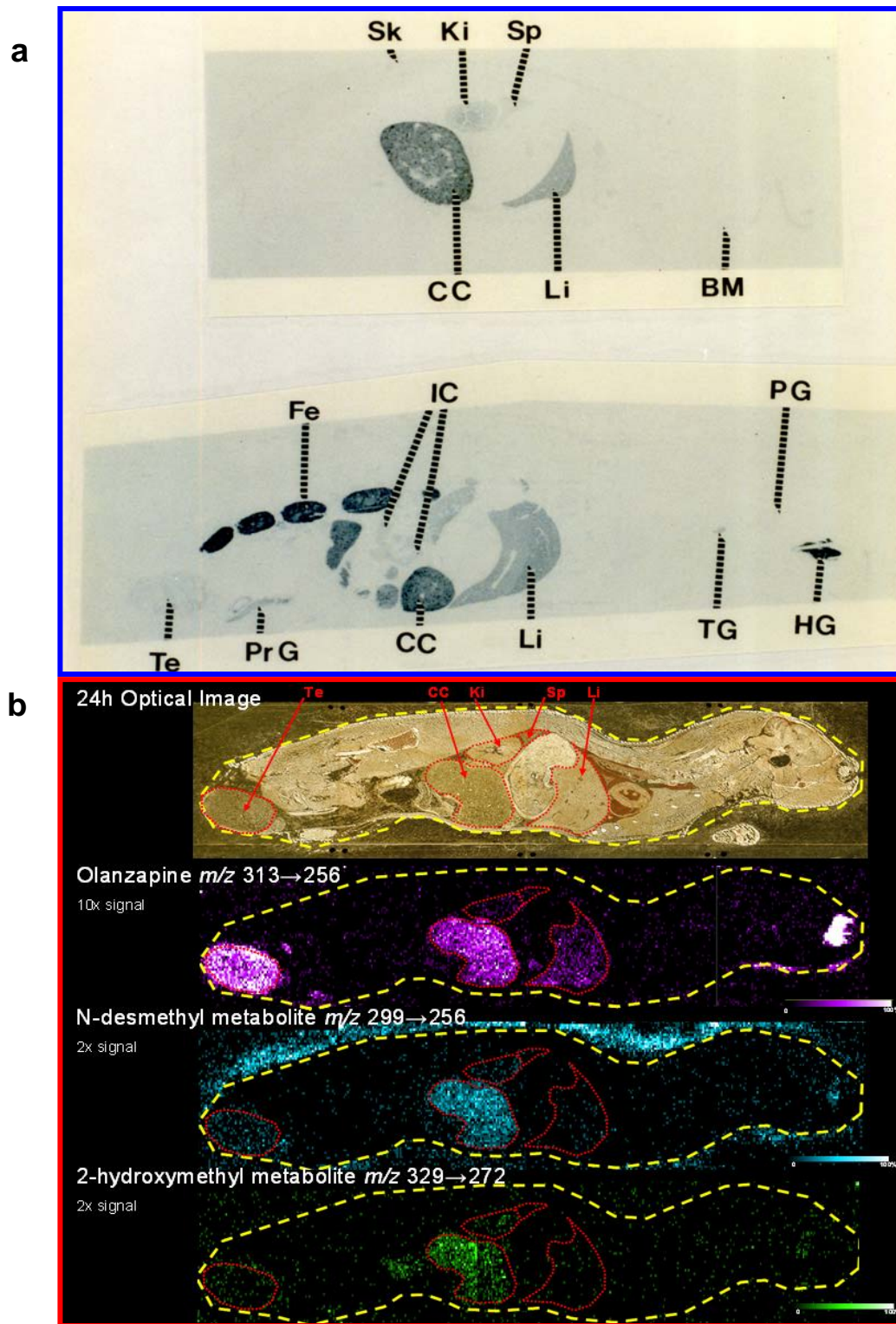


Figure 31. Comparison of WBA and MALDI MS/MS detection of olanzapine at 24 h post-dose in a whole-rat sagittal tissue section. Signals amplified for visualization. a) whole-body autoradiography of [^{14}C] OLZ shows distribution of all labeled compounds^[85], b) MALDI MS/MS detects individual OLZ and metabolite distribution.

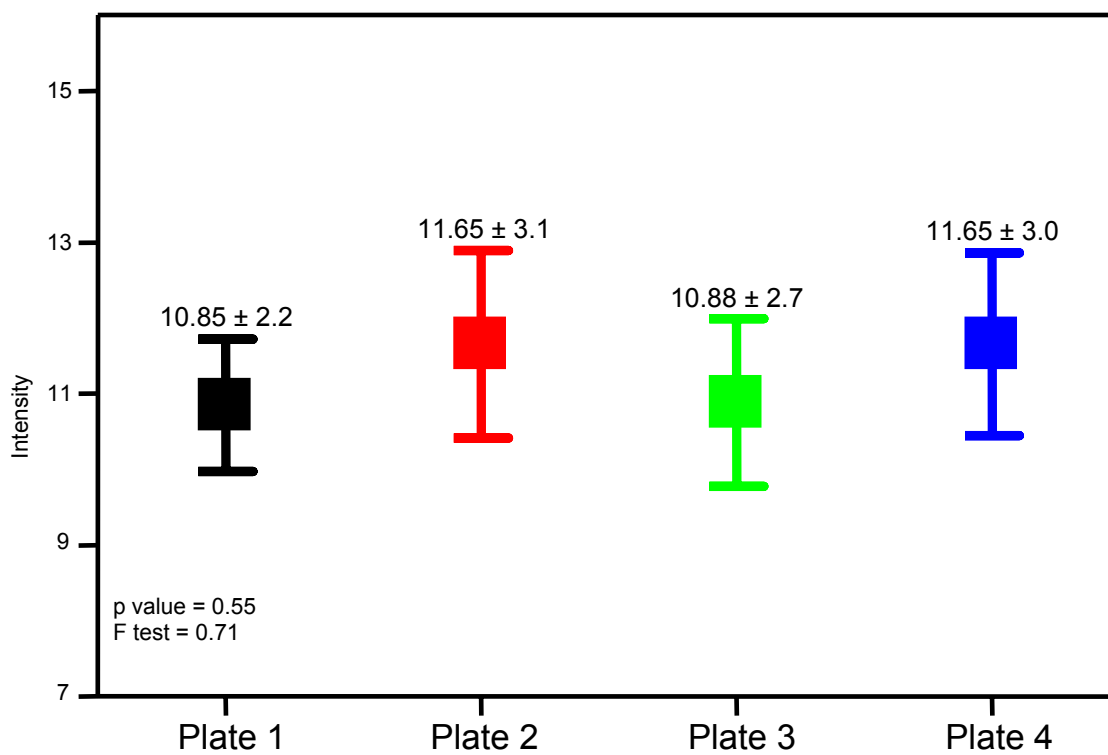


Figure 32. Plot of the average OLZ MALDI MS/MS signal from skeletal muscle across four sample plates demonstrates the reproducibility of the imaging methodology.

significant differences, indicating a highly reproducible whole-body image can be acquired using the methodology described here.

Olanzapine Quantitation by HPLC-MS/MS

For validation of the OLZ signal intensity variations observed across different tissues in a whole-rat MALDI MS/MS image, quantitation by traditional HPLC-MS/MS methods were employed. OLZ was extracted from dosed organ homogenates to determine the bulk concentration of drug in brain, liver, and kidney (Table 6). The ratios of the HPLC-MS/MS values were compared to the ratios of the normalized OLZ MALDI MS/MS signal from the tissue brain, liver, and kidney regions (Table 7). At all time points, imaging signal ratios correlated very well to the extraction study. Similar results were obtained for the metabolite MALDI MS/MS image signals; however at the request of Eli Lilly and Co., that data cannot be shown. Nevertheless, quantitation results indicate that the MALDI MS/MS imaging methodology can be used to detect the relative amount of drug in tissues across a whole-body section tissue.

Discussion

Olanzapine (brand name Zyprexa) is a drug of the thienobenzodiazepine class and is generally used to treat mood disorders such as schizophrenia and acute mania in bipolar patients. As with many atypical antipsychotic drugs, the precise mechanism of action for OLZ is unknown. However, it has been proposed that OLZ works by blocking certain serotonin type 2 (5HT₂) and

Table 6. Bulk quantitation results of OLZ from tissue extracts.

OLZ	HPLC-MS/MS Quantitation ($\mu\text{g/g}$)		
	2 h	6 h	24 h
Brain	57.3 \pm 18.7	3.74 \pm 1.43	2.64 \pm 0.78
Liver	91.5 \pm 21.3	30.2 \pm 6.15	29.7 \pm 5.94
Kidney	117.0 \pm 4.81	52.9 \pm 4.45	13.7 \pm 2.47

Table 7. Comparison of OLZ tissue ratios from MALDI MS/MS imaging signals to HPLC-MS/MS quantitation

OLZ	MALDI MS/MS Imaging			HPLC-MS/MS Quantitation		
	2 h	6 h	24 h	2 h	6 h	24 h
Liver/Brain	1.59 \pm 0.75	11.2 \pm 3.77	N/A	1.60 \pm 0.44	8.07 \pm 2.37	11.3 \pm 2.82
Kidney/Liver	1.29 \pm 0.50	N/A	0.49 \pm 0.26	1.28 \pm 0.18	1.75 \pm 0.25	0.46 \pm 0.09
Kidney/Brain	2.06 \pm 0.86	N/A	N/A	2.04 \pm 0.38	14.1 \pm 3.31	5.18 \pm 1.24

dopamine receptors.^[86] Pharmacokinetic studies of OLZ indicate that it is well absorbed after a single-dose oral administration, reaching peak plasma concentration within 5-8 h in humans^[86] and within 45 min for rats.^[87] At 2 h post-dose, WBA data revealed that radioactivity associated with [¹⁴C]OLZ was readily distributed throughout the tissue of an entire rat^[85]; however, no information as to the molecular identity of the drug was obtainable by this technique. The MALDI MS/MS images obtained in this study are the first examples of simultaneous drug and metabolite imaging in whole animals, thus allowing for the systemwide evaluation of each compound in a single animal section.

Biochemically, three families of cytochrome P450, CYP1, CYP2, and CYP3, are known to participate in the metabolism of drugs.^[88] Previous studies suggest that OLZ is eliminated extensively by first-pass metabolism, acting as a substrate for the cytochrome P4501A2 and P4502D1-5 enzymes in rat (analogous to human CYP1A2 and CYP2D6), with 40% of the OLZ dose metabolized before reaching systemic circulation.^[86] Olanzapine's t_{max} for peak concentration in rat tissues was determined in previous PK studies to be 2 h postdose.^[85, 89] In the 2 h MALDI MS/MS images, the drug is clearly localized in the target organs brain and spinal cord. The prominent signal for OLZ in the liver is consistent with significant drug elimination by first-pass metabolism. However, OLZ was also seen localized to the bladder, indicating elimination in an unchanged form, consistent with previous drug data which found that 7% of the OLZ dose was recovered in the urine in its original form.^[86]

The study also shows that liver, kidney, and bladder had prominent signals for OLZ and its metabolites, N-desmethyl and 2-hydroxymethyl metabolite. On the basis of the MALDI MS/MS images, the 2-hydroxymethyl metabolite, produced by the CYP2D1-5 enzymes, was detected as the more abundant metabolite over the N-desmethyl olanzapine. This may be due to several factors: 1) five isoforms of the CYP2D enzymes exist in rat^[88] (as opposed to the single form present in human, CYP2D6) allowing for increased substrate (OLZ) uptake and metabolite (2-hydroxymethyl olanzapine) turnover; 2) differences in the relative expression and catalytic activity of CYPs in rat liver versus human liver can result in large variations in the *in vivo* metabolic clearance of OLZ; and 3) external sources of variability such as diet, exercise, and environmental exposure can modulate activity of the CYP2D enzymes. It has been determined that at steady-state conditions (multiple dosing) in human the 10-N-glucuronide and N-desmethyl metabolites are the major circulating metabolites produced by direct glucuronidation and CYP1A2 pathways, respectively.^[86] In the case of rat metabolism, little is known about the involvement and preference of CYPs after a single oral dose of OLZ; however, the formation of glucuronide metabolites is an insignificant pathway for metabolic clearance of drugs^[90], and these metabolites were not detected in this study. Additional studies will be needed to identify all major metabolic pathways and enzymes responsible for the clearance of OLZ in rats.

Since the traditional means of quantifying a drug from tissue requires excision of the tissue or organ, homogenization and extraction, and analysis on a

LC-triple quadrupole system, these same classical procedures were performed in this study. The comparison of the imaging MALDI MS/MS OLZ signal in the target organ, brain, and other major organs (liver and kidney) to the HPLC MS/MS quantitation study of dosed tissue homogenates showed good correlation. However, an analysis by MALDI MS/MS gains the advantage of preserving the spatial distribution of the analyte within a tissue sample. The strong correlation of relative drug quantities validates the dynamic signal intensities detected by MALDI MS/MS in a whole-animal tissue section. In addition, this study demonstrates the reproducibility of the MALDI MS/MS imaging methodology, since consistent signals were accurately obtained from the individual analysis of multiple plates over several days.

In this study, MALDI MS/MS was successfully applied to whole-rat sagittal sections. Individual distributions of olanzapine and its subsequent metabolites were monitored across an entire rat in a label-free and molecularly specific manner by the novel imaging MALDI MS/MS methodology. In addition, the MALDI MS/MS images accurately represented the relative quantities of OLZ present in tissues across the whole-rat section.

Materials and Methods

Materials

The MALDI matrix, 2,5-dihydroxybenzoic acid (DHB), was purchased from Sigma Chemical Co. (St. Louis, MO). Olanzapine (OLZ) drug and metabolite

standards were produced by Lilly Research Laboratories (Eli Lilly and Co., Indianapolis, IN). HPLC grade acetonitrile, methanol, and hexane were purchased from Fisher Scientific (Suwanee, GA). HPLC grade cyclohexane was purchased from Acros Organics (Geel, Belgium). Fischer 344 rats were purchased from Charles River Laboratory, Inc. (Wilmington, MA). For animal dosing, Zyprexa tablets (OLZ) were obtained from the Vanderbilt University Hospital Pharmacy. All animal studies were approved by the Institutional Animal Care and Use Committee at Vanderbilt University.

Tissue Preparation

OLZ drug was administered at pharmacologically relevant doses (p.o. 8 mg/kg) to 10 week-old male Fischer 344 rats, which had fasted overnight prior to start of study. Animals were euthanized at 2, 6, and 24 h post OLZ dose by isoflurane anesthesia followed by exsanguinations via cardiac puncture. Control and dosed animal carcasses were frozen in hexane/dry ice and stored at -80 °C. Individual animal carcasses were frozen in a block of ice, and 20 µm thick whole-body sagittal tissue sections were collected on acetate film tape (3M, St. Paul, MN) using a Leica CM3600 cryomacrocut (Leica Microsystems, Inc., Germany) at -20 °C. Tissue sections were allowed to freeze-dry overnight at -20 °C. Whole-body tissue sections were then mounted onto consecutive gold-coated MALDI target plates (Applied Biosystems, Inc., Foster City, CA) using conductive double-sided tape (3M). All plates were stored in a vacuum desiccator until analyzed. Each plate from a single 20 µm thick dosed whole-body tissue section

were individually spray-coated with 20 mL of DHB (40 mg/mL) in 70% methanol, 2 μ M 2-ethyl olanzapine internal standard spike, using a glass spray nebulizer (Kontes, Vineland, NJ). At 30 cm from the target plate, a cycle (3 spray passes) of matrix coatings was applied for 25-30 cycles, with 1-3 min ambient drying time between cycles. All matrix coated tissue sections were allowed to dry under ambient conditions for \sim 1 h prior to MALDI MS/MS analysis.

MALDI MS/MS Imaging

Image analyses were performed on a QStar XL (MDS Sciex, Concord, Canada) equipped with an oMALDI source (20 Hz 337 nm nitrogen laser) and a hybrid QqTOF mass analyzer to obtain MS/MS data. Fragmentation was achieved using a collision energy of 30 eV with an argon collision gas at a pressure of 0.04 mTorr. OLZ and metabolite detection was performed following the transitions: 1) OLZ m/z 313 \rightarrow 256, 2) N-desmethyl olanzapine m/z 299 \rightarrow 256, 3) 2-hydroxymethyl olanzapine m/z 329 \rightarrow 272, and 4) internal standard m/z 327 \rightarrow 270. Two transitions, analyte and internal standard, were monitored per pixel with 4 s accumulation time per transition (total of 8 s/pixel). Each image was automatically acquired at 600 x 400 μ m lateral resolution with a pixel shift of 200 μ m for each subsequent analyte image.

Data Processing

After completion of the MALDI MS/MS image acquisition, each plate was individually processed using the oMALDI server 5.0 software. Images were

normalized against internal standard signal and total signal threshold was set for each analyte image: 1) OLZ = 65, 2) N-desmethyl olanzapine = 9, and 3) 2-hydroxymethyl olanzapine = 9. Images were saved as jpeg files and imported into custom reconstruction software (Chapter II) to produce a single whole-body analyte image. Reconstruction error was found to be <48 μm (less than one MALDI MS/MS image pixel and 2 jpeg pixels).

For the OLZ image signal quantitation study, regions of interest were extracted from the MALDI MS/MS images using the oMALDI server 5.0 software. Average signal intensity and standard deviation for the image region were recorded. Extraction normalization factors (Chapter II) were applied to the average signal from each region: 1) brain = 1.0, 2) kidney = 2.0, and 3) liver = 1.4. Ratios of the normalized OLZ signal averages from each organ were then compared to the ratios of the bulk HPLC-MS/MS quantitation values extracted from tissue homogenates.

Drug and Metabolite Quantitation

Extraction study was modeled after published protocols of OLZ quantitation from dosed tissues.^[87, 89, 91] Each excised brain, liver, and kidney organ (N=3 per organ) was weighed and mass recorded. Organs were sampled in triplicate, and for each 100 mg of tissue, 1 mL of deionized water and 3 μg of internal standard was added and the mixture was homogenized (15 mL glass homogenizer, Fisher Scientific) until the homogenate appeared uniform by visual inspection. Homogenate was transferred to a 20 mL borosilicate glass test tube

(Fisher Scientific). Homogenizer was rinsed 2 times with 1 mL deionized water and rinse was added to test tube. A 1:1 volume of 0.5 M NaOH was added to the test tube and vortexed. A 10 mL volume of cyclohexane extraction solvent was added, test tubes capped, and inverted at 4 °C for 2 h. After inversion, the test tubes were centrifuged for 20 min. Organic layer was then transferred to a new test tube to dry under nitrogen gas at 37 °C. Samples were reconstituted in 300 µL of 10 mM ammonium acetate in 50% acetonitrile. Standard curves were prepared by spiking a control homogenate with the OLZ standard, which covered a concentration range of 1-1000 ng/g.

Samples were randomized and analyzed in triplicate on an ESI TSQ Quantum triple-quadrupole system (Thermo Scientific, Waltham, MA) equipped with an autosampler (set at 4 °C) and HPLC system. A C12 Synergi MAX-RP 150 x 2 mm column (Phenomenex, Torrance, CA) was used with a fast gradient run of mobile phase A (5:95 acetonitrile:0.5% acetic acid in water, 10 mM ammonium acetate) to mobile phase B (95:5 acetonitrile:0.5% acetic acid in water, 10 mM ammonium acetate).

CHAPTER V

IMAGING MALDI MASS SPECTROMETRY FOR THE DISCOVERY OF MOLECULAR FEATURES INDICATIVE OF EARLY DRUG EFFICACY

Introduction

Essential to the success and approval of a drug by the FDA, pharmacodynamic (PD) studies are required to evaluate the pharmacological response of a therapeutic candidate. PD studies usually occur in the development stage using small animal models to determine mechanisms of action, as well as, acceptable parameters of a compound before advancing on into the clinical trials.^[11] These parameters include establishing therapeutic efficacy, dosing schedule, and potential toxicity of an administered compound.^[11, 13, 80, 92] Several mechanisms can be responsible for the observed pharmacological effects of a compound and are often unpredictable by *in vitro* studies performed in the discovery phase. For this reason, animal studies are an invaluable tool to help assess the PD profile of a drug *in vivo*.

Evaluation of a drug's PD profile is traditionally based on the phenotypic response of an animal. These responses can be determined from behavioral studies, diagnostic imaging, or detection of a biochemical endpoint.^[71, 80] The latter has become a major driving force for the evaluation of pharmacological response due to the recent discovery of many biomarkers. These biomarkers are obtained by extensive genomic and proteomic studies and can be selected to represent a desired biological endpoint.^[3, 61, 93] Unfortunately, biomarkers are not

available for the evaluation of all therapeutic pathways, since the *in vivo* mechanisms of action for most new drug compounds are not completely understood. As a result, evaluations based on phenotypic responses such as a decrease in tumor burden determined by an imaging study or physiological improvements observed by a behavioral study are heavily relied upon.

In addition, these biochemical or physiological changes are related to the PK profile of the drug.^[11, 14, 64, 80] In other words, the concentration-effect relationship is used to provide a comprehensive picture of the activity of a drug, perhaps uncovering its mechanism of action. Drug concentrations are typically determined from plasma samples; however, with a few exceptions, most drugs exert their pharmacological activity in a target tissue and not the plasma.

Furthermore, protein binding of drugs in the plasma can influence the rate of uptake into tissues, while at the same time, a drug's binding affinity to a target can also influence the amount of drug localized in a particular tissue.^[80]

Therefore, kinetically, the rate of drug diffusion into tissue and the amount of drug sustained in tissue are independent processes. Often times, this relationship is not equal and plasma drug concentrations alone do not accurately represent the extent of drug in tissues, further complicating any conclusions that can be drawn from the PK/PD studies. Correlating the spatial distribution of a drug in a target tissue with an observed pharmacological response is an essential component to understanding the PK/PD profile of a drug and still remains a difficult task to accomplish.^[80]

Imaging MALDI mass spectrometry has the potential to be used for the simultaneous detection of drug distribution and subsequent proteome changes from a single tissue sample. Previous work has shown that MALDI-TOF MS can be a valuable discovery tool for the identification of disease biomarkers by analyzing the proteome directly from a tissue section.^[37, 55, 57, 94] MALDI-TOF MS analyses of proteome effects following drug administration have also been reported in the literature.^[37, 95] MALDI MS analyses have capacity to identify surrogate biomarkers indicative of pharmacological endpoints long before a phenotypic response manifests and can be used to rapidly evaluate the therapeutic efficacy or toxicity of a candidate compound. In addition, the previous chapter demonstrated the power of MALDI MS/MS analyses for the detection of exogenous drug distribution across multiple tissues present in an entire whole-rat sagittal tissue section.

Consequently, MALDI MS based imaging technologies were used in this study to detect the distribution of exogenous lithium and the subsequent pharmacological response in the proteome of mice with and without exposure to radiation. This case study was chosen since previous work has uncovered radiation as a known cause of neurocognitive impairments in the brain of children and adults^[96, 97], while recent work has demonstrated that chronic lithium administration can have a neuroprotective effect against such injuries.^[98, 99] *In vivo* evaluation of lithium efficacy has been performed by behavioral studies of animals that require a minimum 6 week waiting period for a phenotypic response to manifest. To augment this “wait and see” approach, imaging MALDI MS was

used to identify molecular features within the detected proteome that are indicative of early lithium efficacy against radiation-induced damage.

Results

Experimental Design

In this study, MALDI-TOF MS was used to directly analyze the proteins from radiation exposed mice brains with and without chronic lithium treatment to identify molecular features in the mass spectra indicative of early lithium efficacy. The experimental design required separating the stock of mice into two groups, control and those dosed for eight days with 40 mg/mL lithium. On day eight, immediately following the final lithium dose, the two groups were further separated, with one half of each group receiving a single 7 Gy dose of radiation. This experimental design ultimately provided four treatment groups: 1) control, 2) lithium only (Li+/IR-), 3) radiation only (Li-/IR+), and 4) lithium plus radiation (Li+/IR+) mice (Figure 33). At 1 h post lithium/radiation dose, the mice were sacrificed for the imaging LDI and MALDI MS analyses. For both LDI and MALDI MS analyses, three serial sections of whole-mouse head were collected from individual animals onto MALDI target plates, as well as, a single serial section onto a microscope slide for cresyl violet staining. The sections reserved for MALDI MS analysis were spotted with a high-resolution array of SA matrix droplets at 150 μm lateral resolution (Figure 34), while the LDI tissue sections required no further sample preparation. All tissues were analyzed on a MALDI-

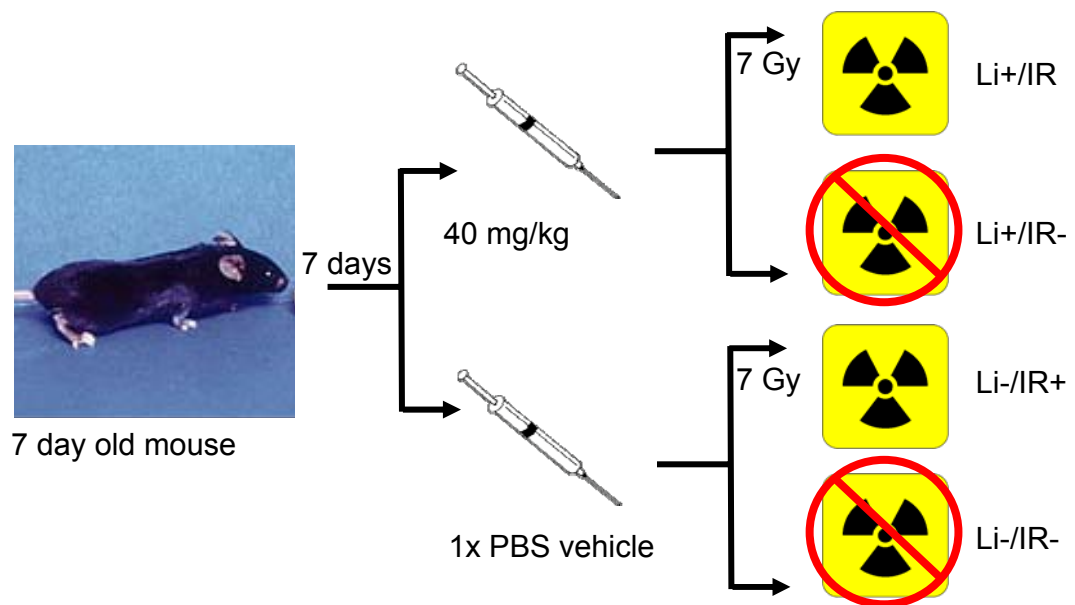


Figure 33. Schematic representation of the experimental design, which provided four treatment groups: 1) control, 2) lithium only (Li+/IR-), 3) radiation only (Li-/IR+), and 4) lithium plus radiation (Li+/IR+) mice.

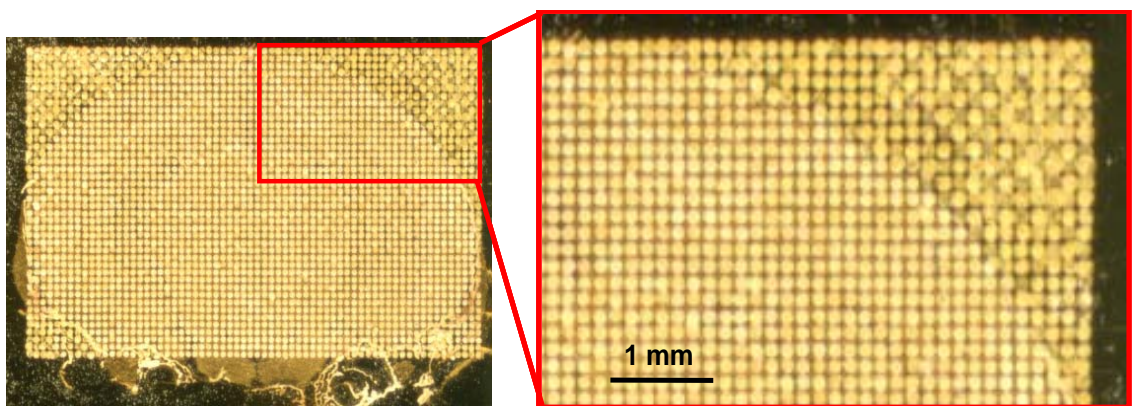


Figure 34. Optical images displaying the high-density array of SA matrix droplets at 150 μm lateral resolution on mouse brain tissue for analysis by MALDI MS. Right panel is a zoomed-in region of the left panel outlined in red.

TOF mass spectrometer under optimized conditions.

From previous studies, it is known that radiation induced neurocognitive effects are a result of injury to the proliferating neuronal progenitor cells in the subgranular zone of the hippocampus.^[98, 100] It has also been shown that chronic lithium treatment can exhibit a protective effect against radiation.^[98, 99] However, for this reason, data only from the hippocampal region was used for the discovery of molecular features indicative of early lithium efficacy. In order to identify the spectra representing only the hippocampus region of interest, the MALDI MS section and its corresponding cresyl violet stained serial section were co-registered after image acquisition to extract the data for statistical analysis (Figure 35). Typically, 100-150 spectra were extracted and contained between 250 to 400 individual protein signals in the mass range of 2-100 kDa. Evaluation of the degree of intra- and inter-sample variability was determined to be ~7 and 14 % CV, respectively (Figure 36). Therefore, for a peak (i.e. feature) to be considered statistically significant, a $>3\sigma$ fold change of 50% must be satisfied for features meeting a 99.9% confidence level. Significant features across all treatment groups were ranked according to a correlation matrix calculated by Kendall's algorithm and paired t-tests were performed for all treatment groups.

LDI MS Imaging of Lithium Distribution in Mouse Brain

To determine the distribution of lithium in the brain, laser desorption/ionization (LDI) mass spectrometry was employed (i.e. matrix-free MALDI MS). Images were acquired at 150 μm lateral resolution with each pixel

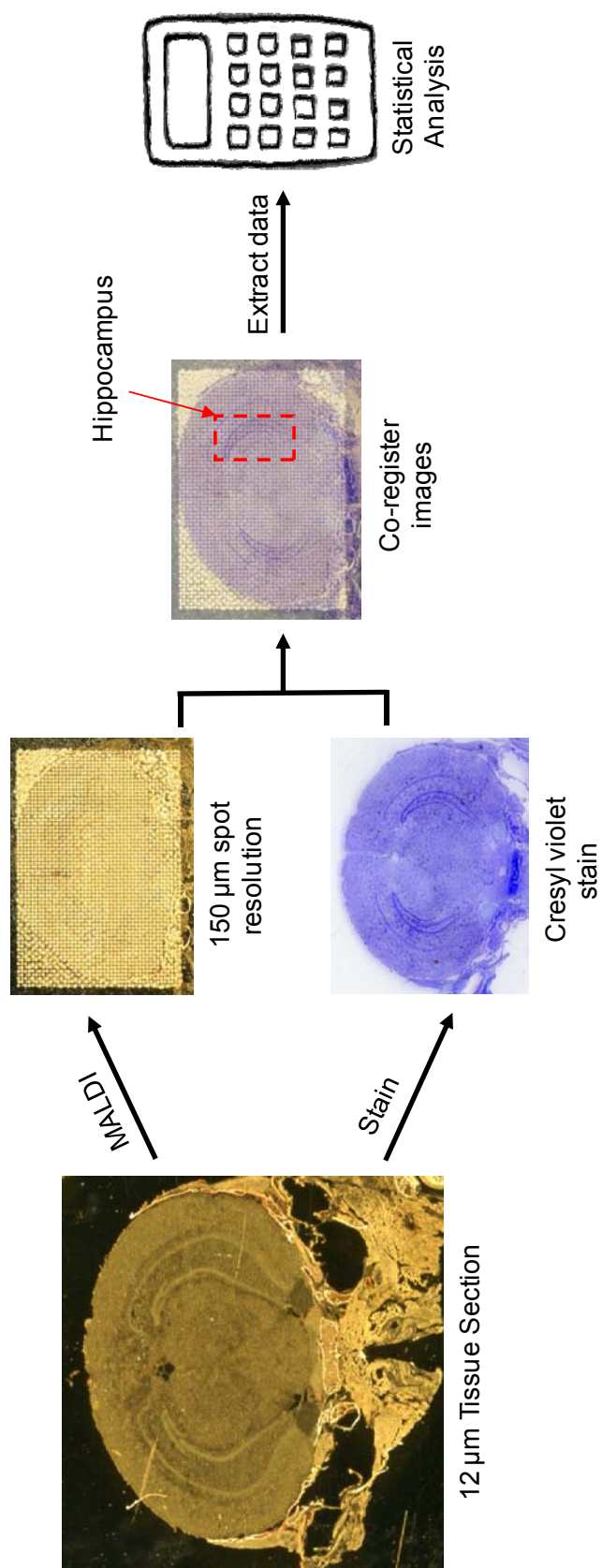


Figure 35. Schematic representation of analytical workflow. Co-registration of the cresyl violet and MALDI sections was performed after image acquisition to identify pixels in the region of interest for data extraction and statistical analysis.

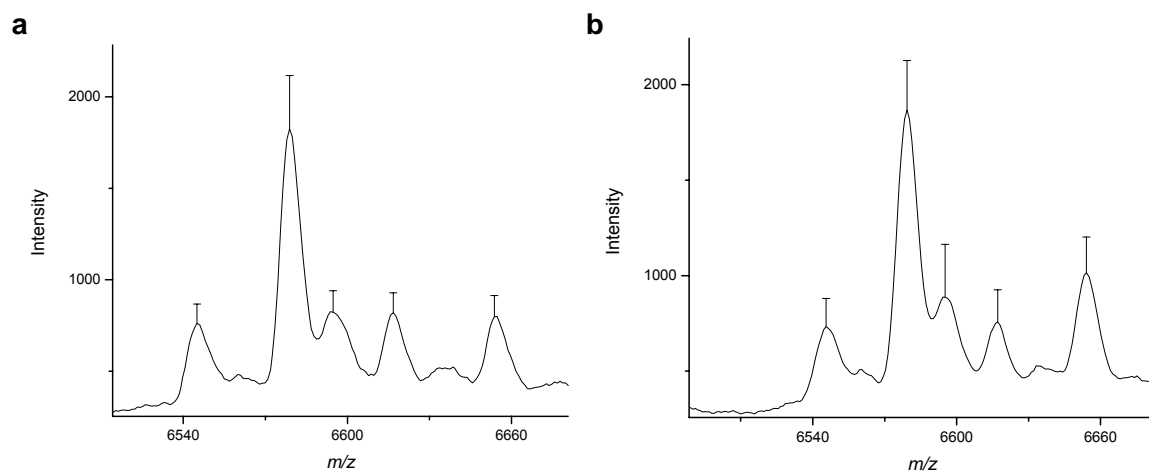


Figure 36. Evaluation of spectral variability in the cortex region of mouse brain. a) example peaks representing intra-sample variability of ~7% CV (average of 10 pixels) and b) inter-sample variability of ~14 % CV (3 animals).

representing the sum of 100 laser shots. The 1 h distribution of lithium was determined to be ubiquitous throughout all the dosed mice brains (Li+/IR- and Li+/IR+) analyzed, with noticeable localization in the gray matter, as well as, the hippocampus (Figure 37). LDI experiments of the non-lithium administered brains (control and Li-/IR+) detected no endogenous lithium to be present.

MALDI MS Imaging of Proteome in Mouse Brain

Preliminary work focused on verifying whether MALDI MS analysis of dosed tissues could monitor the temporal increase or decrease of protein signals as a result of lithium administration. Direct analysis of lithium dosed brain tissue sections at 15, 30, and 60 min post-dose revealed the largest pharmacological response at the 60 min time point (Figure 38). Since, pharmacological response is related to drug concentration, the 1 h time point was selected for the study presented here.

MALDI MS analysis was performed on over 24 individual brain sections, producing over 2500 spectra representing the hippocampus proteome of all four treatment groups. Spectra were separated into classes based on treatment group for statistical analysis, which revealed over 303 features to be statistically significant across the mass range of 2-30 kDa (Figure 39). Pairwise comparisons were performed to identify the subset of features that best indicated lithium efficacy (i.e. Li+/IR+ features most like control and least like Li-/IR+). The following comparisons were made: control vs. radiation only, control vs. lithium plus radiation, and radiation only vs. lithium plus radiation (Table 8). Of the

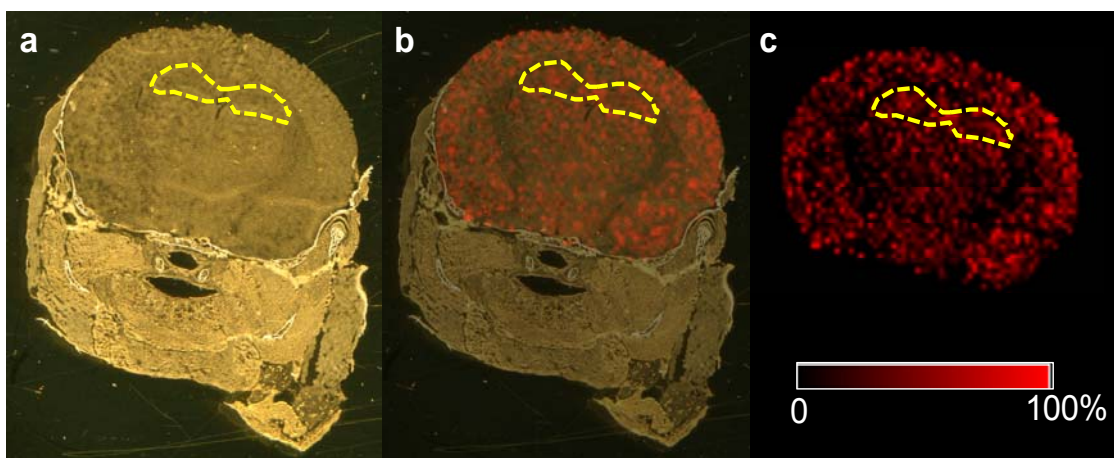


Figure 37. Lithium distribution as detected by imaging LDI-MS. a) optical image of 12 μm whole-mouse head section, b) overlay of optical and ion images, and c) LDI-MS ion image of lithium (m/z 7). Hippocampus region outlined in yellow dashed-line.

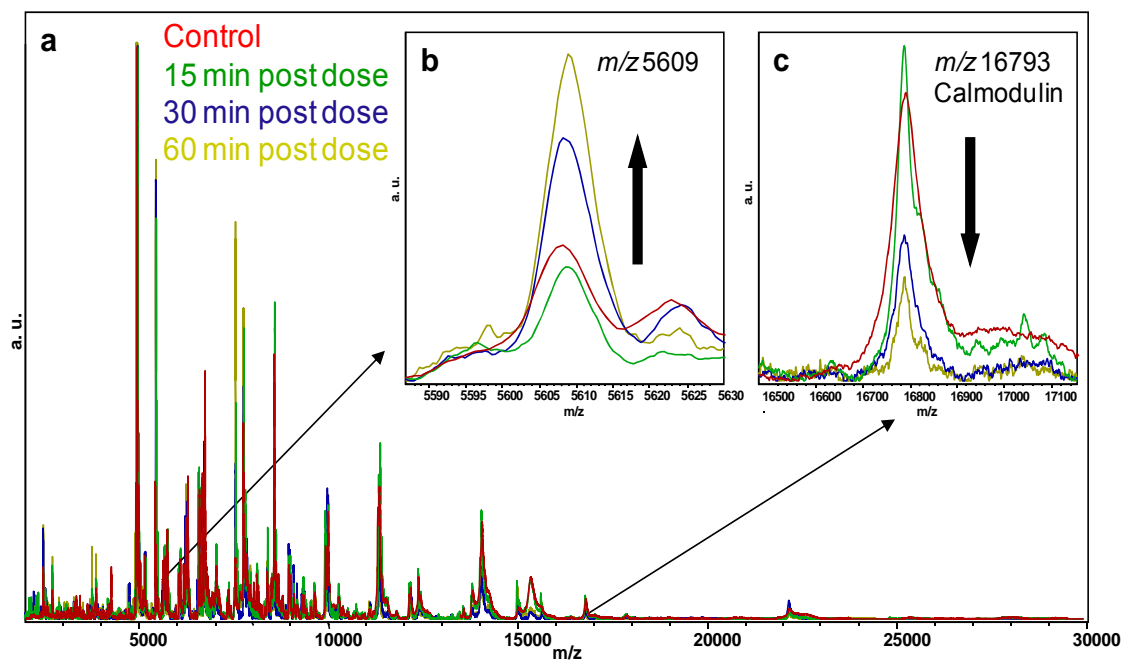


Figure 38. Temporal lithium dose response in proteome of hippocampus region detected by imaging MALDI MS. Two example features of a temporal increase and decrease as a result of lithium administration are shown in the zoom plots.

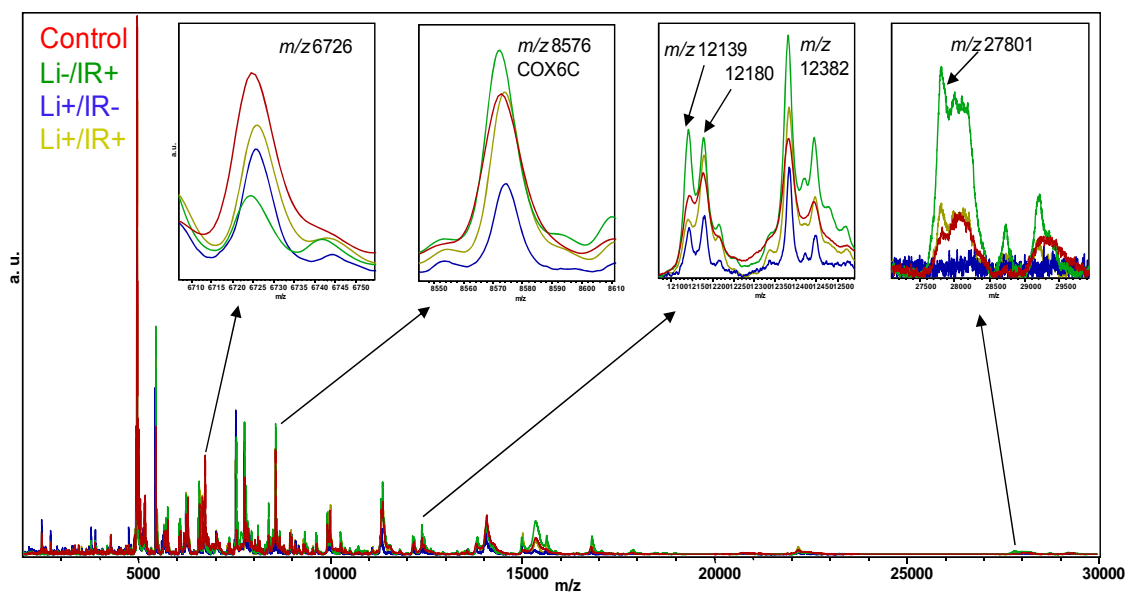


Figure 39. Overlay of average spectra from each treatment group and examples of statistically significant features across the mass range are displayed in the zoom plots.

features shared in common between control and lithium plus radiation samples (239 features), 30 features were found to be statistically significant from radiation only samples. This represents 13% of the total features. Additionally, only 2% of the features (5 out of 303) shared no commonality between control, lithium plus radiation, and radiation only samples. Therefore, 85% of the features are in common across the three treatment groups. It can be concluded that the 30 features detected by MALDI MS analysis are in fact true differences between the treatment groups and not a systematic analytical error. A list of the 30 features can be seen in Table 9 and these features can be considered as early indicators of lithium efficacy.

The average signal intensities of the significant molecular features were plotted for comparison across the treatment groups (Figure 40). Based on the plot, lithium treatment can be seen to reduce the effects of altered protein expression as a result of radiation exposure when compared to mice exposed to radiation without the lithium treatment. The average Li+/IR+ signal was found to be statistically indistinguishable from control.

The contributions of lithium administration and radiation exposure on the detected lithium plus radiation (Li+/IR+) protein signals were evaluated. Pairwise comparisons of the features measured as statistically significant between control and Li+/IR+ samples were performed against the lithium only and radiation only samples (Table 10). Of the 64 features found to be different between control and Li+/IR+ groups, 34 features were statistically indistinguishable between the lithium only and radiation only groups. Therefore, it was determined that 9

Table 8. Results of the pairwise comparisons for the statistically significant features.

Analysis	No. of Features in Common	Total Features	Percentage of Features
Control vs. Li-/IR+	206	303	68%
Control vs. Li+/IR+	239	303	79%
Li-/IR+ vs. Li+/IR+	240	303	79%
Control and Li+/IR+ vs. Li-/IR+	204	239	85%
Control vs. Li+/IR+ vs. Li-/IR+	204	303	67%
	No. of Significant Features		
Control and Li+/IR+ vs. Li-/IR+	30	239	13%
Control vs. Li+/IR+ vs. Li-/IR+	5	303	2%

Table 9. List of 30 statistically significant features indicative of lithium efficacy.

<i>m/z</i>	Fold-Change	Up / Down	t calculated	p value (t test)	p value (Wilcoxon)
3360	1.82	Down	11.04	<0.000001	0
3437	1.51	Down	9.42	<0.000001	0
3653	1.76	Down	12.16	<0.000001	0
3856	2.26	Down	17.51	<0.000001	0
3865	2.01	Down	15.09	<0.000001	0
4542	2.27	Down	15.91	<0.000001	0
4570	1.51	Down	9.77	<0.000001	<0.000001
4668	2.08	Down	14.09	<0.000001	0
4989	2.25	Down	19.70	<0.000001	0
6726	2.52	Down	12.09	<0.000001	0
7623	2.03	Up	22.03	<0.000001	<0.000001
7671	2.14	Up	14.51	<0.000001	<0.000001
7706	2.11	Up	12.21	<0.000001	<0.000001
7721	2.05	Up	14.24	<0.000001	<0.000001
7800	1.87	Up	29.2	<0.000001	<0.000001
7816	1.64	Up	13.37	<0.000001	<0.000001
7838	1.62	Up	14.24	<0.000001	<0.000001
8424	2.38	Up	30.46	<0.000001	<0.000001
8485	1.60	Up	14.04	<0.000001	<0.000001
8631	1.51	Up	11.65	<0.000001	<0.000001
9301	2.19	Down	11.35	<0.000001	0
11070	1.59	Down	11.57	<0.000001	<0.000001
11385	1.52	Up	5.70	<0.000001	0.0000165
12412	1.58	Up	15.80	<0.000001	<0.000001
12436	1.64	Up	18.46	<0.000001	<0.000001
15332	1.86	Up	6.87	<0.000001	<0.000001
15617	2.34	Up	7.68	<0.000001	<0.000001
16793	1.85	Up	16.20	<0.000001	<0.000001
17046	1.51	Up	9.46	<0.000001	<0.000001
27803	1.87	Up	15.72	<0.000001	<0.000001

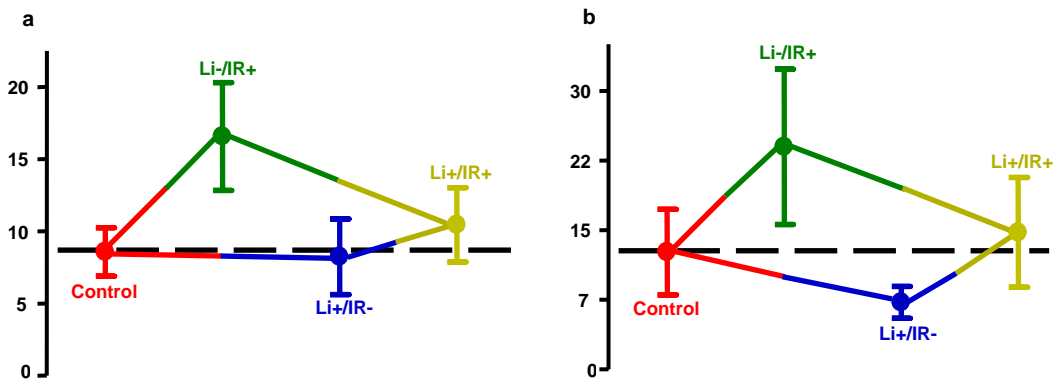


Figure 40. Protein signal plots of the average signal intensity of two features indicative of lithium efficacy show reduced aberrant protein expression as a result of radiation exposure. a) m/z 7800 and b) m/z 16793.

features were induced by the lithium administration, while 17 features were contributed by the radiation exposure, representing 14% and 27% of the features, respectively. Only four features were unable to be attributed to either lithium administration or radiation exposure.

Discussion

Radiation is a common therapy used for the treatment of both primary and metastatic tumors in humans. In the case of brain tumors, cranial radiation treatment causes neurocognitive defects in both children and adults.^[96, 97] Evidence suggests that neurocognitive defects from cranial radiation may involve injury to proliferating neuronal progenitor cells, as well as, radiation-induced apoptosis.^[101-104] Lithium has anti-apoptotic activity and has been previously shown to have neuroprotective effects against a variety of neurological injuries.^[105, 106] Specifically, recent studies have shown that chronic administration of lithium prior to cranial radiation protects against neurological injuries.^[98, 99] Typically, evaluation of lithium efficacy in *in vivo* radiation studies requires a 6 week waiting period for the phenotypic responses of neurological injury to manifest.^[98] In this study, imaging mass spectrometry was used to monitor the brain proteome of mice exposed to cranial radiation with and without chronic lithium treatment to determine potential markers of early lithium efficacy.

LDI MS imaging analysis of the mice brains following chronic lithium treatment for 8 days revealed lithium distribution to be relatively ubiquitous with a noticeable accumulation in hippocampus region of interest. A time course LDI

Table 10. Results of the pairwise comparisons for the features found to be statistically different from control to determine the contribution of lithium or radiation for that difference.

Li+/IR+ Features Significant from Control	No. of Features in Common	Total Features	Percentage of Features
Lithium induced peaks (Li+/IR+ vs. Li+/IR-)	9	64	14%
Radiation induced peaks (Li+/IR+ vs. Li-/IR+)	17	64	27%
Either lithium or radiation induced (Li+/IR- vs. Li-/IR+)	34	64	53%
	No. of Significant Features		
Neither lithium or radiation induced (Li+/IR- vs. Li-/IR+)	4	64	6%

MS imaging experiment (data not shown) detected lithium distribution to have the highest relative abundance at the 1 h time point. A similar analysis of the hippocampus proteome by MALDI MS analysis revealed a temporal increase in pharmacological response, with the largest change in signal detected at the 1 h time point. As a result, the increased pharmacological response detected in the proteome could be directly correlated to the increased concentration of lithium in the highly localized hippocampus region of the mice brains. This finding demonstrates the capacity of imaging MALDI MS to simultaneously relate the PK distribution profile of a drug to its PD response with high spatial resolution.

Statistical analysis of the protein spectra obtained from the hippocampus region of the brain at 1 h post lithium/radiation dose revealed 30 molecular features in the control mice that were conserved in the spectra of the lithium protected radiation mice but significantly aberrant in the radiation only mice. Therefore, it can be concluded that these features are indicative of early lithium efficacy and can be used as markers in future studies to rapidly evaluate the PD profile of lithium.

One of the significant features has been previously identified as calmodulin (m/z 16793). Calmodulin is a calcium-binding protein that is known to indirectly regulate many cellular functions by binding a multitude of proteins involved in inflammation, metabolism, apoptosis, memory, and nerve-growth, to name a few.^[107] Evidence has been reported that chronic treatment of lithium can lead to the robust inhibition of Ca^{2+} influx into the granule cells of the brain.^[108, 109] If less Ca^{2+} is present in these cells, then less calmodulin would be

needed. This physiological response can be seen in the temporal decrease of calmodulin signal following chronic lithium administration by imaging MALDI MS.

On the other hand, reports in the literature have suggested that increased Ca^{2+} levels are seen in mitochondria from brain cells that are undergoing apoptosis.^[110, 111] It is believed that this increase in Ca^{2+} is caused by prolonged activation of the mitochondrial permeability transition pores.^[112] Interestingly, chronic lithium treatment has been shown to inhibit glycogen synthase kinase-3, a known pro-apoptotic enzyme, while increasing anti-apoptotic proteins such as Bcl-2.^[98, 113, 114] The proteins are known to mediate the Ca^{2+} levels in mitochondria by the activation or inactivation of the mitochondrial permeability transition pores. MALDI MS analysis revealed nearly a 2-fold increase in calmodulin levels in the radiation only mice as compared to control and Li+/IR+ mice. Radiation exposure is known to cause DNA damage and subsequent apoptosis.[ref] Perhaps the increased expression of calmodulin is a result of the activation of endogenous repair mechanisms attempting to chelate the excess Ca^{2+} . Thus, the statistically significant detection of calmodulin as an indicator of early lithium efficacy can be thoroughly rationalized.

In summary, the MALDI MS data obtained in this study were able to provide 30 molecular features indicative of lithium efficacy. Correlating lithium distribution to proteome response in the hippocampus by LDI and MALDI MS analyses provided a means to directly correlate drug distribution with pharmacological response and provided insight into the concentration-effect relationship. Further work needs to be performed to determine the identity of the

molecular features in order to rationalize the biological significance of these proteins and for validation for use of these features as early markers of lithium efficacy in future studies.

For example, the molecular feature previously identified as calmodulin was shown to have significant expression levels as result of lithium protection against radiation-induced damage in hippocampal cells. The hippocampus is the center for learning and memory and calmodulin has a known role in short- and long-term memory.^[101] Now, targeted experiments can be performed to further elucidate the exact function of calmodulin in this process. In addition, imaging LDI MS experiments can be performed to monitor the endogenous Ca^{2+} levels to corroborate the detected expression changes of calmodulin in the hippocampus region.

Given that the ultimate goal of PD studies is to relate the pharmacological response to dose-concentration or concentration-effect relationships of a therapeutic compound and its metabolites, a technology such as imaging MALDI MS can provide an invaluable tool to rapidly and reproducibly relate the tissue distribution of a drug to the observed pharmacological response within the same animal while maintaining spatial resolution.

Materials and Methods

Materials

The MALDI matrix, 3,5-dimethoxy-4-hydroxycinnamic acid (sinapinic acid, SA), and lithium chloride salt were purchased from Sigma Chemical Co. (St. Louis, MO). HPLC grade acetonitrile and ethanol were purchased from Fisher Scientific (Suwanee, GA). C57BL mice were provided by the department of radiation oncology at Vanderbilt University (Nashville, TN). All animal studies were approved by the Institutional Animal Care and Use Committee at Vanderbilt University.

Tissue Preparation

Lithium chloride drug was chronically administered at pharmacologically relevant doses (i.p. 40 mg/kg) to 7 day-old C57BL mice for seven days prior to start of study. On day eight, control (non-lithium dosed) and chronic lithium administered mice were divided into four treatment groups: control, lithium only (Li+/IR-), radiation only (Li-/IR+), and lithium treated radiation exposed (Li+/IR+) mice (N=2-3 mice per treatment group). A final lithium dose was administered and immediately following, the radiation mice were given a 7 Gy dose. All mice were euthanized at 1 h post lithium/radiation dose by exsanguination through the eye. Control and dosed carcasses were frozen in hexane/dry ice and stored at -80 °C. Individual animal carcasses were decapitated and the heads sectioned at 12 µm thickness using a Leica 3050S cryomicrotome (Leica Microsystems, Inc.,

Bannockburn, IL) at -20 °C. Six serial tissue sections from the hippocampus region of interest were thaw-mounted onto two gold MALDI target plates (3 section/plate) and additional serial sections were collected onto microscope slides for cresyl violet staining^[115]. Tissue sections reserved for LDI and MALDI-TOF MS analysis were allowed to dry in a vacuum dessicator for ~2 hr prior to matrix deposition. MALDI MS tissue sections were rinsed 2x in 70% ethanol wash for 30 s and 1x in 95% ethanol wash for 15 s, then individually spotted with 25 mg/mL SA prepared in 60:40 acetonitrile:0.6% TFA in water using a Portrait 630 Reagent Multispotter (Labcyte, Sunnyvale, CA) at 150 µm lateral resolution. All matrix coated tissue sections were allowed to dry under ambient conditions for ~1 h prior to MALDI MS analysis.

LDI and MALDI MS Imaging

LDI and MALDI MS image analyses were performed on an Autoflex II (Bruker Daltonics, Inc., Billerica, MA) MALDI-TOF mass spectrometer equipped with Smartbeam laser technology (200 Hz 355 nm Nd:YAG laser) using the FlexImaging 2.0 software (Bruker Daltonics, Inc.). LDI data were collected at 150 µm lateral resolution in positive, reflector mode with an accelerating voltage of 19 kV and a reflector voltage of 20 kV. LDI spectra represent the mass range of 1-40 Da and the sum of 100 laser shots per pixel (Smartbeam modulation turned off). MALDI MS data were obtained over the mass range of 2-100 kDa in positive, linear mode with an accelerating voltage of 20 kV, and under optimized

delayed extraction conditions (300 ns). A total of 400 laser shots were summed over each matrix spot.

Data Processing

After completion of the LDI and MALDI image acquisitions, data were processed for baseline correction (convex-hull), normalized, and ion images displayed (peak integration) using the FlexImaging 2.0 software (Bruker Daltonics, Inc.). For the extraction of MALDI MS data, image data sets were co-registered to cresyl violet stained serial sections using the FlexImaging 2.0 software. Pixels corresponding to the hippocampus region, as defined by the stained section, were selected and exported for statistical analysis.

Statistical Analysis

Extracted spectra from the hippocampus region were loaded according to treatment groups into ClinProTools 2.0 (Bruker Daltonics, Inc.) statistical analysis software. All spectra were baseline subtracted using a convex-hull algorithm and normalized. Null spectra, as well as, spectra failing to meet a mean signal to noise ratio (S/N) of 2.0 across the analyzed mass range were rejected and thus not included in the statistical analysis. Spectra were realigned allowing for a possible 1500 ppm mass window shift and a 20% minimum peak-to-peak match. Those spectra unable to be realigned by the preceding parameters were withheld from data analysis. The peaks achieving a S/N of 3.0 after all processing steps were individually integrated to determine peak area.

For statistical analysis, peak areas representing each class were averaged and their standard deviations calculated. Pair-wise peak comparisons were made between classes. Deviations were pooled and mean peak areas were compared using a t-test, where the calculated t values had to surpass a 99.9% confidence levels in order to be considered as significant. Bartlett's test was performed to verify the likeness of variance and the inter-animal variability was measured to be ~14%. Therefore, only peaks meeting a 99.9% confidence level while exceeding a minimum of 1.5 fold change ($>3\sigma$) were deemed to be statistically significant. A correlation matrix was calculated by Kendall's algorithm to rank peaks closely associated with those measured as significant.

CHAPTER VI

CONCLUSIONS AND PERSPECTIVES

Endogenous and Exogenous Compound Analysis in Whole-Animal Tissues by Imaging MALDI Mass Spectrometry

Through the course of this research, a dosed tissue model assay was developed to provide a method for the prediction of matrix/solvent preferences of exogenous compounds in dosed tissues for analysis by MALDI MS/MS. This model assay allows for the analysis of any matrix/solvent combination to determine the optimal conditions for analyzing exogenous small molecules (i.e. drug and metabolite compounds) from dosed tissues. Additionally, the model assay allows for the screening of a large number of drug compounds to determine their potential for an imaging MALDI MS/MS experiment without ever dosing an animal.

In summary, the model assay provided a means to streamline sample preparation parameters by predicting the optimal matrix/solvent combination for analysis of OLZ, as well as other exogenous compounds, in dosed whole-animal tissue section by MALDI MS/MS. Specifically, the model assay identified that matrix/solvent conditions were unique to a drug class (i.e. dictated by the chemical structure of drug), as well as, the targeted tissue for analysis and that DHB in 50% methanol could serve as an adequate universal matrix for first-pass qualitative analyses. This methodology can now be applied to a larger cohort of compounds to further identify more significant trends, perhaps in the future,

providing a guide for matrix/solvent selection based on the chemical structure of the analyte alone.

Succeeding imaging experiments performed by MALDI MS/MS were able to provide the individual, label-free temporal distributions of olanzapine and its metabolites in whole-rat sagittal tissue sections with high sensitivity and reproducibility. Image resolution, instrument parameters, and analyte selection can be tailored for sensitivity and throughput, further maximizing the reproducibility of the imaging MALDI MS/MS application. Highly-accurate relative quantities of olanzapine in brain, liver, and kidney tissues could also be obtained from the MALDI MS/MS ion images when proper normalization factors were considered. These results are in line with previous quantitation studies from dosed tissue homogenates and WBA distribution studies of olanzapine.^[85-87, 89, 90] Therefore, it has been demonstrated that MALDI MS/MS imaging can be applied in the early PK evaluations of an administered therapeutic candidate and its metabolites in a small animal model.

Moreover, PK studies by MALDI MS/MS can be combined with PD studies using MALDI MS. In the case study presented in Chapter V, proteomic analysis by MALDI-TOF MS identified 30 molecular features in the mass spectrum that were indicative of early lithium efficacy for protection against radiation-induced damage in the hippocampal region of a mouse brain. The capacity to detect drug distribution and proteome response from the same tissue sample will have a huge impact on the pharmaceutical industry. Currently, such correlations are performed using unbound plasma concentrations of drug as a surrogate for

actual tissue concentrations. It is believed that pharmacological activity can be related to the unbound drug in the plasma. However, this key assumption is not always valid and can make attempts at understanding the relationship between drug concentration in target tissues and pharmacological response difficult.

Therefore, technologies such as MALDI MS based imaging technologies that can correlate the actual drug distribution in tissues to pharmacological response in an accurate manner will be an essential tool for evaluating the potential success of a candidate drug compound. Establishing and validating the identified biological endpoints could provide new biomarkers indicative of efficacy or toxicity.

Screening for these biomarkers in the proteome by imaging MALDI MS can provide a rapid assessment of therapeutic success or whether reoptimization of the treatment regimen is needed.

Research Perspectives

The promise of drug discovery lies in the potential to understand a disease process at the molecular level and to determine the optimal molecular targets for drug intervention. Currently, there are only 500 molecular targets for which drugs have been developed^[116] and it is estimated that there are at least 10 times as many molecular targets that can be exploited for future drug therapy than are being used today.^[1] Genomics and proteomics offer the promise of providing new selective drug targets for a large number of disease, which in turn spurs the development of many more therapies aimed at smaller patient populations (i.e. individualized medicine). Validation of the new drug targets will require the *in*

vivo PK and PD evaluations of many new compounds aimed at producing a desired therapeutic effect. Better analytical technologies aimed at answering ADME and efficacy or toxicity parameters are needed, while keeping research and development expenditures low.

Imaging mass spectrometry has the potential to improve the understanding of complex molecular events that take place at the protein, peptide, or lipid level of disease, therapeutic response, or even toxicological effects in animal models of disease, while also providing information about the individual distribution of drug and metabolites in animal models. The IMS methodology developed in this study for the analysis of endogenous and exogenous compounds in whole-animal tissue sections is one significant step closer to improving the productivity of pharmaceutical research.

Much of the IMS methodology can be owed to the established WBA protocols, which were expanded upon and optimized for the MALDI MS and MS/MS technologies. Since WBA is a mandatory procedure for drug approval by the FDA, integrating whole-body IMS into the pharmaceutical workflow should be relatively easy. However, the true advantage of the IMS technology lies in the rapid, label-free and molecularly specific MALDI MS/MS analyses that can be performed long before a labeled drug candidate is ever synthesized for WBA. Imaging of whole-animal tissue sections by IMS will be a significant means of early PK and PD assessments of drug candidates. These earlier assessments will streamline the evaluation and selection of lead compounds entering the development phase, where the cost of moving a drug along the pipelines

escalates rapidly. The earlier the PK and PD profiles are established, the more tailored drug research can become. With a more focused understanding of the molecular events that lead to a drug candidate's efficacy or potential side effects that can be gained by an IMS analysis, the pharmaceutical industry will have the capacity to deliver valuable new therapies to the public, extending and improving patients' lives safely and more effectively.

Future Research Directions

This thesis research has developed a methodology to analyze endogenous and exogenous compounds directly from whole-animal tissue sections; however there are still many questions that need to be explored. For example, the olanzapine study was able to demonstrate the quantitative values that can be obtained from a MALDI MS/MS experiment. Relative information about the quantities of drug as it localizes in various tissue in an animal is of value; however, the true worth of this technology would be the capacity to detect *absolute* quantities of drug and metabolites across a whole-animal tissue section in a single imaging experiment. Answering this question will not be trivial as many factors contribute to the signals observed in an imaging MALDI MS/MS analysis. For example, accumulation of a drug in a particular tissue section is not likely to be uniform and therefore a single pixel intensity can not be directly correlated to the bulk quantities identified by HPLC-MS/MS. In addition, heterogeneous crystal formation and non-uniform inclusion of the analyte into the crystals, as well as, shot-to-shot variability of the MALDI process can all

contribute to fluctuations in detected drug signal, making absolute quantitation by MALDI MS/MS a difficult task. However, it is reasonable to assume that a MALDI MS/MS methodology can be developed that will normalize these variations, as was the case in this study, which identified the relative quantities of OLZ by normalizing the ionization and extraction efficiencies of the analyte in various tissues.

Imaging MALDI mass spectrometry has also been shown to correlate the distribution of a drug to aberrant protein expression or distribution in a tissue sample in a qualitative manner. Of greater interest would be the *quantitative* correlation of protein changes to the *absolute* drug quantity at a particular location in the tissue sample. This technology could then be readily applied to identify potential biomarkers of efficacy or toxicity with high precision and accuracy, while possibly providing clues to the mechanism of action seen in the pharmacological response. Furthermore, application of this technique to large sample sets can provide an unbiased, high-throughput means of identifying molecularly specific features unique to individual non-responders of therapy. Identification of these features can aid in the screening of patient populations for likely response to a treatment regimen.

Whole-body imaging has expanded the two-dimensional capabilities that have been previously demonstrated by the IMS technology. Further expanding this technology into the z-direction will allow for the three-dimensional analysis of whole-animal tissue sections and work has already begun in this area. Through the course of this research, a novel methodology was developed to acquire and

reconstruct spatially resolved three-dimensional MALDI MS ion images and to co-register these images to *in vivo* imaging modalities, such as magnetic resonance imaging (MRI), CT, and PET.^[117]

A proof-of-concept experiment was performed using a glioma (GL26) mouse model to correlate the *ex vivo* molecular proteomic information gained in the MALDI MS analysis to the tissue contrasts observed in the *in vivo* images obtained by MRI. Prior to the MALDI MS analysis, MR images were obtained on a 7T magnet (Varian, Inc., Palo Alto, CA) to produce quantitative parametric images of the longitudinal relaxation time (T_1), transverse relaxation time (T_2), and apparent diffusion coefficient (ADC) (Figure 41). After imaging, the mouse was immediately prepared for analysis by MALDI MS (protocol described in Chapter II). During the sectioning process, optical images of each blockface section (40 μm) were acquired using a high-resolution digital camera (Canon, Inc., Lake Success, NY) and reconstructed into a continuous image volume (Figure 42). Whole-mouse head tissue sections from selected regions of the blockface volume encompassing the spatial extent of the tumor were collected for analysis by imaging MALDI-TOF MS (150 μm lateral resolution and 300 shots/pixel). MALDI MS data were inserted and co-registered to the corresponding image slice in the blockface volume. The MRI data was then rigidly co-registered to the blockface volume as well, thus inherently co-registering the MALDI MS to the MRI data.

For example, ion volumes for two proteins, astrocytic phosphoprotein PEA-15 (m/z 15035) and fatty acid binding protein 5 (m/z 15076), were rendered

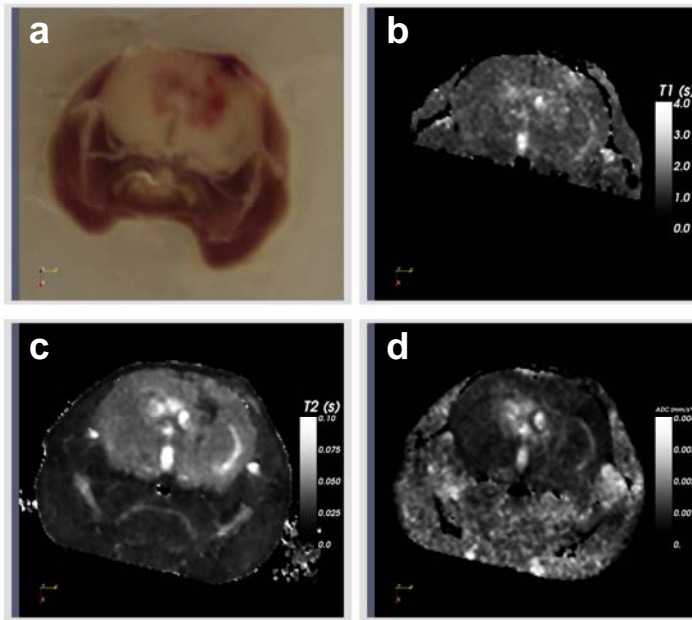


Figure 41. Co-registered blockface and quantitative MR images obtained on a 7T magnet. a) coronal blockface image of glioma mouse head, b) longitudinal relaxation (T_1), c) transverse relaxation (T_2), and d) apparent diffusion coefficient (ADC).

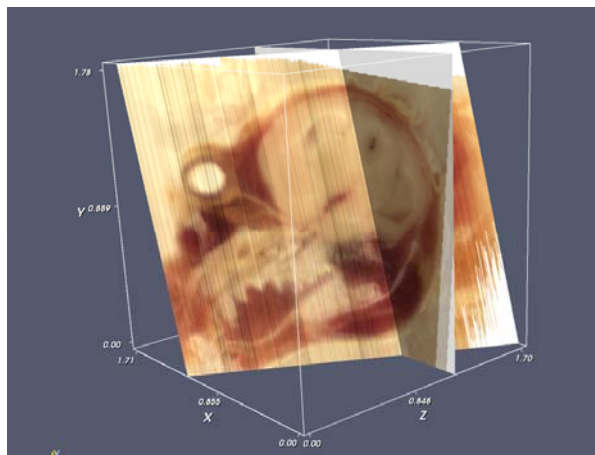


Figure 42. Reconstructed blockface volume of glioma mouse head. The mouse head was sectioned coronally in an anterior to posterior fashion (units in centimeters).

against the corresponding MRI data (Figure 43). These proteins have been previously identified as elevated in grade III gliomas^[94], and were detected in the tumor region as indicated by the blockface volume and area of tumor contrast in the MRI. These results indicate good correlation between the two imaging modalities. In addition, the 3D MALDI-MS volume was automatically binned using a K-means algorithm and the voxels with the highest intensity bin had the corresponding T1, T2, and ADC values averaged. The areas of high protein concentration as detected by MALDI MS are in agreement with the contrast variations detected in the MRI analysis (Table 11). This result demonstrates the power of relating molecular information gained in the MALDI MS analysis to tissue composition contrasts observed in the MRI data.

The ability to relate proteomic information, both spatially and quantitatively, with *in vivo* imaging data has important implications. For example, 3D MALDI MS analysis can now provide contextual information that can open the door to understanding the complex molecular interactions that take place in an animal volume. This approach also enables MALDI MS images to be placed in an *animal-specific* frame of reference, thus permitting the data to be precisely interpreted against specific anatomical information. Moreover, functional information from the *in vivo* studies, such as tumor angiogenesis or tissue degradation, can be correlated with proteomic profiles to help elucidate the molecular mechanisms of health and disease. *In vivo* imaging technologies such as CT and PET already have their place in the pharmaceutical workflow, and the application of this novel 3D methodology can also be extended to allow for the

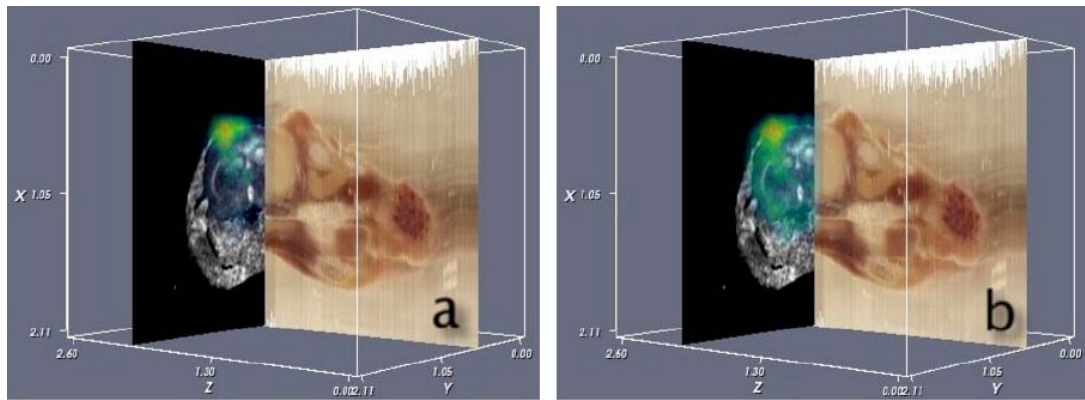


Figure 43. Co-registered blockface volume, 3D MALDI MS (yellow), and ADC MR data (gray scale). a) astrocytic phosphoprotein PEA-15 and b) fatty acid binding protein 5 (units in centimeters).

Table 11. Comparison of voxels with high 3D MALDI-MS ion signal and corresponding average T1, T2, and ADC parameters from the co-registered MR data.

3D MALDI-MS to MRI Correlation	T1 (s)	T2 (ms)	ADC (10 ⁻³ mm ² /s)
Tumor	0.85±0.82	33.5±18.2	0.92±0.62
Injection Insult	1.27±0.46	38.4±11.8	0.97±0.44
Striatum	0.88±0.70	46.6±7.7	0.92±0.24

co-registration of MALDI MS/MS drug distribution data to validate and identify the drug target, and any end-points related to the ADME and PK/PD profile of a compound.

Conclusions

In conclusion, a compelling technology has been demonstrated for the analysis of endogenous and exogenous in whole-animal tissue sections by imaging MALDI MS. The most challenging aspects of the MALDI based imaging technology were the interfacing of a whole-body tissue section to the mass spectrometer, and data reconstruction. Encouragingly, the novel methodology developed through this research can now be successfully applied to whole-animal samples in a robust and reproducible manner. Such a technology has a huge potential to revolutionize the productivity in pharmaceutical research by providing a rapid, label-free and molecularly specific *ex vivo* analysis. For example, applications of this imaging MALDI MS/MS methodology to study the temporal distribution of a therapeutic compound and, more importantly, its metabolites can provide valuable spatial information which are otherwise missed by traditional nuclear imaging techniques or lost in HPLC quantitation studies, thus providing a means to determine the ADME and PK profile of an administered drug. Additionally, imaging the resulting proteome effects of drug administration by MALDI MS can provide valuable PD profiles that can determine a drug's efficacy or toxicity. Correspondingly, preliminary work has also demonstrated the potential of 3D MALDI to serve as a powerful complement to

WBA and PET by providing sample-specific molecular information that can be easily implemented into the pharmaceutical workflow. However, MALDI MS based imaging still has its limitations and is not amenable to every drug compound or protein of interest, and is an invasive technique. Nevertheless, the powerful analyses that can be performed by MALDI imaging of whole-animal sections need to be exploited to know its true value, since there still much to be learned from this technology. It will be exciting to see the impact this technology will have on the advancement of pharmaceutical research and our understanding of PK and PD properties of drugs at the molecular level.

REFERENCES

- [1] J. Drews, *Science* **2000**, 287, 1960-1964.
- [2] M. J. Cunningham, *Journal of Pharmacological and Toxicological Methods* **2000**, 44, 291-300.
- [3] G. C. Kennedy, *Drug Development Research* **1997**, 41, 112-119.
- [4] E. Butt and K. Marcus in *Differential Phosphoproteome Analysis in Medical Research, Vol. 28* Eds.: M. Hamacher, K. Marcus, K. Stuhler, A. v. Hall, B. Warscheid and H. E. Meyer), Wiley-VHC, Federal Republic of Germany, **2006**, pp. 209-220.
- [5] P. R. Graves and T. A. J. Haystead, *Microbiology and Molecular Biology Reviews* **2002**, 66, 39-63.
- [6] D. B. Martin and P. S. Nelson, *TRENDS in Cell Biology* **2001**, 11, s60-s65.
- [7] J. A. DiMasi, *Regulatory Toxicology and Pharmacology* **1994**, 19, 228-235.
- [8] J. A. DiMasi, R. W. Hansen and H. G. Grabowski, *Journal of Health Economics* **2003**, 22, 151-185.
- [9] T. Kennedy, *Drug Discovery Today* **1997**, 2, 436-444.
- [10] L. L. Miller, *Drug Information Journal* **1992**, 26, 251-260.
- [11] W. A. Lee and N. Bischofberger, *Chemicke Listy* **1995**, 89, 22-29.
- [12] I. R. Baxendale, J. J. Hayward, S. V. Ley and G. K. Tranmer, *ChemMedChem* **2**, 768-788.
- [13] L. P. Schacter, C. Anderson, R. M. Canetta, S. Kelley, C. Nicaise, N. Onetto, M. Rozenzweig, L. Smaldone and B. Winograd, *Seminars in Oncology* **1992**, 19, 613-621.

- [14] M. Honing in *The Role of LC-MS in Drug Discovery and Development, an Overview, Vol. 8* Eds.: M. L. Gross and R. M. Caprioli), Elsevier Ltd., Oxford, UK, **2006**, pp. 393-401.
- [15] D. V. Patel and E. M. Gordon, *Drug Discovery Today* **1996**, *1*, 134-144.
- [16] E. J. Martin, J. M. Blaney, M. A. Siani, D. C. Spellmeyer, A. K. Wong and W. H. Moos, *Journal of Medicinal Chemistry* **1995**, *38*, 1431-1436.
- [17] C. M. Masimirembwa, R. Thompson and T. B. Andersson, *Combinatorial Chemistry & High Throughput Screening* **2001**, *4*, 245-263.
- [18] P. S. Dittrich and A. Manz, *Nature Reviews Drug Discovery* **2006**, *5*, 210-218.
- [19] S. H. Hoke, K. L. Morand, K. D. Greis, T. R. Baker, K. L. Harbol and R. L. M. Dobson, *International Journal of Mass Spectrometry* **2001**, *212*, 135-196.
- [20] M. Karas, D. Bachmann and F. Hillenkamp, *Analytical Chemistry* **1985**, *57*, 2935-2939.
- [21] M. Karas, D. Bachmann, U. Bahr and F. Hillenkamp, *International Journal of Mass Spectrometry and Ion Processes* **1987**, *78*, 53-68.
- [22] K. Tanaka, H. Waki, Y. Ido, S. Akita, Y. Yoshida and T. Yoshida, *Rapid Communications in Mass Spectrometry* **1988**, *2*, 151-153.
- [23] M. Karas and F. Hillenkamp, *Analytical Chemistry* **1988**, *60*, 2299-2301.
- [24] R. C. Beavis and B. T. Chait, *Rapid Communications in Mass Spectrometry* **1989**, *3*, 436-439.
- [25] K. Dreisewerd, R. Lemaire, G. Pohlentz, M. Slazet, M. Wisztorski, S. Berkenkamp and I. Fournier, *Analytical Chemistry* **2007**, *79*, 2463-2471.
- [26] R. Cramer, F. Hillenkamp and J. Richard Haglund, *Journal of the American Society for Mass Spectrometry* **1996**, *7*, 1187-1193.

- [27] A. Overberg, M. Karas, U. Bahr, R. Kaufmann and F. Hillenkamp, *Rapid Communications in Mass Spectrometry* **1990**, *4*, 293-296.
- [28] R. Castaing and G. Slodzian, *Journal of Microscopie* **1962**, *1*, 395-410.
- [29] F. Hillenkamp, E. Unsold, R. Kaufmann and R. Nitsche, *Nature* **1975**, *256*, 119-120.
- [30] M. Stoeckli, P. Chaurand, D. E. Hallahan and R. M. Caprioli, *Nature Medicine* **2001**, *7*, 493-496.
- [31] J. S. Fletcher, N. P. Lockyer and J. C. Vickerman, *Surface and Interface Analysis* **2006**, *38*, 1393-1400.
- [32] R. M. Caprioli, T. B. Farmer and J. Gile, *Analytical Chemistry* **1997**, *69*, 4751-4760.
- [33] S. J. Atkinson, P. M. Loadman, C. Sutton, L. H. Patterson and M. R. Clench, *Rapid Communications in Mass Spectrometry* **2007**, *21*, 1271-1276.
- [34] P. Chaurand and R. M. Caprioli, *Electrophoresis* **2002**, *23*, 3125-3135.
- [35] Y. Hsieh, R. Casale, E. Fukuda, J. W. Chen, I. Knemeyer, J. Wingate, R. Morrison and W. Korfmacher, *Rapid Communications in Mass Spectrometry* **2006**, *20*, 965-972.
- [36] J. Pierson, J. L. Norris, H.-R. Aerni, P. Svenningsson, R. M. Caprioli and P. E. Andren, *Journal of Proteome Research* **2001**, *3*, 289-295.
- [37] M. L. Reyzer, R. L. Caldwell, T. C. Dugger, J. T. Forbes, C. A. Ritter, M. Guix, C. L. Arteaga and R. M. Caprioli, *Cancer Research* **2004**, *62*, 9093-9100.
- [38] M. L. Reyzer, Y. Hsieh, K. Ng, W. A. Korfmacher and R. M. Caprioli, *Journal of Mass Spectrometry* **2003**, *38*, 1081-1092.
- [39] S. A. Schwartz, M. L. Reyzer and R. M. Caprioli, *J. Mass Spectrom.* **2003**, *38*, 699-708.

- [40] F. J. Troendle, C. D. Reddick and R. A. Yost, *J. Am. Soc. Mass Spectrom.* **1999**, *10*, 1315-1321.
- [41] D. Touboul, H. Piednoel, V. Voisin, S. De La Porte, A. Brunelle, F. Halgand and O. Laprevote, *European Journal of Mass Spectrometry* **2004**, *10*, 657-664.
- [42] T. J. Garrett and R. A. Yost, *Analytical Chemistry* **2006**, *78*, 2465-2469.
- [43] M. R. Groseclose, M. Andersson, W. M. Hardesty and R. M. Caprioli, *Journal of Mass Spectrometry* **2007**, *42*, 254-262.
- [44] M. L. Reyzer and R. M. Caprioli, *Journal of Proteome Research* **2005**, *4*, 1138-1142.
- [45] P. Chaurand, S. A. Schwartz and R. M. Caprioli, *Current Opinion in Chemical Biology* **2002**, *6*, 676-681.
- [46] M. Guilhaus, V. Mlynski and D. Selby, *Rapid Communications in Mass Spectrometry* **1997**, *11*, 951-962.
- [47] B. A. Mamyrin, *international Journal of Mass Spectrometry* **2001**, *206*, 251-266.
- [48] R. S. Brown and J. J. Lennon, *Analytical Chemistry* **1995**, *67*, 1998-2003.
- [49] J. Gross and K. Strupat, *Trac-Trends in Analytical Chemistry* **1998**, *17*, 470-484.
- [50] C. E. Costello, *Current Opinion in Biotechnology* **1999**, *10*, 22-28.
- [51] G. Siuzdak, *Proceedings of the National Academy of Sciences of the United States of America* **1994**, *91*, 11290-11297.
- [52] I. V. Chernushevich, A. V. Loboda and B. A. Thomson, *Journal of Mass Spectrometry* **2001**, *36*, 849-865.
- [53] R. A. Yost and R. K. Boyd, *Methods in Enzymology* **1990**, *193*, 154-200.

- [54] P. Chaurand, S. Fouhecourt, B. B. DaGue, B. J. Xu, M. L. Reyzer, M.-C. Orgebin-Crist and R. M. Caprioli, *Proteomics* **2003**, 3, 2221-2239.
- [55] K. Yanagisawa, Y. Shyr, B. J. Xu, P. P. Massion, P. H. Larsen, B. C. White, J. R. Roberts, M. Edgerton, A. Gonzalez, S. Nadaf, J. H. Moore, R. M. Caprioli and D. P. Carbone, *The Lancet* **2003**, 362, 433-439.
- [56] P. Chaurand, M. E. Sanders, R. A. Jensen and R. M. Caprioli, *American Journal of Pathology* **2004**, 165, 1057-1068.
- [57] S. A. Schwartz, R. J. Weil, M. D. Johnson, S. A. Toms and R. M. Caprioli, *Clinical Cancer Research* **2004**, 10, 981-987.
- [58] M. Stoeckli, T. B. Farmer and R. M. Caprioli, *J. Am. Soc. Mass Spectrom.* **1999**, 10, 67-71.
- [59] A. J. Sinskey, S. N. Finkelstein and S. M. Cooper, *PharmaGenomics* **2004**, 4, 16-19.
- [60] M. Rudin and R. Weissleder, *Nature Reviews Drug Discovery* **2003**, 2, 123-131.
- [61] R. M. Stephen and R. J. Gillies, *Pharmaceutical Research* **2007**, 24, 1172-1185.
- [62] S. N. Finkelstein, A. J. Sinskey and S. M. Cooper, *PharmaGenomics* **2004**, 4, 20-24.
- [63] M. Singh and V. Waluch, *Advanced Drug Delivery Reviews* **2000**, 41, 7-20.
- [64] A. J. Fischman, N. M. Alpert and R. H. Rubin, *Clinical Pharmacokinetics* **2002**, 41, 581-602.
- [65] Food and Drug Administration in 21CFR312.23, Vol. www.fda.gov, **2005**.
- [66] S. Ullberg, *Acta Radiologica Supplementum* **1954**, 118, 1-110.

- [67] E. G. Solon, S. K. Balani and F. W. Lee, *Current Drug Metabolism* **2002**, *3*, 451-462.
- [68] S. Ullberg, *Sci Tools, The LKB Instrument Journal* **1977**, 1-29.
- [69] L. Dencker, B. S. Larsson, R. Dargy, S. Ullberg and H. Tjalve, *Pure and Applied Chemistry* **1991**, *63*, 1271-1277.
- [70] R. A. D'Souza, E. A. Partridge, D. W. Roberts, S. Ashton, A. Ryan, A. B. Patterson, Z. Wilson and C. C. Thurrell, *Xenobiotica* **2007**, *37*, 328-340.
- [71] C. M. Masimirembwa, U. Bredberg and T. B. Andersson, *Clinical Pharmacokinetics* **2003**, *42*, 515-528.
- [72] S. L. Cohen and B. T. Chait, *Analytical Chemistry* **1996**, *68*, 31-37.
- [73] J. C. Jurchen, S. S. Rubakhin and J. V. Sweedler, *Journal of the American Society for Mass Spectrometry* **2005**, *16*, 1654-1659.
- [74] P. Chaurand, B. B. DaGue, R. S. Pearsall, D. W. Threadgill and R. M. Caprioli, *Proteomics* **2001**, *1*, 1320-1326.
- [75] P. Chaurand, S. A. Schwartz and R. M. Caprioli, *Journal of Proteome Research* **2004**, *3*, 245-252.
- [76] J. L. Norris, D. S. Cornett, J. A. Mobley, M. Andersson, E. H. Seeley, P. Chaurand and R. M. Caprioli, *International Journal of Mass Spectrometry* **2007**, *260*, 212-221.
- [77] A. N. Krutchinsky and B. T. Chait, *Journal of the American Society for Mass Spectrometry* **2002**, *13*, 129-134.
- [78] L. Crossman, N. A. McHugh, Y. S. Hsieh, W. A. Korfmacher and J. W. Chen, *Rapid Communications in Mass Spectrometry* **2006**, *20*, 284-290.
- [79] L. Sleno and D. A. Volmer, *Rapid Communications in Mass Spectrometry* **2006**, *20*, 1517-1524.

- [80] J. H. Lin, *Current Drug Metabolism* **2006**, 7, 39-65.
- [81] P. Lonroth, P. A. Jansson and U. Smith, *American Journal of Physiology* **1987**, 253, E228-E231.
- [82] N. Jezyk, W. Rubas and G. M. Grass, *Pharmaceutical Research* **1992**, 9, 1580-1586.
- [83] R. Lahana, *Drug Discovery Today* **1999**, 4, 447-448.
- [84] S. J. Atkinson, B. Prideaux, J. Bunch, K. E. Warburton and M. R. Clench, *Chimica Oggi-Chemistry Today* **2005**, 23, 5-8.
- [85] S. H. Chay and J. L. Herman, *Arzneimittel-Forschung/Drug Research* **1998**, 48, 446-454.
- [86] Eli Lilly and Company in *Zyprexa Prescribing Information*, Vol. PV 3391 AMP, **12/12/2003**.
- [87] M. Aravagiri, Y. Teper and S. R. Marder, *Biopharmaceutics & Drug Disposition* **1999**, 20, 369-377.
- [88] D. F. V. Lewis, C. Ioannides and D. V. Parke, *Environmental Health Perspectives* **1998**, 106, 633-641.
- [89] J. Bao and B. D. Potts, *Journal of Chromatography B* **2001**, 752, 61-67.
- [90] K. Kassahun, E. Mattiuz, R. Franklin and T. Gillespie, *Drug Metabolism and Disposition* **1998**, 26, 848-855.
- [91] M. J. Bogusz, K. D. Kruger, R. D. Maier, R. Erkwow and F. Tuchtenhagen, *Journal of Chromatography B* **1999**, 732, 257-269.
- [92] Food and Drug Administration in *FDA and the Drug Development Process: How the Agency Ensures that Drugs are Safe and Effective*, Vol. (Ed. D. o. H. a. H. Services), www.fda.gov, **2002**, pp. FS 02-05.

- [93] M. Oellerich, M. J. Barten and V. W. Armstrong, *Therapeutic Drug Monitoring* **2006**, 28, 35-38.
- [94] S. A. Schwartz, R. J. Weil, R. C. Thompson, Y. Shyr, J. H. Moore, S. A. Toms, M. D. Johnson and R. M. Caprioli, *Cancer Research* **2005**, 65, 7674-7681.
- [95] D. W. Kim, J. Huamani, M. L. Reyzer, D. Mi, R. M. Caprioli and D. E. Hallahan, *International Journal of Radiation Oncology Biology Physics* **2006**, 66, S554-S554.
- [96] A. T. Meadows, D. J. Massari, J. Fergusson, J. Gordon, P. Littman and K. Moss, *Lancet* **1981**, 2, 1015-1018.
- [97] L. Jannoun and H. J. G. Bloom, *International Journal of Radiation Oncology Biology Physics* **1990**, 18, 747-753.
- [98] E. M. Yazlovitskaya, E. Edwards, D. Thotala, A. L. Fu, K. L. Osusky, W. O. Whetsell, B. Boone, E. T. Shinohara and D. E. Hallahan, *Cancer Research* **2006**, 66, 11179-11186.
- [99] M. Inouye, H. Yamamura and A. Nakano, *Journal of Radiation Research* **1995**, 36, 203-208.
- [100] D. Thotala, D. E. Hallahan and E. M. Yazlovitskaya, *International Journal of Radiation Oncology Biology Physics* **2006**, 66, S97-S97.
- [101] B. Deweer, B. Pillon, J. B. Pochon and B. Dubois, *Behavioural Brain Research* **2001**, 127, 209-224.
- [102] W. Peissner, M. Kocher, H. Treuer and F. Gillardon, *Molecular Brain Research* **1999**, 71, 61-68.
- [103] R. Nagai, S. Tsunoda, Y. Hori and H. Asada, *Surgical Neurology* **2000**, 53, 503-506.
- [104] I. Ferrer, T. Serrano, S. Alcantara, A. Tortosa and F. Graus, *Journal of Neuropathology and Experimental Neurology* **1993**, 52, 370-378.

- [105] S. Nonaka, N. Katsube and D. M. Chuang, *Journal of Pharmacology and Experimental Therapeutics* **1998**, 286, 539-547.
- [106] S. Nonaka and D. M. Chuang, *Neuroreport* **1998**, 9, 2081-2084.
- [107] D. Voet and J. G. Voet, *Biochemistry*, J. Wiley & Sons, Hoboken, **2004**, p.
- [108] N. Shalbuyeva, T. Brustovetsky and N. Brustovetsky, *Journal of Biological Chemistry* **2007**, 282, 18057-18068.
- [109] S. Nonaka, C. J. Hough and D. M. Chuang, *Proceedings of the National Academy of Sciences of the United States of America* **1998**, 95, 2642-2647.
- [110] D. G. Nicholls, *Current Molecular Medicine* **2004**, 4, 149-177.
- [111] P. Bernardi, A. Krauskopf, E. Basso, V. Petronilli, E. Blalchy-Dyson, F. Di Lisa and M. A. Forte, *Febs Journal* **2006**, 273, 2077-2099.
- [112] D. W. Choi, *Journal of Neurobiology* **1992**, 23, 1261-1276.
- [113] R. W. Chen and D. M. Chuang, *Journal of Biological Chemistry* **1999**, 274, 6039-6042.
- [114] G. N. Bijur, P. De Sarno and R. S. Jope, *Journal of Biological Chemistry* **2000**, 275, 7583-7590.
- [115] P. Chaurand, S. A. Schwartz, D. Billheimer, B. G. J. Xu, A. Crecelius and R. M. Caprioli, *Analytical Chemistry* **2004**, 76, 1145-1155.
- [116] J. Drews and S. Ryser, *Drug Discovery Today* **1997**, 2, 365-372.
- [117] T. K. Sinha, S. Khatib-Shahidi, T. E. Yankeelov, K. Mapara, M. Ehtesham, D. S. Cornett, B. M. Dawant, R. M. Caprioli and J. C. Gore, *accepted in Nature Methods* **2007**.